THE EFFECT OF GEOMETRICAL SCALE UPON MPD THRUSTER BEHAVIOR

by

James Hunter Gilland

Princeton University
School of Engineering and Applied Science
Department of Mechanical and Aerospace Engineering

Submitted in partial fulfillment of the requirements for the degree of Master of Science in Engineering from Princeton University, 1988

Prepared by:

James Hunter Gilland

Approved by:

R. G. Jahn
Professor R. G. Jahn
Thesis Adviser

W. J. Kelly
Dr. A. J. Kelly
Thesis Reader

June 1988

ABSTRACT

Half Scale versions of the Princeton Benchmark and Flared Anode self field MPD thrusters have been investigated and compared to full scale thruster behavior to determine the influence of scale and design upon MPD performance. Thruster performance determined from impulsive thrust and terminal voltage measurements has been found to depend primarily on propellant flow rate and the ratio of electrode radii, but not on thruster size. Current distributions obtained from magnetic field probes are independent of scale for both thruster designs. Voltage depends upon current, electrode geometry, and propellant flow rate. Because of the scale invariance of the above performance parameters, subscale thrusters show limited promise in low power applications.

ACKNOWLEDGEMENTS

This thesis results from work aided or encouraged by several people. I am indebted particularly to Professor Robert Jahn and Dr. Arnold Kelly for their support, both financial and academic, which allowed me to perform this research. I am also thankful for the broad education provided me by the Princeton faculty in both the Mechanical and Aerospace and Physics Departments. Mr. Waldo von Jaskowsky, Mr. George Miller, and Mr. Dave Tregurtha were also invaluable for their experience and wisdom in the practicalities and history of MPD research; thanks to them, MPD thrusters made it from my notes to the vacuum tank. The education I received from these people both in and out of the classroom will stay with me well beyond the writing of this thesis.

My time at Princeton has also been enhanced by my interaction with my fellow graduate students, particularly Roydon Fraser, John Barnett, Roger Myers, Jay Polk, Kok Meng Lue, and Edgar Choueiri. A great many discussions and arguments ended in enlightenment and understanding for all of us on subjects ranging from Plasma Physics to Socialism. Debating with Roydon over completely inane subjects on the way to Thomas Sweets' ice cream parlor provided a much needed catharsis after a week in the lab. Roydon's cheer and goodwill were always infectious, and he has been a steadfast friend.

Special thanks also to the Mercer Bucks Running Club, whose Tuesday Night track and pizza nights were a reminder of a world beyond the ivy halls and vacuum tanks of Princeton. I've found that running with friends can answer many "unsolvable" problems, which are just waiting for your return. If they aren't solved, they at least fall into perspective. Thanks to Mike Ruggio, who shares my joy in competing, and who proved to be a good training partner and friend, even if he did beat me in races.

Finally, thanks to my loved ones, who waited (for the most part) patiently for this work to be finished, even if they weren't sure why it took so long. Your support was always appreciated, even though your advice sometimes met with stiff resistance. Mom and Dad, it is finally finished, and you can leave it on the coffee table and read it any time you want.

My thanks to Myra Creighton, who was more than patient with me, and who proved to be a valuable assistant as well as confidante, particularly when sitting through hours of experiments with only comic books and textbooks to keep her busy. She not only has my eternal gratitude, but is now able to say Magnetoplasmadynamic Thruster without blushing. I hope that she will always put up with me in my work.

This thesis is done; I hope the knowledge and friendships it created continue.

This work was supported by the National Aeronautics and Space Administration under contract number 954997, and by grants from Rocket Research, Inc. and the U.S. Department of Energy, Plasma Physics Laboratory, Princeton, NJ.

This thesis carries number 1811-T in the records of the Department of Mechanical and Aerospace Engineering.

TABLE OF CONTENTS

Abstract ii

Chapter I: INTRODUCTION 1

The MPD Accelerator 2
Review of Scaling Research 4

Chapter II: EXPERIMENTAL APPARATUS AND TECHNIQUES . . . 8

Introduction 8
The MPD Thruster 8
Vacuum System 11
The Power Supplies 12
Diagnostics 13
Terminal Characteristics 13
Magnetic Field Probing 14
Thrust Stand 15
Data Acquisition 17

Chapter III: Scaling of the Benchmark Thruster 18

Terminal Characteristics 18
Voltage Waveforms 19
Voltage-Current Characteristics 19
Onset Current 24
Thrust-Current Characteristics 28
B-probing 33
Summary 33

Chapter IV: Scaling of the Flared Anode Thruster 35

Terminal Characteristics 36
Voltage Waveforms 37
Voltage-Current Characteristics 38
Onset 39
Thrust-Current Characteristics 41
B-Probing 44
Summary 48

Chapter V: Performance Comparison: Scale and Geometry 49

Scaling 49
Scaling of the Benchmark Thruster 51
Scaling of the Flared Anode Thruster 52
Geometry Performance Comparison 54

Chapter VI: Summary and Conclusions 57

Summary 57
Scaling 57
Geometry 58
Conclusions 59
Future Work 60

Appendix A: Calibration Procedures 62

Mass Flow Calibration 62
Operation and Calibration of Magnetic Field Probes . . 64

REFERENCES 68

Chapter I

INTRODUCTION

Although chemical rocket propulsion has proved adequate for near Earth missions, a need has arisen for a form of space propulsion with higher specific impulse for missions of longer duration, such as outer planet exploration and orbital transfer (1). These missions are expected to require specific impulse values of 2000 to 5000 seconds. Electric propulsion has often been proposed as a viable means of propulsion for such missions. Two forms of electric rockets are particularly promising for missions of this type: Electrostatic and Electromagnetic rockets.

Electrostatic thrusters use an electrostatic potential to accelerate propellant ions to high velocities. These devices are capable of achieving high levels of specific impulse, greater than 10000 seconds, but space charge effects limit their thrust densities to low values (~ 5 N/m^2). Electromagnetic propulsion uses electromagnetic forces to accelerate a conducting quasi-neutral plasma propellant and consequently do not suffer from space charge effects. The primary force in these devices, the Lorentz (jxB) body force, acts upon a plasma in the presence of a magnetic field. These devices produce specific impulse lev-

els ranging from 2000 to 5000 s, at thrust densities on the order of 100 kN/m² (2). This thesis describes research that has been conducted to understand the behavior of self-field, Lorentz force Magnetoplasmadynamic (MPD) thrusters as a function of geometric scale. Emphasis has been placed on the possibility of designing subscale MPD thrusters that can be used with the low megawatt level space power plants envisioned for the near future.

1.1 The MPD Accelerator

The MPD thruster, a coaxial plasma accelerator, is exemplified by the "benchmark" thruster, as shown in Figure 1.1. In this device, the cylindrical cathode is surrounded by an annular anode. A gaseous propellant is injected from the insulated rear wall of the chamber into the space between the two electrodes. Application of a several thousand volt potential difference across the electrodes ionizes the gas and a diffuse arc is formed. At kiloampere (kA) current levels, the coaxial geometry of the MPD thruster allows it to act as a self-field plasma accelerator, in which the current flowing through the cathode establishes an azimuthal magnetic field which then interacts with the current flow through the plasma to accelerate the plasma outward and compress it toward the axis via the Lorentz body force. Thrust is thereby produced by the expulsion of the plasma at high speeds out of the chamber.

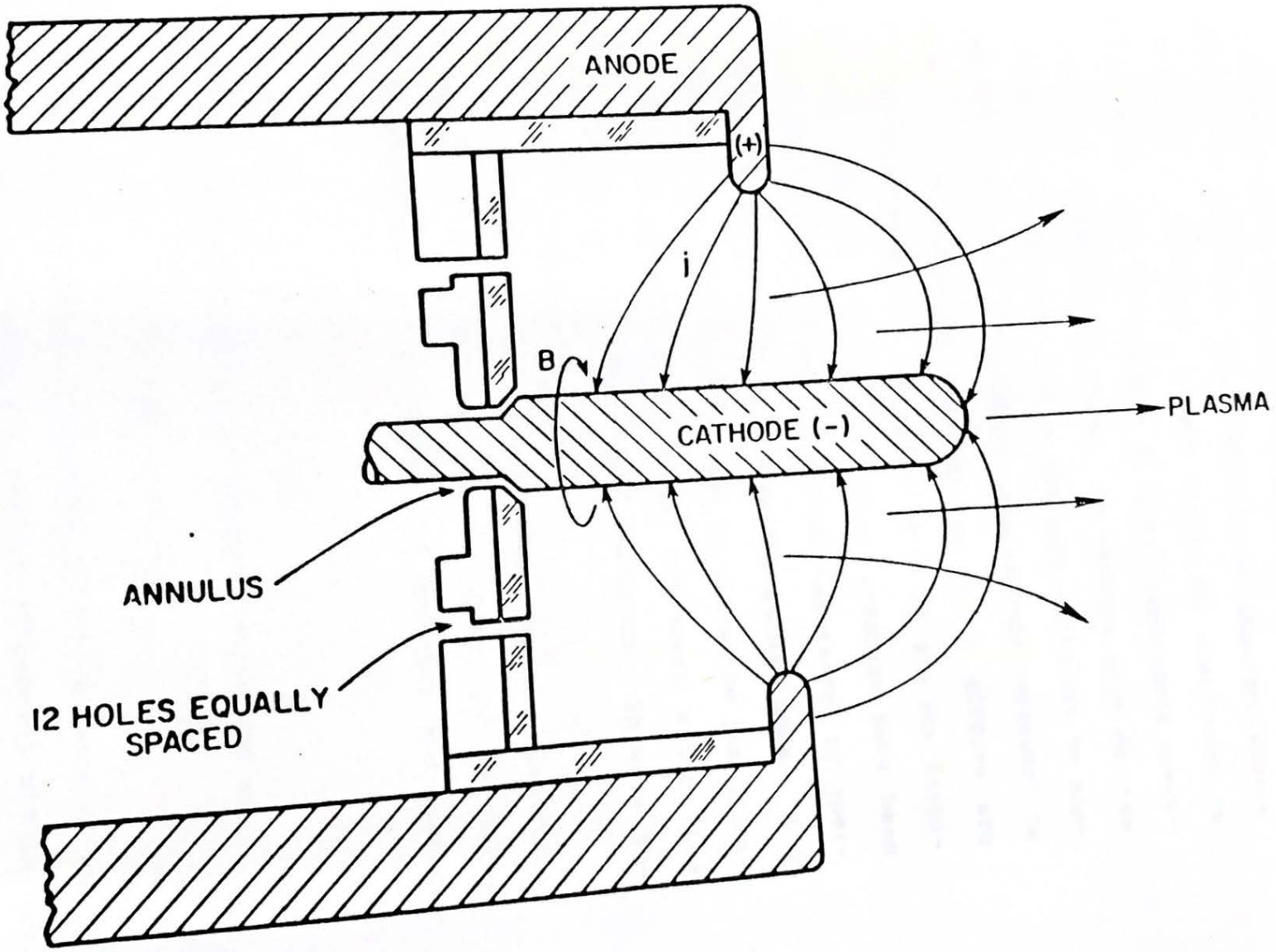

Figure 1.1

MPD CONFIGURATION

In order to obtain appreciable amounts of electromagnetic thrust, the MPD thruster must be operated at thousand ampere current levels. Since the voltage across the electrodes is on the order of tens to hundreds of volts, continuous operation requires megawatts of power. In testing such devices in laboratory environments, it is not only difficult to supply appropriate power; the pumping requirements necessary to operate at the low pressures required for a diffuse arc while injecting propellant at rates up to 20 g/s are formidable with existing technology. These problems have been circumvented in the Electric Propulsion Laboratory by operating the MPD thruster in a protracted pulsed mode. A 1 millisecond flat pulse is sufficient to allow the gas dynamic and electromagnetic acceleration processes within the thruster to attain a steady state condition. This is the "quasi-steady" operating mode (3).

The electromagnetic thrust dominates over the electrothermal thrust in these devices. This quantity can be calculated theoretically as a function of geometry and current level:

$$T = bJ^2$$

where b is a geometry-dependent constant expressed as

$$b = \frac{\mu_0}{4\pi} \ln(R_a/R_c)$$

The logarithmic term represents the effective ratio of anode radius to cathode radius for current attachment within the

thruster. Expressions for specific impulse and thrust efficiency can also be determined from the thrust equation:

$$I_{sp} = T/\dot{m} = bJ^2/\dot{m}$$

$$\eta = T^2/2\dot{m}JV = b^2J^3/2\dot{m}V$$

As is obvious from the above equations, thrust, I_{sp}, and efficiency all increase with current level. However, other processes come into play within the thruster to create a limit in the currents at which the thruster can operate for a given propellant flow rate. This limit is called the onset condition. At onset, high frequency voltage oscillations and both insulator and electrode erosion occur, effectively limiting the current levels at which a given thruster can operate. The current at which the peak-to-peak voltage oscillations reach 10% of the mean voltage amplitude has been defined as the "so-called" onset current (J*); this value is used as the upper limit of thruster operation (4).

1.2 Review of Scaling Research

Research in MPD propulsion has centered upon questions of performance and lifetime. Both questions have been approached experimentally by varying electrode and mass injection geometries, so that a limited amount of information concerning the effects of these parameters on performance already exists (4,5,16,19). All of these studies used thrusters of comparable size, and all operated in the mega-

watt range. The primary goal of many of these studies was to improve performance through increasing the onset current.

One of the obstacles the MPD thruster faces in terms of application in space is the problem of available power. At this time, no multimegawatt electrical space power source exists to provide appropriate power for steady state operation of the MPD thruster. When viewed in this light, the drive to increase the onset current, while ultimately beneficial, leaves open the problem of how to provide thrusters that are applicable to existing space power supplies. This problem forms the central concern of this thesis.

MPD experimental scaling research has been conducted previously at Princeton's Electric Propulsion Laboratory. In these studies the approach has been to reduce the size of the standard "full scale" MPD thruster by a factor of two while maintaining similitude of the electrode geometries in order to isolate the effects of size upon the acceleration processes.

Initial experimental findings by Mead (6) with the Half Scale Benchmark Thruster (HSBT) examined terminal voltage characteristics in relation to scale and mass flux. In that first study, a half scale version of the Benchmark thruster was tested at low mass flow rates (0.125 - 3 g/s) to determine the range of performance possible in the smaller device. Voltage measurements and theoretical calculations of electromagnetic thrust indicated that the HSBT might have

an advantage over the Full Scale Benchmark Thruster (FSBT) at low powers (6). This study also indicated some scaling of thruster voltage with mass flux; however, no physical explanation for this dependence was put forth. A second experimental investigation of the HSBT by Kaplan (7) investigated voltage characteristics and current distributions of both scales for similar mass fluxes. These results included performance calculations obtained from current patterns, and indicated that the HSBT had marginal utility at low powers compared to the FSBT. These experiments concentrated on operation of the half scale device with mass fluxes equal to those used in the full scale, in order to preserve similarity of interelectrode conditions. Half scale mass flow rates ranging from 0.75 to 4.5 g/s in these experiments were then compared to full scale thruster behavior at flow rates of 3-18 g/s. This study showed that the full scale thruster was capable of reaching higher peak efficiencies than the half scale models, and that there was no advantage in efficiency by operating at low powers (Figure 1.2) (7).

The above studies consisted of measurements and theoretical performance calculations for a single electrode configuration. To develop a more useful foundation for making judgements about scaling, a second electrode configuration with a flared continuously conducting anode was introduced into the study. This was done in an effort to separate the effects of geometry and scale with respect to their influ-

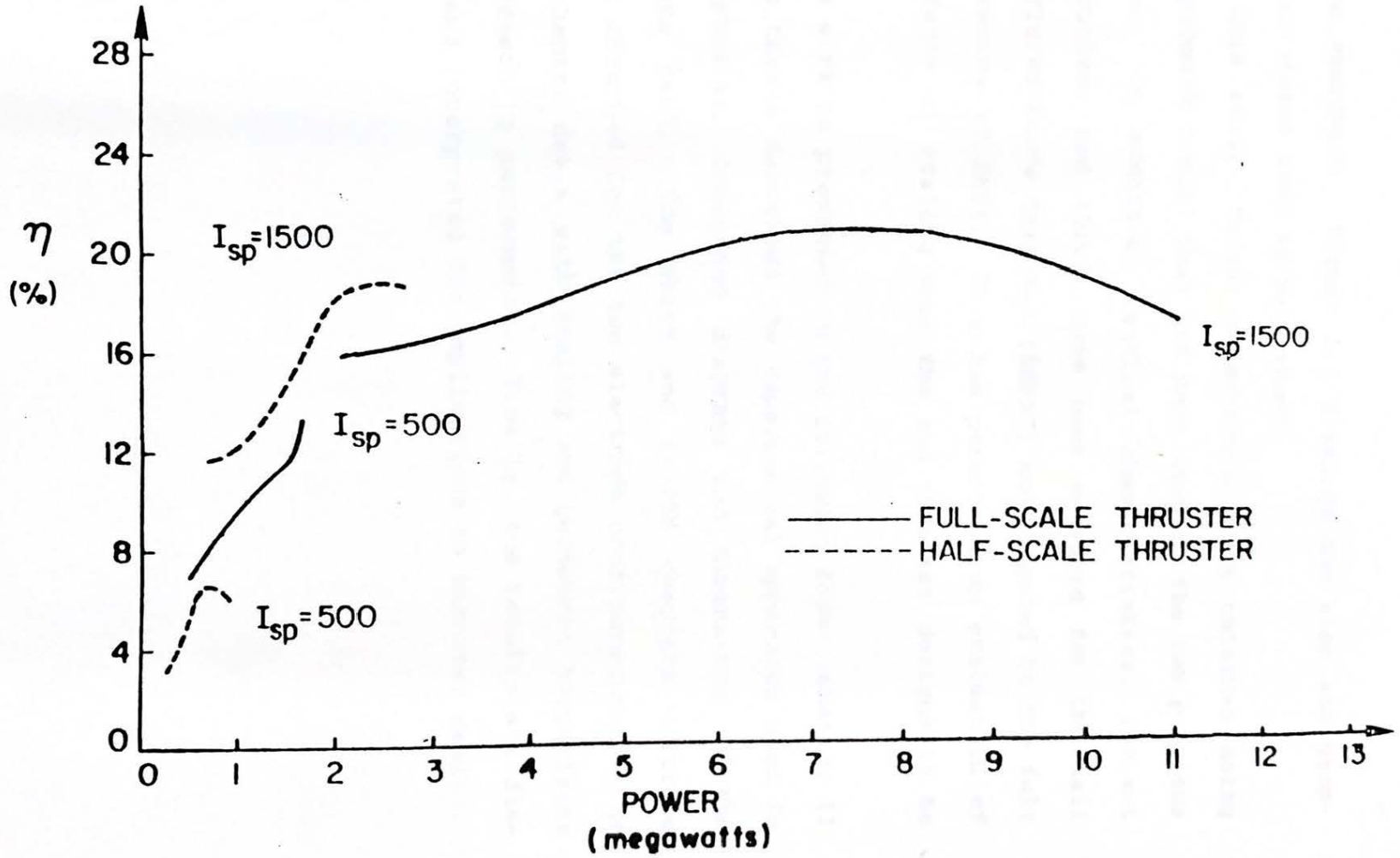

COMPARISON OF EFFICIENCIES BETWEEN THRUSTERS (II)

Figure 1.2

ence on operation. Figure 1.3 displays the size and geometry variations used in this study.

In this study, thrust measurements were obtained using the benchmark design that had been used in the two previous studies. In addition, terminal characteristics, current distribution, and thrust have been measured for the Half Scale Flared Anode Thruster (HSFAT) and compared to the full scale device (FSFAT). This has permitted an evaluation of the effects of scaling upon the two thruster designs to be made.

This work is presented in the following form: Chapter II of this thesis describes the experimental apparatus used in these studies, including diagrams and dimensions of the thrusters used. The third and fourth chapters describe results obtained for the two electrode configurations. The fifth chapter deals with scaling and geometric comparisons with respect to performance. Finally, the results are discussed and interpreted for implications to thruster design.

SCALE–DESIGN MATRIX

HALF SCALE BENCHMARK THRUSTER	HALF SCALE FLARED ANODE THRUSTER
FULL SCALE BENCHMARK THRUSTER	FULL SCALE FLARED ANODE THRUSTER

Figure 1.3

Chapter II

EXPERIMENTAL APPARATUS AND TECHNIQUES

2.1 Introduction

The Electric Propulsion Laboratory has been active in MPD research for over 25 years. The apparatus and techniques which have been developed over this period are described briefly in this chapter; detailed descriptions can be found in reports and theses published by this laboratory.

2.2 The MPD Thruster

Two MPD thruster designs were used in this study: the so-called "Benchmark" and the "Flared Anode." Both of these devices are coaxial, with differing arc chamber and electrode construction, as illustrated in Figures 1.1 and 2.1.

The Benchmark thruster is the reference design for Princeton's Electric Propulsion Laboratory. It consists of a cylindrical chamber insulated with Pyrex at the walls and a boron nitride backplate at the rear of the chamber. At the front of the cylinder is an annular aluminum anode, with a cylindrical cathode with a hemispherical tip located on the chamber axis. The cathodes used in these experiments in both thrusters were constructed of 2% thoriated tungsten.

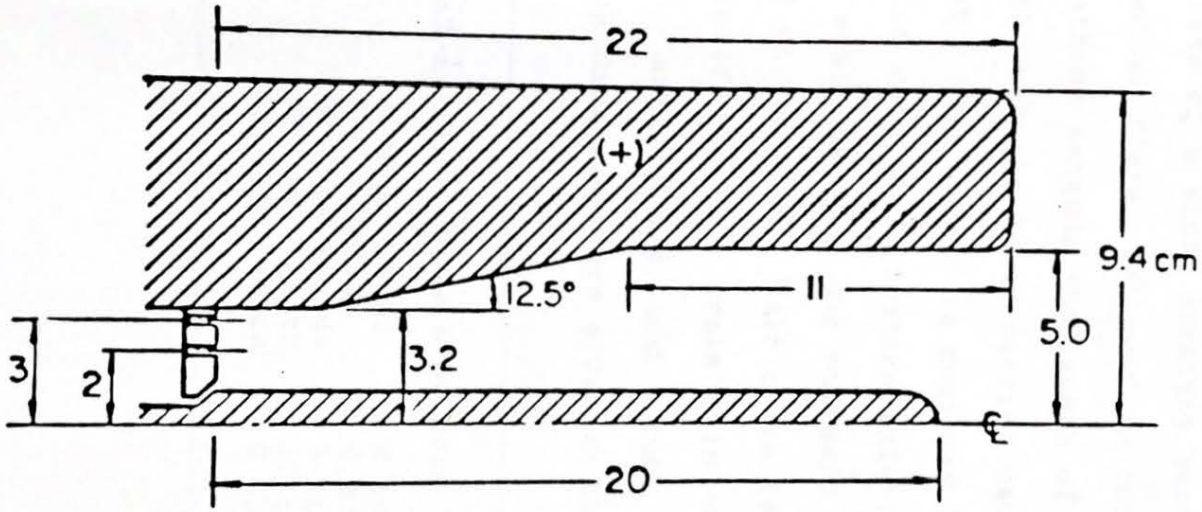

Modified Flared Anode Thruster

Figure 2.1

The Flared Anode thruster design arose from a desire to exploit the choking characteristics of MPD flow (8). The chamber is longer than that of the benchmark, and the walls are formed by the continuous copper anode. The anode cross section consists of a short straight section, followed by a 25 degree conical flare, followed by another straight section. The cathode extends the length of the chamber. Mass is injected through the boron nitride backplate at the rear of the chamber. This design is depicted in Figure 2.1.

Two sizes of each configuration exist: "Full" and "Half" scale. Full scale denotes the standard multimegawatt size commonly used in the past. Half scale is then 1/2 the linear dimensions of the full scale. In other words, length scales by 1/2, area by 1/4, and volume by 1/8. The full scale benchmark dimensions are given in Table 1:

Table 1: Full Scale Benchmark Thruster

Chamber Depth	8 cm
Anode Radius	9.4 cm
Orifice Radius	5 cm
Cathode Length	10 cm
Cathode Radius	0.95 cm

The Full Scale Flared Anode dimensions are listed in Table 2:

Table 2: Full Scale Flared Anode Thruster

Chamber Depth	22 cm
Anode Radius	9.4 cm
Orifice Radius	5 cm
Cathode Length	20 cm
Cathode Radius	0.95 cm

Argon gas is used as propellant in all experiments. The gas is injected into the chamber at two locations on the backplate of each thruster; half the flow rate is injected through an annulus at the base of the cathode and half is injected through 12 evenly spaced holes located at a fixed radius from the central axis. In the case of the Half Scale Benchmark Thruster (HSBT), the outer injection ports are located at a radius of 1.9 cm; in the Half Scale Flared Anode Thruster (HSFAT), the outer ports are located near the anode at a radius of 1.5 cm in order to correspond to the location of the mass injection ports used in the FSFAT.

Mass flow rate is controlled by choked orifices located upstream of the backplate. By choking the flow, the mass flow rate through the sonic orifices can be regulated by the upstream stagnation pressure. Stagnation pressure, in turn, is measured and regulated at a plenum upstream of the sonic orifices. Calibration tests show that the mass flow rate is

linear with respect to plenum pressure, as is expected for an ideal gas; however, the proportionality constant obtained empirically is less than that calculated from fluid mechanical theory (Appendix A). This is attributed to the non-ideal aspects of flow within the propellant distribution system, such as viscous losses in the small channels and losses from the turning of the flow at sharp corners.

2.3 Vacuum System

MPD thrusters operate with interelectrode chamber pressures of approximately 10 torr. In order to duplicate the low density background conditions of space and maintain the necessary diffuse arc, the thrusters are operated within large dielectric vacuum chambers at back pressures on the order of 10E-5 torr. Two vacuum tanks were used in the course of these experiments: a Plexiglas diagnostic chamber and a fiberglass performance test vessel.

The Plexiglas chamber measures 1.83 m long and 0.92 m inner diameter. This tank was kept evacuated by two mechanical roughing pumps and an oil diffusion pump. The diagnostic facility is used to obtain terminal characteristics and magnetic field distributions. Probing is accomplished using a remote controlled electrical probe rack with three degrees of freedom.

The fiberglass chamber is 5 m long and 2 m in diameter. This chamber is also kept at a pressure of approximately

10E-5 torr by two 1.3 m diameter oil diffusion pumps. The chamber is equipped with a thrust stand for performance measurements.

2.4 The Power Supplies

The MPD thruster is operated in a pulsed mode by which quasisteady operation is attained. Typical pulses are 1 millisecond in length, at instantaneous powers up to several megawatts. The pulses are supplied by an L-C ladder network designed to produce rectangular current waveforms 0.5-2 milliseconds in length. Each facility has a separate ladder network and power supply, and both systems are configured to produce the required rectangular wave forms (Figure 2.2).

The capacitor bank used with the Plexiglas tank is the more versatile of the two systems. It consists of 80 stations with four 26.1 μF capacitors per station. These stations are arranged in four rows of 20 stations each, and each station is connected by a 1.5 μH "jellyroll" inductor. Several series and parallel configurations can be created to achieve current pulses of various shapes and durations. The bank is connected to the MPD diagnostic facility through an electrolytic ballast resistor which matches the impedance of the bank to that of the thruster. The bank is charged by a DEL High Voltage DC Power Supply; switching is accomplished using a high speed solenoid valve and gas discharge switch (9). Propellant is injected for 15-20 milli-

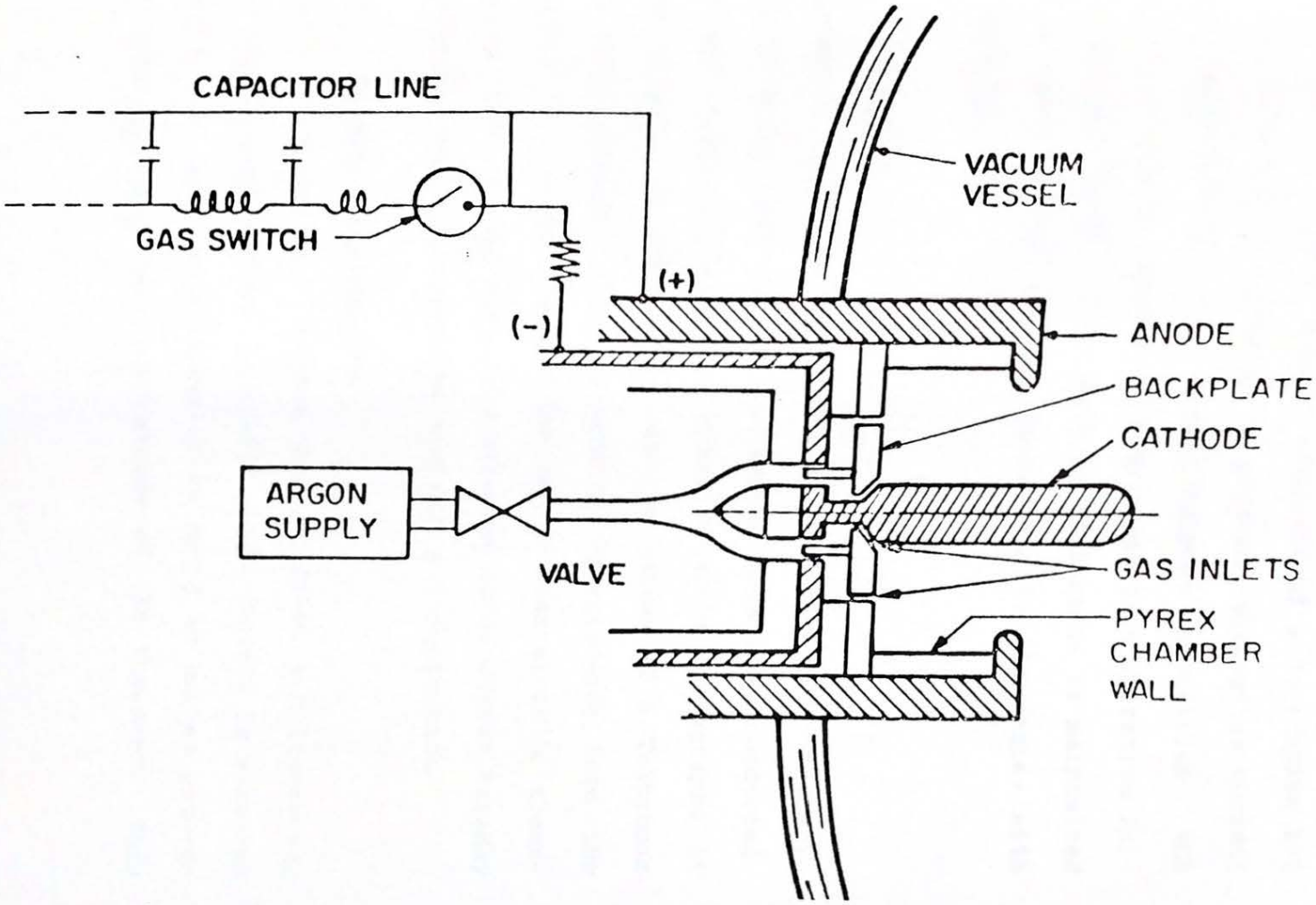

Figure 2.2

EXPERIMENTAL FACILITIES

seconds prior to activating the gas switch that connects the thruster to its power supply. This allows the propellant distribution to become steady and uniform before the discharge is initiated by the gas switch.

The fiberglass power supply consists of a 20-station L-C network which can be adjusted to produce rectangular current pulses ranging from 0.5 to 2 milliseconds in duration. SCR thyristor switches capable of 1 Hz repetitive operation initiate the discharge (10). Ballast resistance is maintained with a water cooled tubular steel resistor in series with the thruster.

2.5 Diagnostics

Experiments involving terminal characterization, magnetic field probing, and thrust measurement have been conducted. Data are acquired primarily using Polaroid photographs of probe signals as they appear on the screen of a Tektronix 7844 oscilloscope. Electromagnetic interference from the thruster is reduced through the use of coaxial cable transmission lines and by placing a grounded metal screen Faraday cage around the oscilloscopes and related electronics.

2.5.1 Terminal Characteristics

Thruster current and voltage are measured simultaneously over the duration of the discharge. The current is measured using a low inductance copper-sheet shunt in series between the capacitor bank and the cathode of the thruster. This

shunt was calibrated using a Pearson Electronics No. 301 X current transformer. The voltage drop across the shunt is displayed and photographed on the shielded oscilloscope screen.

Terminal voltage is measured differentially across the anode and cathode using two Tektronix 6013A 1000:1 high voltage probes, which were calibrated prior to each experiment. Once calibrated, the probes remained calibrated over the course of the experiments. The power supply and terminal measurements were quite repeatable. The primary measurement error (~5%) is associated with reading data from the photographs.

2.5.2 Magnetic Field Probing

The magnetic fields within the thruster are measured by inserting a small multiturn coil of insulated wire into the discharge. This coil is encapsulated in a closed glass rod and the coil itself is coated with epoxy to protect it from the discharge. Total probe diameter for this experiment was 4 mm.

The magnetic probe coil produces an emf in response to the changing magnetic flux through its center. This voltage is proportional to the change in field strength with respect to time. The coil signal is integrated using an active integrator to produce a voltage which is proportional to the magnetic field strength at the probe location. The probe can be positioned precisely in 3 directions; axial, hori-

zontal, and vertical,as well as rotated in the horizontal plane, using the remote controlled electrical probe rack in the Plexiglas test facility.

Through the use of Ampere's Law in conjunction with the assumption of azimuthal symmetry within the discharge, enclosed current contours can be calculated from the magnetic field strengths measured throughout the thruster. Electromagnetic thrust can be obtained by summing the axial components of the Lorentz force over the thruster surfaces perpendicular to the thruster axis (4,5). In the case of the benchmark thruster, calculated thrust was found to approximate actual thrust stand performance; the Flared Anode thruster has shown significant deviations from the value predicted from magnetic field measurements.

2.5.3 Thrust Stand

Thrust is measured using a thrust stand built according to a design by Fairchild Republic and modified by R. Burton (10) for use in the fiberglass vacuum chamber. The stand consists of the thruster, a horizontal free swinging thrust arm, and an Bentley Nevada rf position transducer. The transducer is located directly below the thruster's central axis.

The thruster is located at the free end of the thrust arm, with the other end attached to a vertical axis which permits it to swing freely on two friction-free flexural pivots (Figure 2.3). The horizontal arm also contains the

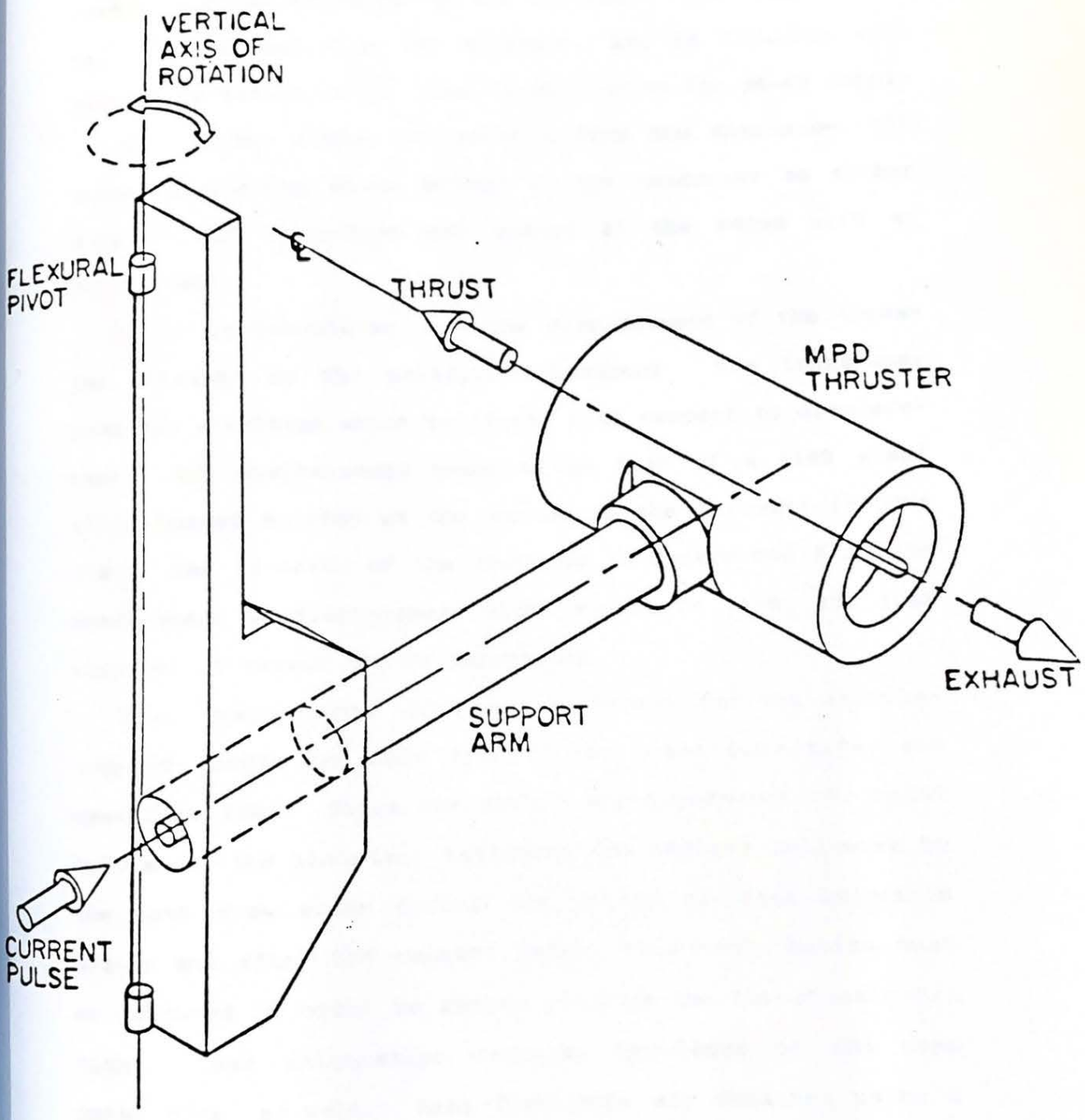
VERTICAL
AXIS OF
ROTATION
FLEXURAL
PIVOT
THRUST
MPD
THRUSTER
EXHAUST
SUPPORT
ARM
CURRENT
PULSE

Figure 2.3

coaxial current conductor to the thruster. The stand assembly is insulated from the discharge and is floating with respect to the thruster. The connection to the power supply at the chamber window is isolated from the discharge with rubber insulating disks bolted to the conductor on either side of the connection and sealed at the edges with an O-ring seal.

Thrust is calculated from the displacement of the thruster obtained by the position transducer. The transducer produces a voltage which is linear with respect to displacement. The displacement measured is that of a 4140 steel alloy target mounted at the bottom of the thruster (Figure 2.4). The velocity of the thruster is determined from the measurement of displacement with respect to time, and from this result thrust can be calculated.

Other measurements which are necessary for the calculation of thrust are cold flow thrust, mass flow rate, and mass flow time. Since the thrust stand measures the total impulse of the thruster, including the impulse delivered by the mass flow alone during the period of mass injection before and after the current pulse, this contribution must be measured in order to remove it from the thrust calculations. This calculation requires knowledge of the mass pulse time, as well. Mass flow data are obtained using a piezoelectric pressure transducer located downstream of the regulating plenum. Cold thrust is measured with the thrust

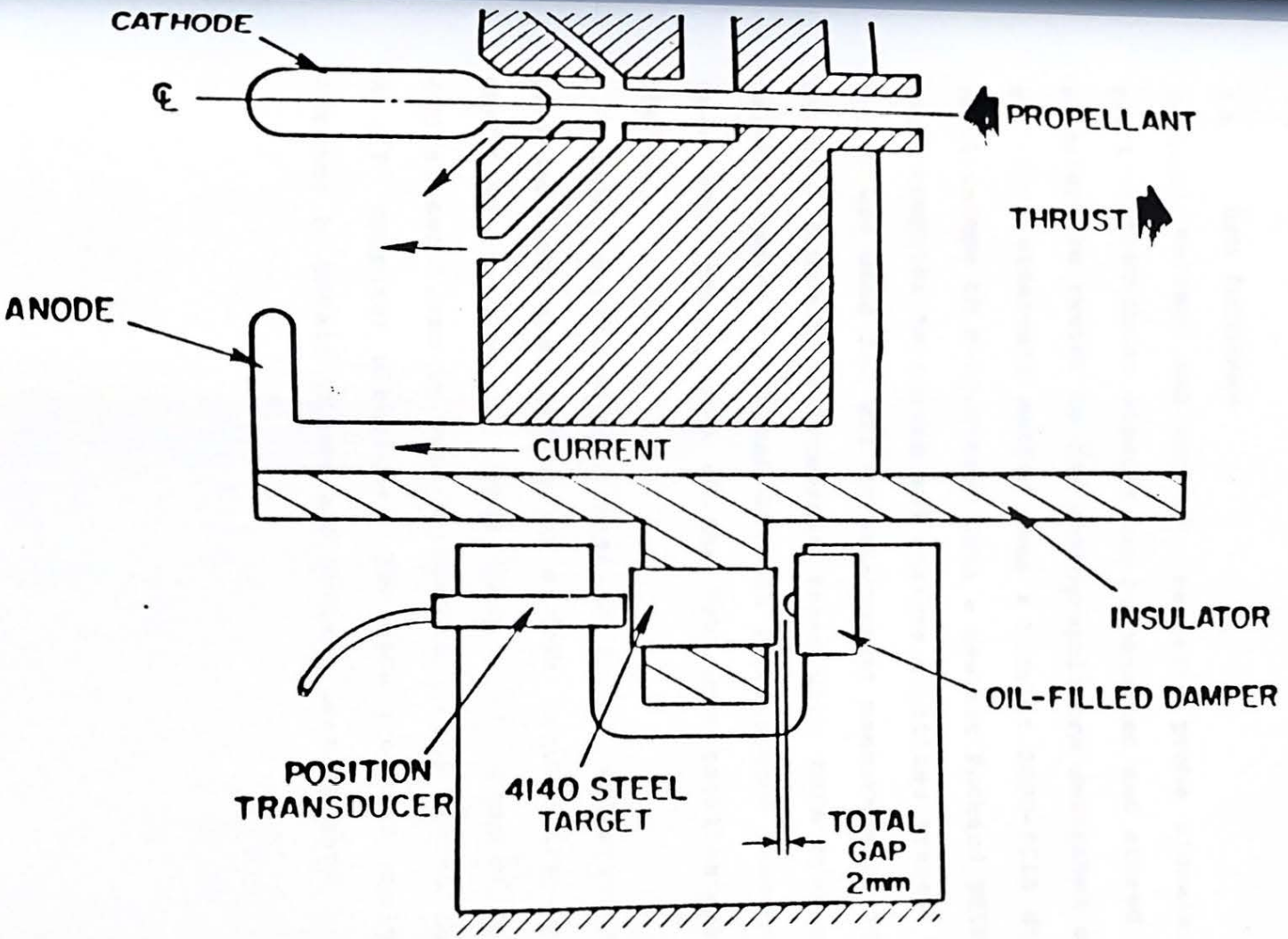

Figure 2.4 Thrust Stand Proximitor Mounting

stand by pulsing the mass injection system without generating a discharge.

2.5.4 Data Acquisition

Terminal voltage and current, magnetic probe signals, and position transducer signals can be obtained and stored using an alternate system to the photographic one described earlier. This alternate method uses a Nicolet 2090-IIIA digital oscilloscope in conjunction with a Hewlett Packard 9816 personal computer to record and analyze digitized traces. This system was used for all thrust-current measurements in this thesis. Current measurements taken with this system were found to agree to within 5% with simultaneous measurements taken from photographs of the Tektronix oscilloscope display.

Nicolet oscilloscope traces of thrust and current were recorded and analyzed using a data acquisition program, FASTTRANS, written by James Polk. This program receives digital oscilloscope data automatically and stores the data on 3.5" computer diskettes. The data are then analyzed by computer to obtain thrust and current measurements.

Chapter III

SCALING OF THE BENCHMARK THRUSTER

The Benchmark thruster described in chapter I serves as the reference design for comparisons of performance and physical processes at the Princeton Electric Propulsion Laboratory. The data collected for the Half-Scale Benchmark Thruster (HSBT) now consist of current, voltage, and thrust characteristics in addition to magnetic field probing. These data are described and compared with respect to the large full scale data base that exists.

3.1 Terminal Characteristics

Experimental HSBT terminal characteristics now include thrust-current measurements in addition to voltage-current measurements obtained in the Plexiglas and fiberglass facilities. Electrical terminal data to be discussed here are voltage and current transient behavior, quasisteady voltage as a function of current, and the onset current as a function of propellant mass flow rate.

3.1.1 Voltage Waveforms

The HSBT displays typical quasisteady behavior (Figure 3.1); that is, the voltage trace is rectangular, with no initial or end transients to distort the 1 ms plateau. Current and voltage show a rapid rise (10-50 μs), followed by a 1 ms plateau and a final drop off to zero. Voltage and current levels measured at a point 700 μs into the pulse were taken to be representative of the quasisteady operating state (cf. Figure 3.2). These terminal data are qualitatively similar to those obtained with the full scale device. The experimental results are discussed in the forthcoming sections.

3.1.2 Voltage-Current Characteristics

Three separate tests of the Half Scale Benchmark Thruster have been made in both facilities by two different researchers. The first voltage measurements were collected by Kaplan (7) in the Plexiglas vacuum facility, while this thesis reports data taken in both test facilities. While the first set of voltage-current measurements agreed with Kaplans's findings, the second set did not. These later data exhibited the same qualitative behavior seen in the initial findings, but the magnitude of the voltage was consistently 40% lower. This second experiment was done under identical conditions of mass flow rate and tank pressure, using calibrated instruments. No explanation, either physical or systematic, could be found for this behavior, which occurred repeatably and consistently throughout the experi-

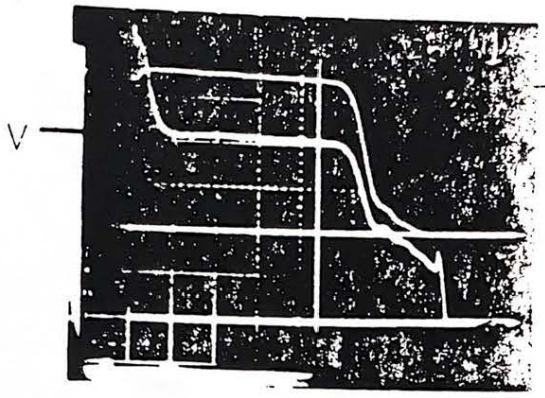

VOLTAGE AND CURRENT TRACES

BELOW ONSET

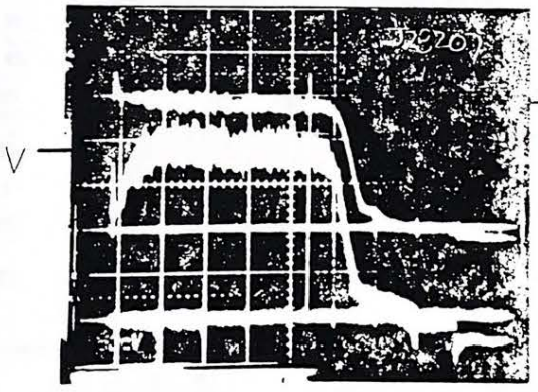

VOLTAGE AND CURRENT TRACES

AT ONSET

Figure 3.1

HALF SCALE BENCHMARK VOLTAGE CHARACTERISTICS

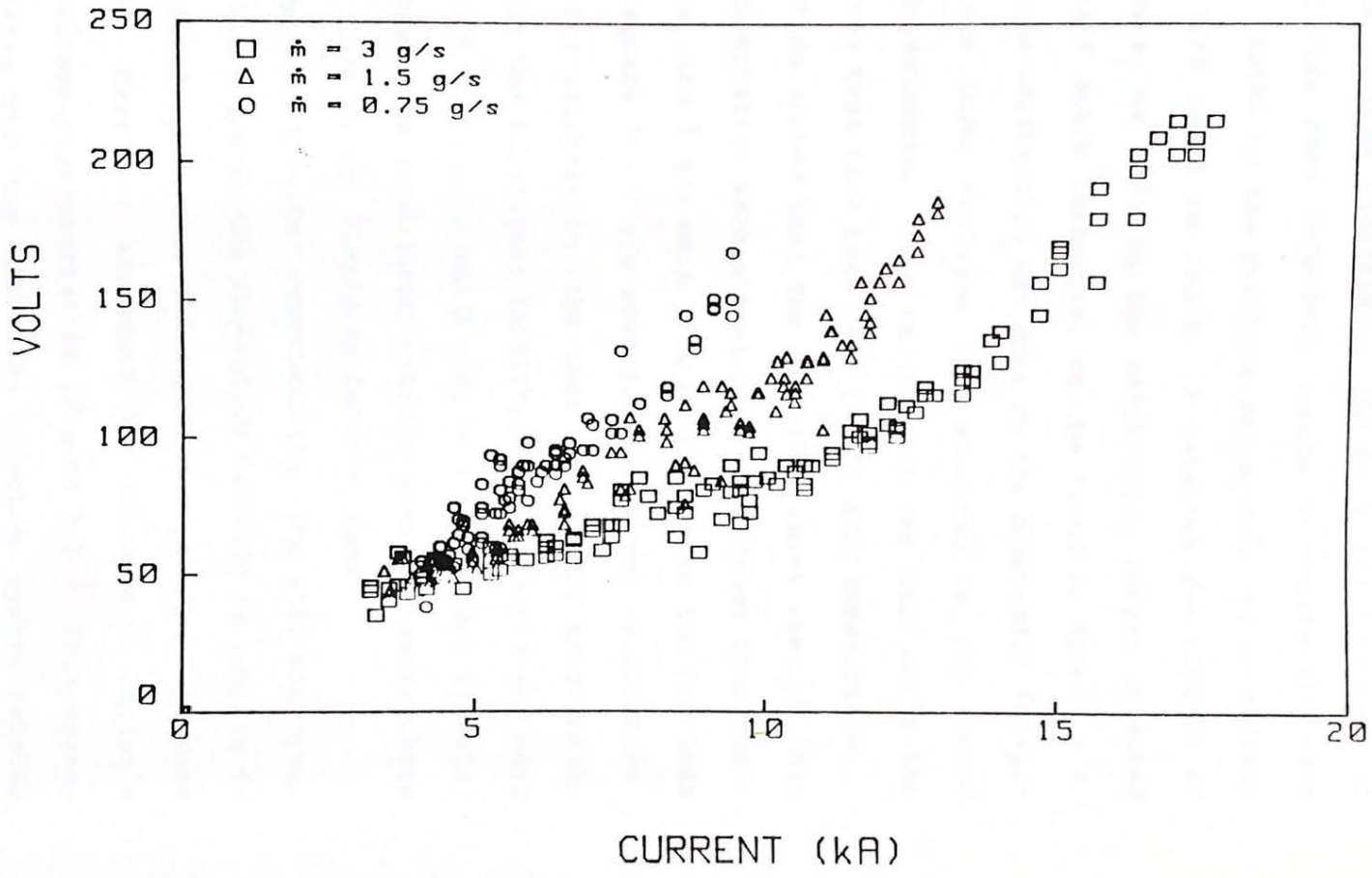

Figure 3.2

ment. This voltage discrepancy led to a recalibration of the choked flow mass injection system to verify the mass flow rates stated by the previous researcher, as no records of calibration could be found. A detailed description of the procedure, as well as the calibration curves obtained for both half scale thrusters, can be found in Appendix A. The mass flow calibration was done in the diagnostic facility after the lower voltages were measured in the second round of experiments. This calibration was done using the same orifices that have been used in all HSBT experiments.

Calibration showed that the mass flow rates used in initial experimentation were actually a third higher than quoted; that is, the 3 g/s mass flow conditions in the previous HSBT work equate to 4 g/s according to recent calibration. Following the calibration, the next set of HSBT experiments were done in the fiberglass facility, using the correct mass flow rates of 0.75, 1.5, and 3 g/s, as well as some repeated tests at the same conditions used by previous researchers and in the most recent Plexiglas facility data.

As a check of thruster repeatability, the HSBT was operated at 2 and 4 g/s in the fiberglass facility to compare to Plexiglas facility voltage characteristics at the same mass flow rates. Excellent agreement was found with Kaplan's original voltage characteristics (Figure 3.3). This agreement indicates that the HSBT mass injection system behaved in a manner consistent with Kaplan's experiments in both

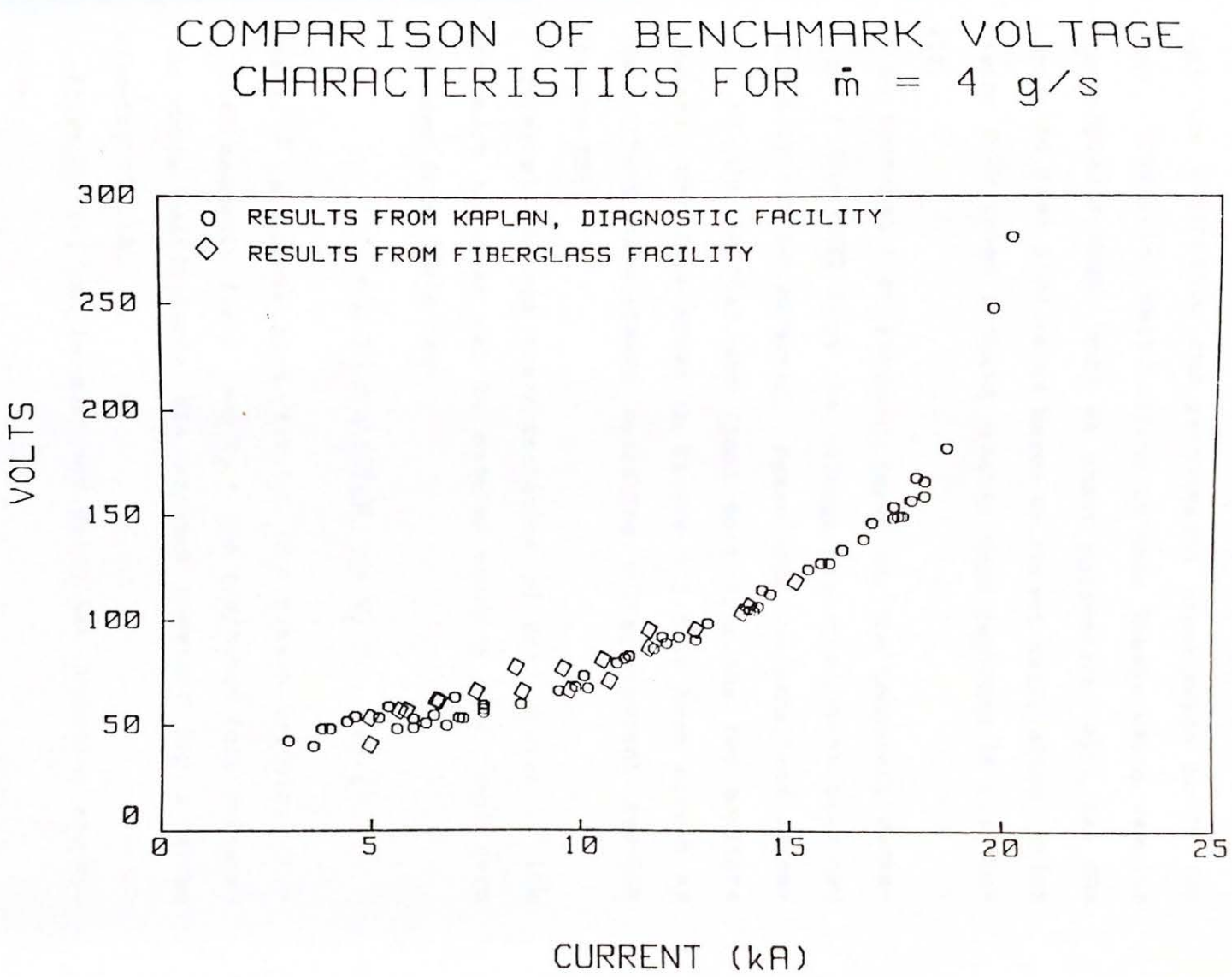
COMPARISON OF BENCHMARK VOLTAGE CHARACTERISTICS FOR ṁ = 4 g/s
RESULTS FROM KAPLAN, DIAGNOSTIC FACILITY
RESULTS FROM FIBERGLASS FACILITY
VOLTS
300
250
200
150
100
50
0
0
5
10
15
20
25
CURRENT (kA)

Figure 3.3

facilities. The mass flow calibration reported here for both the diagnostic and performance experiments holds for both. Therefore, calculations in this thesis using results from Kaplan's work, such as onset parameters, will use the corrected mass flow rates based on recent calibration, which yields flow rates a third greater than reported in his thesis.

No systematic or physical cause for the temporary deviation of the HSBT from the voltage characteristics measured initially can be advanced. Based upon the excellent agreement of the initial and final data from the two separate systems, the data shown in Figure 3.2 have been chosen as the correct quasisteady operating voltage-current results for the HSBT.

Terminal voltage characteristics of both scales of the Benchmark thruster can be modeled using a functional form obtained from Ohm's law:

$$V = \int \frac{\vec{j}}{\sigma} \cdot \delta\vec{l} + \int (\vec{u} \times \vec{B}) \, \delta\vec{l} + V_f \qquad (3\text{-}1)$$

where σ = plasma conductivity, u = plasma velocity, B = induced magnetic field, and V_f = the electrode fall voltage. The above coefficients are assumed constant for a given geometry (11,12).

Equation 3-1 can be analyzed using the following assumptions:

1.) All thrust is electromagnetic in origin ($T=bJ^2$).

2.) The plasma is moving at the equivalent exhaust velocity $U_{eq} = T/m = bJ^2/\dot{m}$

3.) The linear term (the Ohmic term) is calculated assuming axially uniform radial current density, $J/2\pi rL$. With this simplification, the line integral of the field from the anode to the cathode reduces to

$$J/(2\pi L\sigma)\ln(R_a/R_c)$$

This term is scale dependent; however, at the current levels of interest in MPD arcs, the second term dominates (12).

4.) The magnetic field is calculated assuming uniform radial current flow and azimuthal symmetry. Then $B = \mu_0 J(1-z/L)/2\pi r$.

5.) The fall voltage is considered independent of current, and represents the cumulative effects of electrode sheaths and other losses.

Integrating along the radial current paths from anode to cathode, the first term is the ohmic voltage. The second term is the field arising from the motion of the plasma, and is called the "back emf". It is expressed as UXB, where U is the particle velocity and B is the magnetic field. Using the above assumptions for the plasma velocity and magnetic field, and integrating along the interelectrode separation results in U_{eq} multiplied by $\mu_0 J\ln(R_a/R_c)/2\pi$, which produces a term proportional to $b^2J^3/\dot{m}$. These assumptions produce the final expression

$$V = J/(2\pi L\sigma)\ln(R_a/R_c) + kb^2J^3/\dot{m} + V_f \quad (3\text{-}2)$$

where k is a constant dependent upon current and velocity distributions within the thruster.

This general functional form was fit to terminal voltage data of both scales and thruster configurations in order to determine its applicability. Statistical regression of voltage data to this function yielded coefficients which represent the measured voltage characteristics of the thruster (Figure 3.4), The cubic coefficient obtained from the regression, 0.08 V/kA for J in kA, is within a factor of two of the square of the electromagnetic thrust coefficient calculated from HSBT thrust measurements ($2b^2 = 0.08$). Ohmic coefficients and fall voltages are in agreement with values previously observed in this laboratory (11).

HSBT voltage shows the same functional dependence upon current as the FSBT, as shown by equations 3-3, curve fit for J in kA and mass flow in grams per second (g/s):

$$V = 1.26*J + 0.082*J^3/\dot{m} + 48.2 \quad \text{(Half Scale)}$$

$$V = 1.65*J + 0.064*J^3/\dot{m} + 24.5 \quad \text{(Full Scale)} \qquad (3\text{-}3)$$

Equations 3-3 were obtained from non-linear curve fits of HSBT data for propellant flow rates of 0.75, 1.5, and 3 g/s, which are equal in terms of mass flux to full scale mass flow rates of 3, 6, and 12 g/s, to FSBT mass flow rates of 3 and 6 g/s. Terminal voltages of both scales for these mass flow rates are shown in Figure 3.5. Note that the case of

COMPARISON OF HSBT VOLTAGE CHARACTERISTICS TO CURVE FIT RESULTS

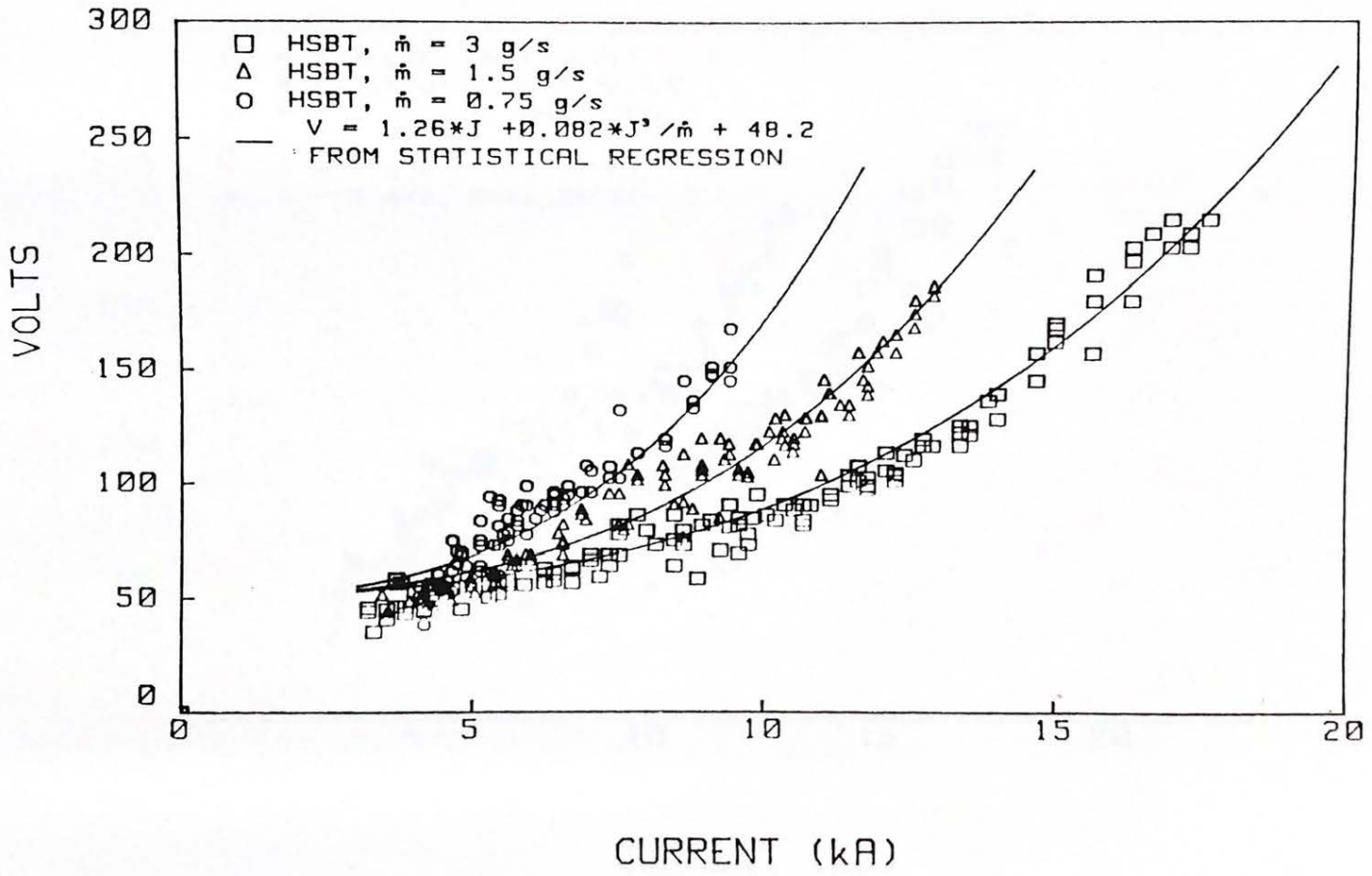

Figure 3.4

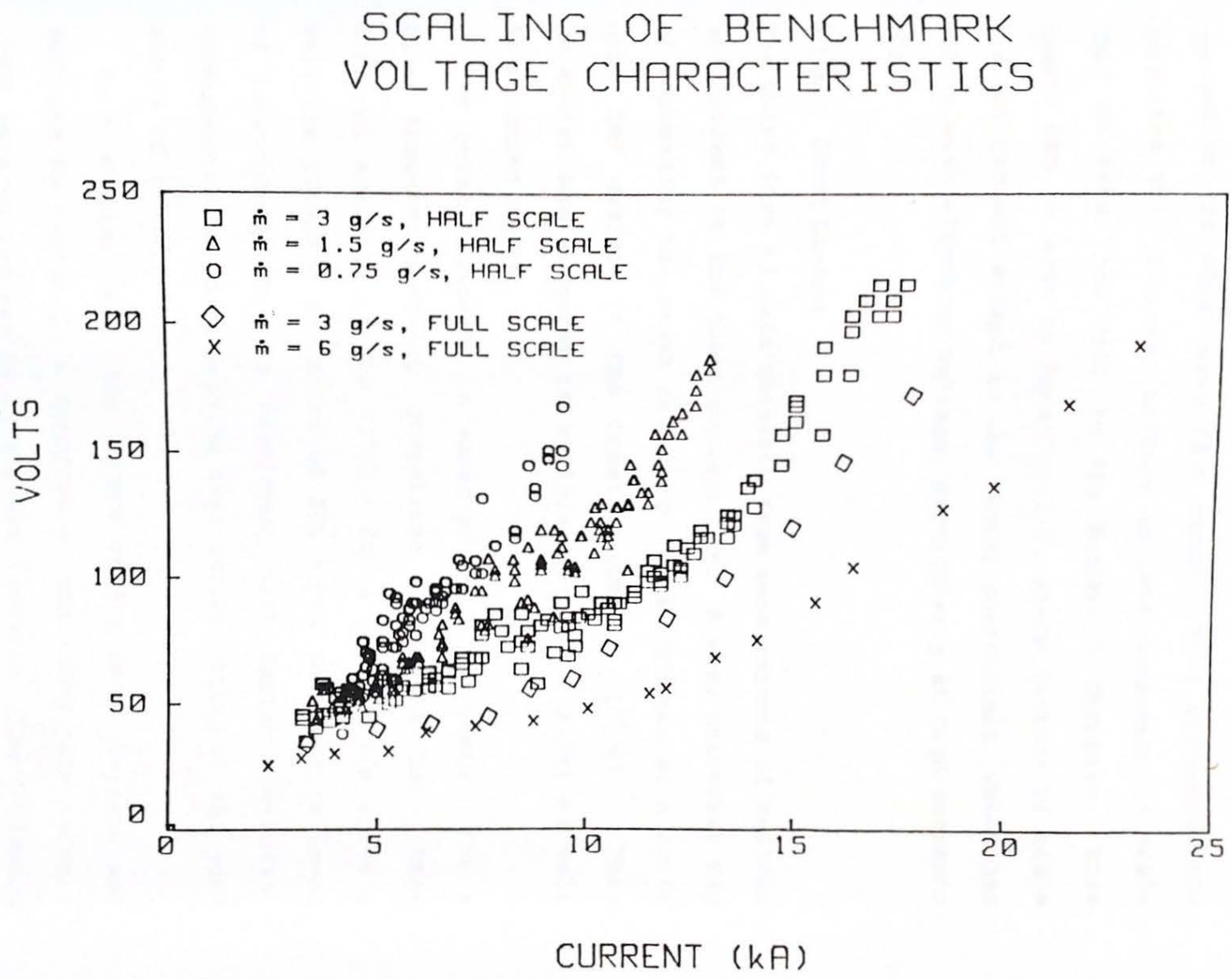
SCALING OF BENCHMARK
VOLTAGE CHARACTERISTICS
□ ṁ = 3 g/s, HALF SCALE
△ ṁ = 1.5 g/s, HALF SCALE
○ ṁ = 0.75 g/s, HALF SCALE
◇ ṁ = 3 g/s, FULL SCALE
× ṁ = 6 g/s, FULL SCALE
VOLTS
250
200
150
100
50
0
0
5
10
15
20
25
CURRENT (kA)

Figure 3.5

equal mass flow rate shows close agreement across scales, as opposed to the equal mass flux cases. This correspondence indicates that thruster voltage is less dependent on scale than on mass flow rate in the Benchmark Thruster. This result can be seen in Equation 3-2, where factors of scale are not present except in the linear coefficient, which has only a weak effect on voltage, particularly at high currents (12).

3.1.3 Onset Current

The third form of data obtained from measurements of voltage and current is the onset current, J*. A more universal way of expressing the onset condition for a thruster of a given size and design is the onset parameter, $(J^2/\dot{m})^*$. This parameter has appeared in various theories (13,14) as well as in experiments. (15)

The onset parameter is expected to be a constant for a given thruster geometry, propellant, and scale (14). Statistical analysis of the $(J^2/\dot{m})^*$ for a given scale shows a relative standard deviation of 20% about the mean; a level of uncertainty that is consistent with Kaplan's results. Consequently the data provide weak corroboration of the constancy of $(J^2/\dot{m})^*$.

In a similar vein, the square of the onset current was analyzed by Kaplan as a function of mass flow rate using a least squares regression to a power function. The following relations (from Kaplan's data corrected for the calibrated mass flow rates) were obtained:

$$\text{Half Scale} \quad (J^*)^2 = 82.8 * \dot{m}^{0.95}$$

$$\text{Full Scale} \quad (J^*)^2 = 136 * \dot{m}^{0.72}$$

A regression of the form $(J^*)^2 = k\dot{m}$, as predicted by theory, produced the following relations for the same onset data.

$$\text{Half Scale} \quad (J^*)^2 = 76.1 * \dot{m}$$

$$\text{Full Scale} \quad (J^*)^2 = 65.8 * \dot{m}$$

Comparisons of the two fits at Full Scale and Half Scale are shown in Figures 3.6 and 3.7. Note that either curve follows the data within the error bars; statistically, neither fit can be said to be superior to the other.

Onset current data were taken at 2 and 4 g/s argon flow rates in the Plexiglas tank with the HSBT, and at 0.75, 1.5, and 3 g/s in the fiberglass facility. The 2 and 4 g/s onset currents were found to agree well with previous results. Onset data obtained in the fiberglass facility require some interpretation before a comparison can be made to other data, and are discussed in the following paragraphs.

Qualitatively, two types of voltage oscillations are present in the HSBT data from the fiberglass performance facility (Figure 3.8). High frequency hash at 10 % of the mean amplitude appears at much lower currents than measured in the Plexiglas facility. The relative amplitude of these oscillations is near 10% for all higher currents, causing a wide spread in values for the onset current. At current levels closer to the onset levels measured in the Plexiglas

HALF SCALE BENCHMARK THRUSTER
ONSET ANALYSIS

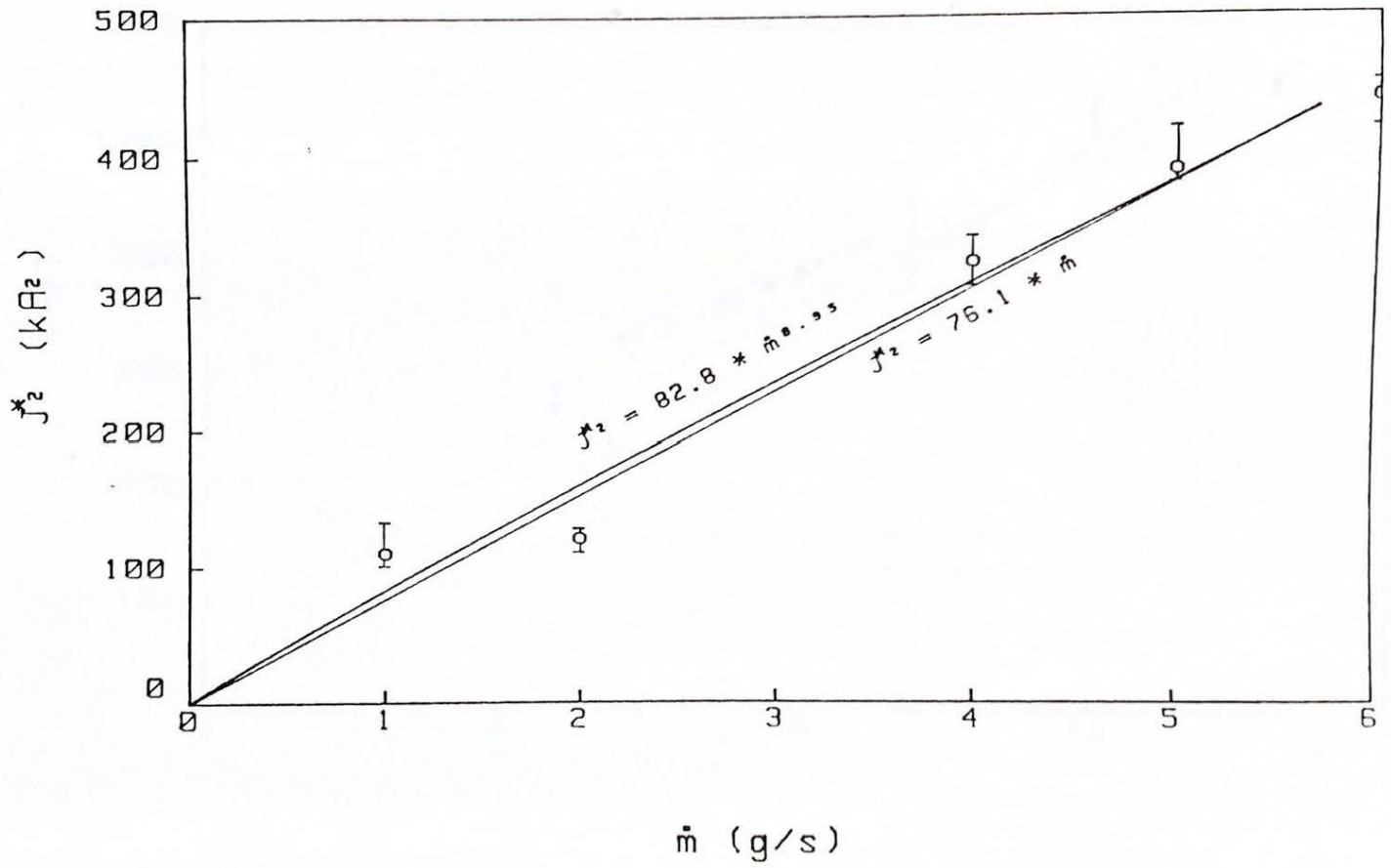

Figure 3.6

FULL SCALE BENCHMARK THRUSTER
ONSET ANALYSIS

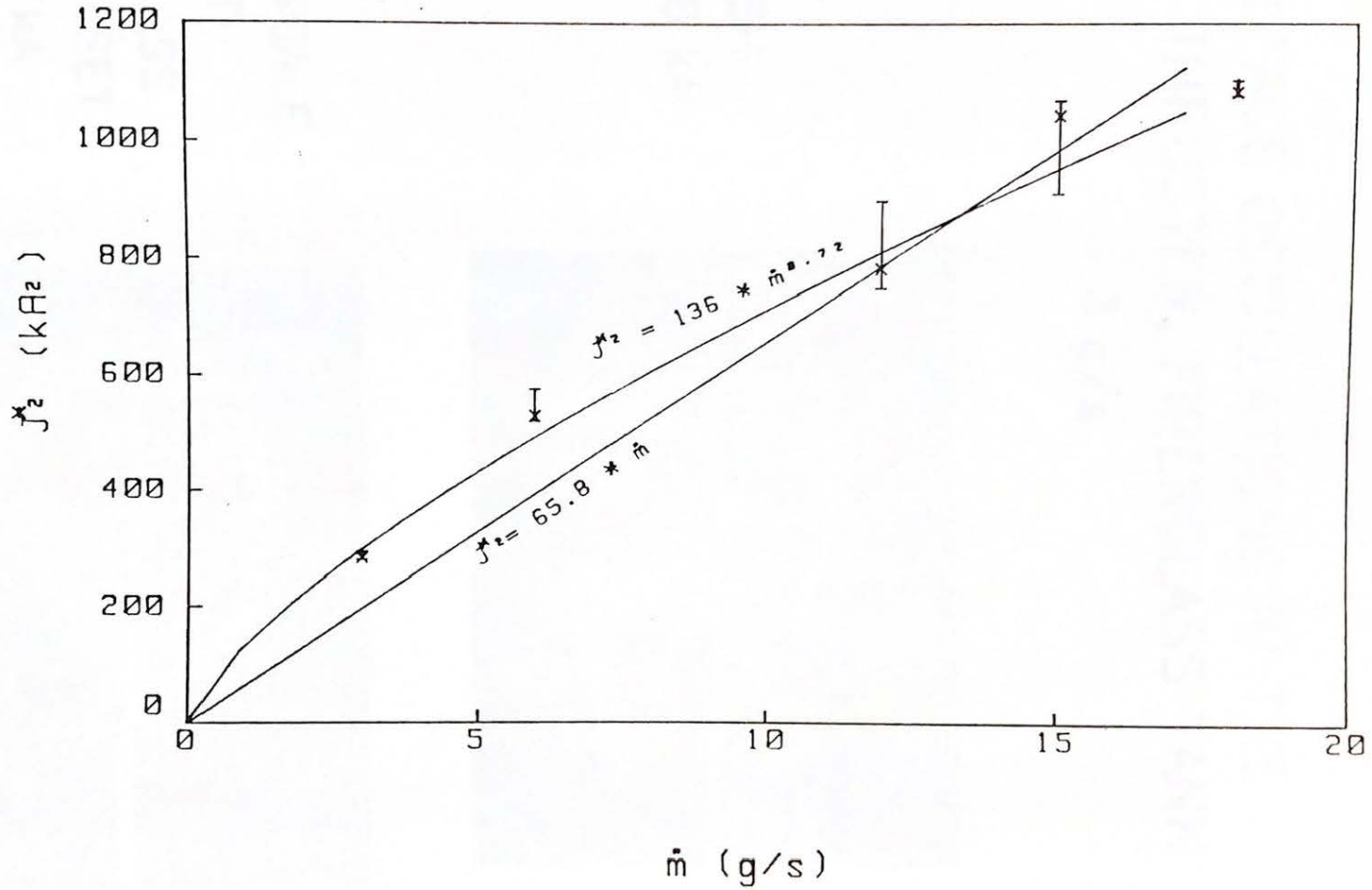

Figure 3.7

VOLTAGE OSCILLATIONS IN THE HSBT THRUSTER, FIBERGLASS TANK

3 g/s

10% HASH
J = 11.8 kA

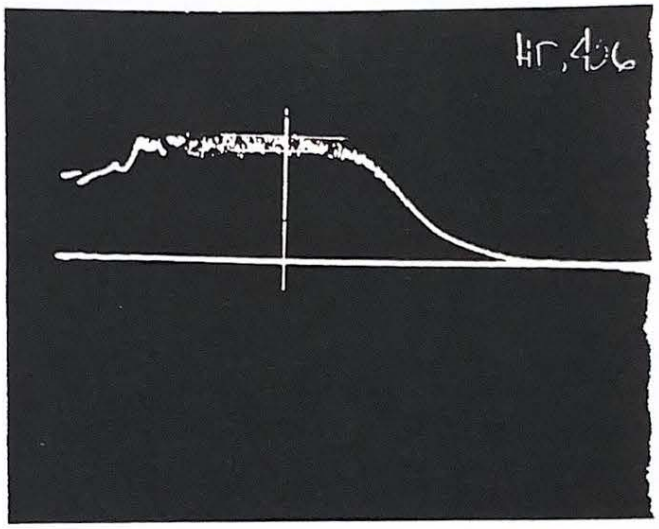

LARGE SCALE
HASH AT
PLEXIGLASS
TANK ONSET
J=17.6 kA

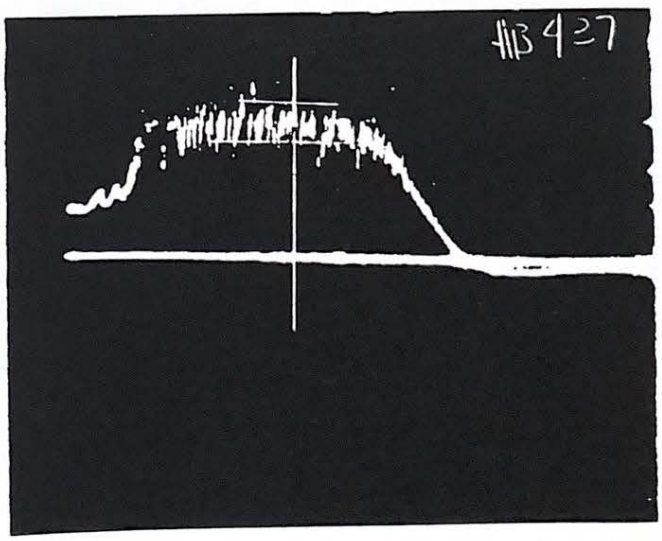

Figure 3.8

facility much higher amplitude, lower frequency oscillations appear suddenly and are present at all currents greater than the onset level. Comparisons using this threshhold as the value for onset leads to agreement with earlier values.

A similar statistical analysis of this second set of onset data was also performed. The onset parameter showed a relative standard deviation of 13% about an average of 88.9 kA^2-s/g for this data; experimental variation was 10%. Linear and power curve fits were applied to these data. The linear curve fit of the large amplitude onset data produced behavior somewhat similar to that seen before:

$$(J^*)^2=48.4*\dot{m} \qquad \text{10\% hash}$$

$$(J^*)^2=81.8*\dot{m} \qquad \text{large amplitude hash}$$

The power curve fits are also similar to those seen before:

$$(J^*)^2=69.5\dot{m}^{0.66} \qquad \text{10\% hash}$$

$$(J^*)^2=97.6\dot{m}^{0.78} \qquad \text{large amplitude hash}$$

The large amplitude onset curves, which show the closest agreement with previous measurements, are plotted in Figure 3.9.

To summarize the onset findings, the half-scale benchmark thruster has been found to show consistent onset behavior in all experiments, if the large-scale oscillations described above are considered to be the onset condition in the case of the fiberglass facility experiments. Statistical analy-

HALF SCALE BENCHMARK THRUSTER
ANALYSIS OF RECENT ONSET DATA

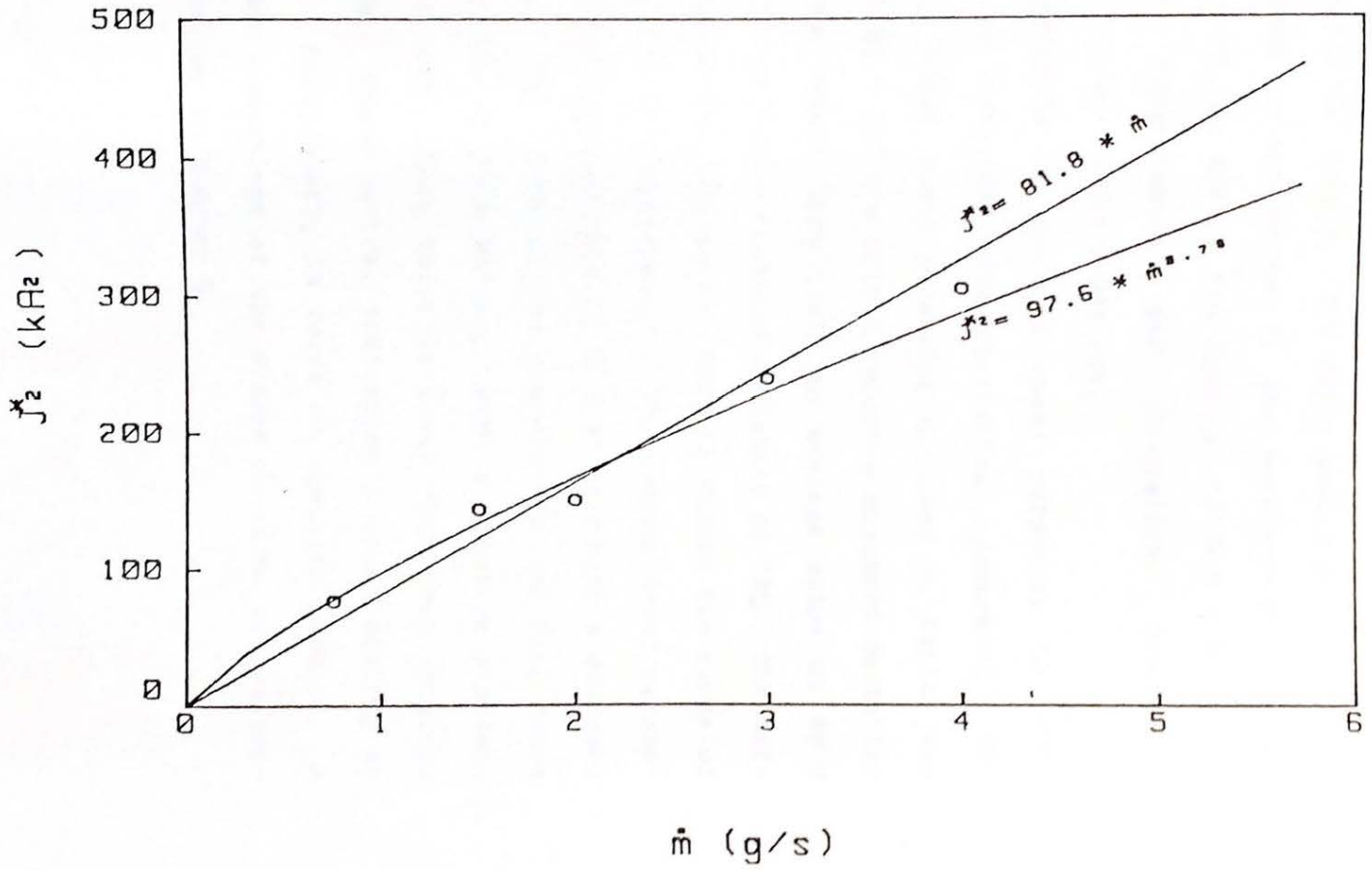

Figure 3.9

sis of onset current as a function of mass flow shows similar behavior in all trials. The small sample population and the associated uncertainties in the measurement of onset current warrent the use of the familiar $(J^2/\dot{m})^* = \text{constant}$, which has experimental and theoretical precedents (13,14,15), rather than a power law.

The experimentally measured onset parameter for both scales can be compared using statistical regression. The average half scale onset parameter obtained by Kaplan was found to be 80.6 kA^2-s/g with a relative standard deviation of 23%. The latest data yield an average value of 88.9 kA^2-s/g with a relative standard deviation of 13%. The difference between the two values, 10%, is within the range of uncertainty for this measurement. The average onset parameter for all half-scaled data is 84.8 kA^2-s/g with a standard deviation of 18%. This can be compared to the full scale onset parameter of 75.4 kA^2-s/g, with a relative standard deviation of 20%. This value is lower than that obtained with the half scale device, indicating a lower ceiling on performance, particularly in terms of specific impulse. A more complete comparison of the scales in terms of performance will follow in Chapter 5.

3.1.4 Thrust-Current Characteristics

previously, Full Scale Benchmark Thruster (FSBT) thrust data have been obtained by two means: 1.) calculated electromagnetic thrust from magnetic field maps (7); 2.) direct impulsive thrust measurements (10). Comparison of these two methods showed that thrust measured at high currents approximated values inferred from magnetic field measurements.

The electromagnetic thrust coefficient obtained from B-probing was found by Kaplan to depend weakly on $J^2/\dot{m}$ (7). This behavior was identical for both scales of the benchmark. A linear best fit regression of the B-probe thrust calculations for both scales was fitted to the relation:

$$b = \mu_0/4\pi \ * \ln(5.63+0.011*J^2/\dot{m}) \quad (3\text{-}4)$$

over the range of $J^2/\dot{m}$ from 25 to 100 kA^2-s/g (7). Note that the expresson in parentheses above is the effective anode to cathode radius ratio in the theoretical formulation of the electromagnetic thrust equation. With a minimum value of 5.63, this expression is greater than the actual electrode radius ratio of 5.26. Consequently, the B-field measurements indicate performance superior to the strictly geometric predictions.

Equation 3-2 gives b values that range from 0.17 to 0.19 N/kA^2 for currents below onset; the corresponding geometric b value is 0.166 N/kA^2. To determine actual thruster performance, the thrust measurements of the FSBT can be analyzed for their quadratic behavior. A quadratic regression

of full scale thrust as a function of current produces an overall electromagnetic thrust coefficient of b=0.195 N/kA^2, equivalent to the highest value determined from magnetic field probing. The additional thrust measured in the FSBT was accounted for as the electrothermal thrust contribution (10).

HSBT thrust performance was found to be equal to that of the Full Scale Thruster (Figure 3.10). Thrust measurements of the HSBT have also been analyzed to examine the behavior of thrust with respect to current. The extensive thrust measurements taken at mass flow rates of 0.75, 1.5, and 3 g/s were analyzed for repeatabilty and for dependence on current and mass flow. Ideally, electromagnetic thrust should only depend on the square of the current. Although this has been found to be approximately true, some differences in performance with flow rate were also seen. These differences will be discussed later in this section.

Thruster operation is very repeatable, with the chief variation in thrust data being associated with the cold flow thrust measurements for each mass flow rate. These data were taken at the start of an experiment with each flow rate. The behavior of cold thrust measurements was consistent from flow rate to flow rate; that is, the ratios of cold thrust at different mass flows were equal to the ratios of the mass flows themselves. Repeatability of cold flow thrust data in a given experiment was within 5%. However,

SCALING OF BENCHMARK THRUST CHARACTERISTICS

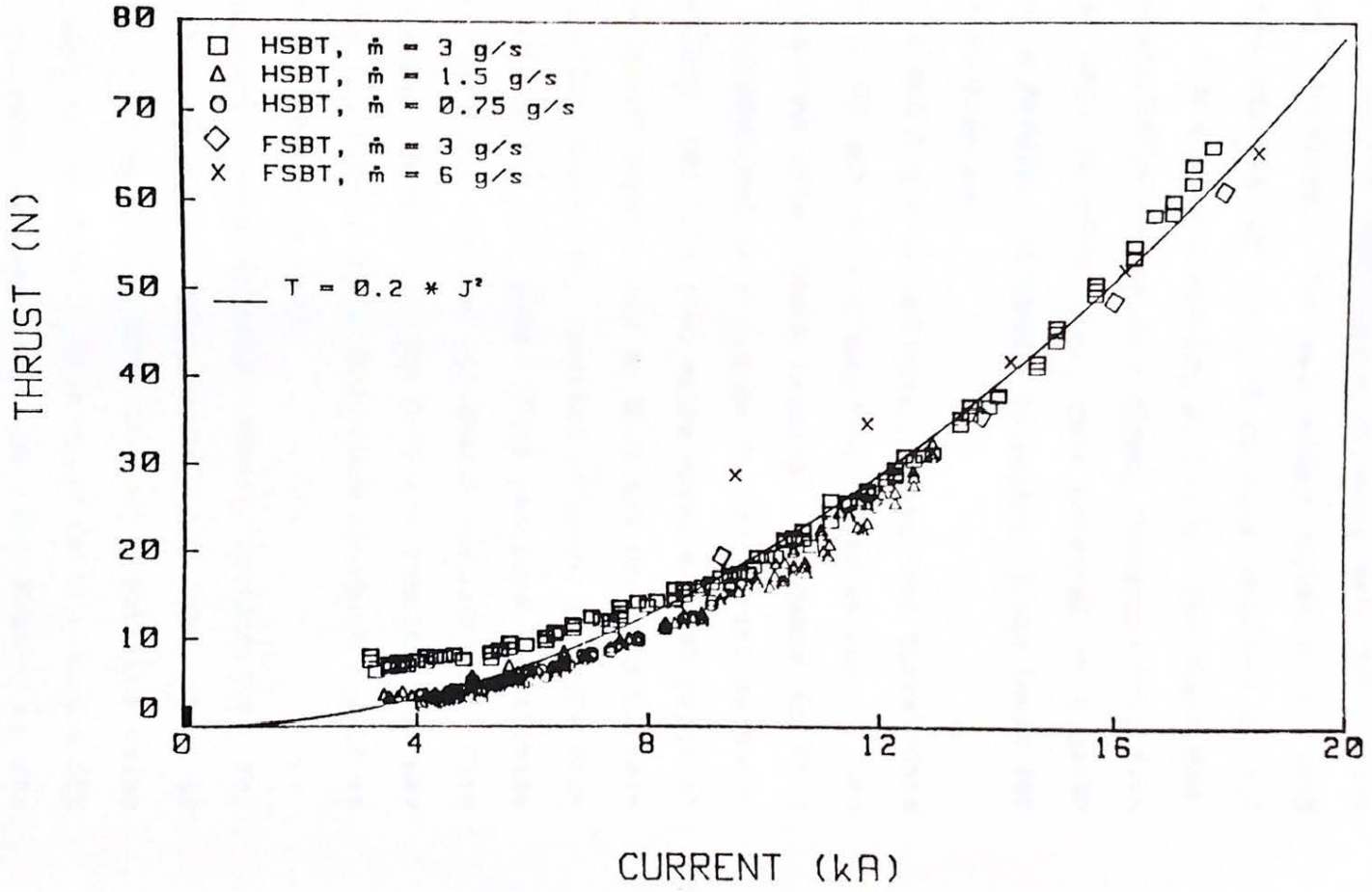

Figure 3.10

comparison of various experiments at equal mass flow rates shows a 10% variation. The day-to-day variation in cold flow produced offsets of +/- 1 N in data obtained at 1.5 g/s, and +/- 3 N during operation at 3 g/s. The small magnitude of these offsets permits a fixed, reference cold flow value to be used to correct all data obtained at a given mass flow as a result. Agreement to within 5% was found for each mass flow data set.

Unlike 1.5 and 3 g/s thrust measurements, hot thrust data obtained at 0.75 g/s showed day-to-day variations of the same magnitude as cold thrust results. A change in cold flow data corresponded to a change in hot thrust measurements; therefore, the cold flow value measured just prior to thrust measurement experiments at 0.75 g/s was used to calculate thrust for those data, instead of using a single value of cold thrust for all data. This was done to minimize the scatter in data due to systematic variations. This behavior is characteristic of the 0.75 g/s results, and may be due to the relatively small displacements which result at low current and mass flow rate.

The resulting electromagnetic thrust coefficients for 0.75, 1.5, and 3.0 g/s are shown in Table 3. The values of b range from 0.16 to 0.20 N/kA^2; the value obtained using all thrust data is .19 N/kA^2. This value falls within a 95% confidence interval between .188 and .193 N/kA^2; as the table shows, variation of the individual mass flow rates is

outside of this region. It is interesting that the electromagnetic thrust coefficient scales with mass flow rate; this may actually be an indication of superior thrust performance at higher mass flow rates. In other words, the electromagnetic thrust coefficient may reach its maximum at flow rates greater than 3 g/s. This suspicion is supported by the relatively high electromagnetic thrust coefficient seen at 3 g/s and above in the HSBT and FSBT. The improvement in performance cannot be related to the parameter $J^2/\dot{m}$, since the thruster covers the same range for all mass flows and scales.

Table 3: Experimental Thrust Coefficients

$\dot{m}$(g/s)	b (N/kA^2)	95% interval
0.75	0.164	0.161 - 0.166
1.5	0.173	0.169 - 0.174
3	0.200	0.197 - 0.202
All	0.190	0.188 - 0.193

In comparison, the HSBT operates in a manner quite similar to the FSBT, particularly at equivalent current levels and mass flow rates. The electromagnetic thrust coefficients of both scales come within 3% of each other at 3 g/s operation, indicating that the same thrust process is occurring within the thrusters for identical mass flow rates. As was seen in the voltage-current characteristics, equal mass flow rates are important to maintain invariance between thruster scales.

Extensive thrust measurements of the HSBT also allow a comparison of measured thrust behavior to that seen in B-probe results. The quantity T/J^2 can be used to represent an "effective" electromagnetic thrust constant based upon thrust measurements (Figure 3.11). At values of $J^2/\dot{m}$ greater than 50 kA^2-s/g, this variable is approximately constant for both the HSBT and FSBT. The constant can be transformed into an effective R_a/R_c ratio, which can then be curve fit as a function of $J^2/\dot{m}$ to compare to the relation obtained by B-probing.

Taken as a whole, the thrust data, curve fit for values of $J^2/\dot{m}$ greater than 40 kA^2-s/g, does not form any definitive pattern. Generally, the effective R_a/R_c increases with $J^2/\dot{m}$ for all mass flow rates, but the trend is obscured by the scattered data. In order to compare to probe results, linear fits were made for each of the mass flow rate thrust data sets. The intercepts and slopes obtained for each of these sets are listed in Table 4.

Table 4: Linear Curve Fits of HSBT R_a/R_c

$\dot{m}$	intercept	slope
0.75	3.94	0.014
1.5	3.42	0.023
3	5.48	0.025
All	5.49	0.0085

SCALING OF BENCHMARK THRUST BEHAVIOR

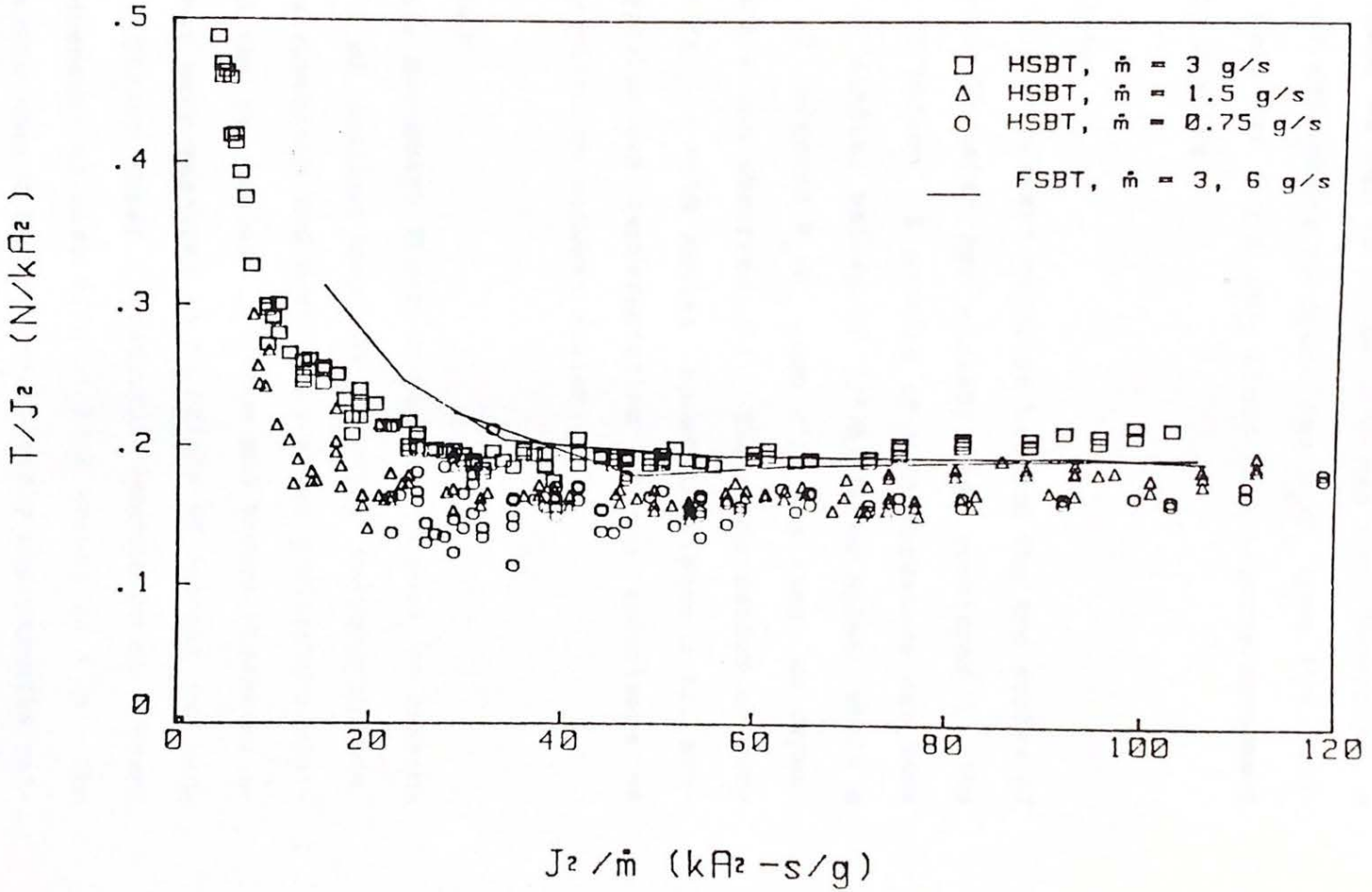

Figure 3.11

Comparing these values to those obtained from B-probing, a similar order dependence is found for R_a/R_c upon $J^2/\dot{m}$; however, only data for 3 g/s show close quantitative agreement with B-probe results.

3.2 B-probing

The similarity in current contours between the two scales of the Benchmark Thruster has already been mentioned in the discussion of thrust. B-probing of both thrusters was done by Kaplan at similar values of $(J^2/\dot{m})$ below onset; while a dependence of inferred R_a/R_c upon $J^2/\dot{m}$ was seen, no dependence on scale was observed (7). The distribution of current contours for both scales, shown in Figure 3.12, provides a qualitative representation of the invariance of current distribution between scales.

3.3 Summary

A Half Scale Benchmark Thruster has been tested to examine the effects of scaling upon MPD behavior and performance. Current distributions had previously shown qualitative similarities in the two scales. Voltage and thrust characteristics have now been measured as functions of current and mass flow rate. Thrust shows a quadratic dependence on current and is independent of mass flow at high values of $J^2/\dot{m}$. The electromagnetic thrust coefficient closely approximates calculations based upon current distributions in either thrus-

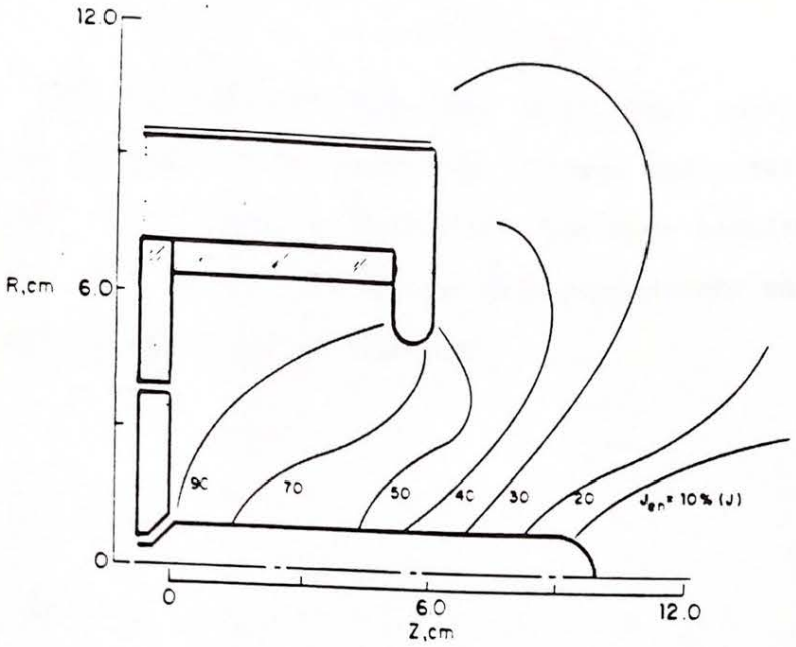

QUASI-STEADY ENCLOSED CURRENT CONTOURS: FULL-SCALE THRUSTER

$\dot{m}$ = 6 gm/sec J = 23.5 kA

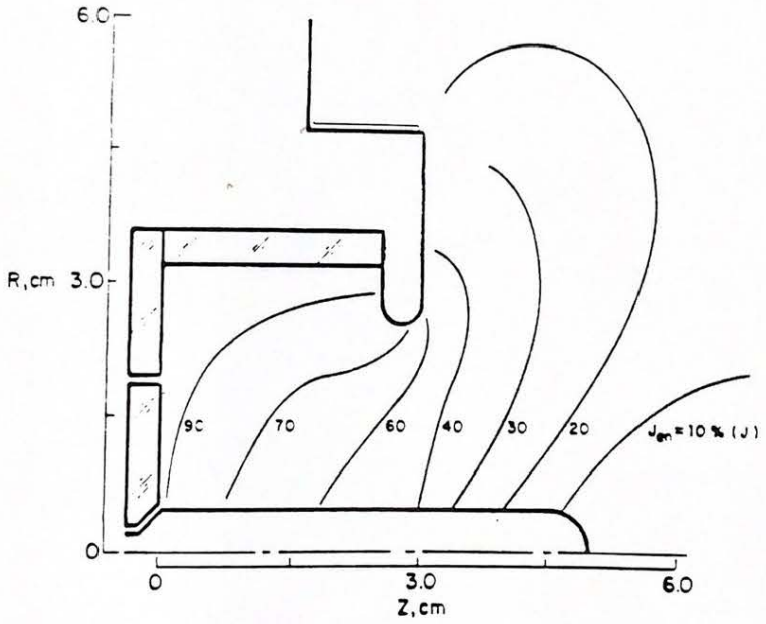

QUASI-STEADY ENCLOSED CURRENT CONTOURS: HALF-SCALE THRUSTER

$\dot{m}$ = 1.5 gm/sec J = 12.4 kA

Figure 3.12

ter size. Voltage exhibits the same functional form in either scale; at equal flow rates, the voltage characteristics of either scale have approximately the same magnitude and behavior. This similarity agrees with predictions based on simple MHD analysis of MPD behavior.

Chapter IV

SCALING OF THE FLARED ANODE THRUSTER

The flared anode design has been advanced as a means by which electromagnetic and electrothermal thrust and therefore thrust efficiency could be improved. The original design using 50/50 mass injection and tested at 6 g/s Argon (8), was characterized with respect to terminal behavior and magnetic field profiles. Electromagnetic thrust and thrust efficiency calculated from the current distributions obtained from B-field probing were interpreted in terms of an inferred electromagnetic thrust constant

$$b=0.15\ N/kA^2 \qquad (4\text{-}1)$$

These results predicted that the flared thruster was more efficient than a straight channel of equal length and exit diameter (16).

The Full Scale Flared Anode Thruster (FSFAT) was also used with 0/100 all- outer mass injection of Argon at 3 and 6 g/s in prior experiments (17). These tests were performed in an attempt to maximize the onset current for a given geometry and mass flow rate. In this case, the onset current at 6 g/s was increased from 21 kA to 41.4 kA. Terminal characteristics, current mappings, and thrust measurements

were obtained for this second flared anode configuration (5).

The primary result of performance measurement of the flared anode thruster came from the comparison of theoretical electromagnetic thrust calculated from magnetic field probing to impulsive thrust measurement. Current distributions predicted electromagnetic thrust performance in close agreement with previous B-probe findings. Actual thrust measurements, however, produced thrust levels 20% lower than inferred values (5). Viscous drag losses within the chamber are thought to be responsible for this inferior performance.

The Half Scale Flared Anode has been characterized by terminal measurements, current mapping, and thrust measurements for this experiment. This design uses 50/50 mass injection, with the outer injection holes located at a radius of 1.5 cm, close to the anode wall. The anode length is equal to the cathode length (10.0 cm), which is a departure from the extended anode used in the full scale device. The anode is constructed of copper, the cathode is thoriated tungsten, and the backplate is made of boron nitride, as in the full scale.

4.1 Terminal Characteristics

Three characteristics of thruster behavior of particular interest can be obtained from measurements of current and electrode voltage: voltage waveform, V-J dependence and onset levels.

4.1.1 Voltage Waveforms

The temporal behavior of the quasisteady current and voltage as a function of propellant flow rate and current provides insight into the behavior of MPD devices with respect to power conditioning requirements. Generally, the quasisteady current and voltage appear as rectangular millisecond pulses (cf. Chapter III). In the benchmark design thruster, these waveforms remain constant throughout the range of current values, with the only change occurring at and above the onset current, where high frequency oscillations appear in the voltage trace.

The 1/2 scale flared anode thruster exhibits a very different behavior over the range of currents up to onset. The low current voltage signal is rectangular like the benchmark thruster. At higher currents, the voltage trace deviates from a flat plateau. Instead, at the initiation of the millisecond pulse, a high voltage peak or hump forms, from which the voltage relaxes to a more quasisteady value (Figure 4.1). As onset is approached, high frequency oscillations appear first at the high voltage level. The hash extends progressively further into the pulse as current levels increase. This behavior occurs at all mass flow rates tested in the HSFAT. Reference to full scale data taken with 50/50, 3 g/s Argon show similar transients in the breakdown; these transients are not seen in the 0/100 voltage traces taken afterwards.

HALF SCALE FLARED ANODE

PEAKED VOLTAGE

0.75 g/s, J = 9.6 kA

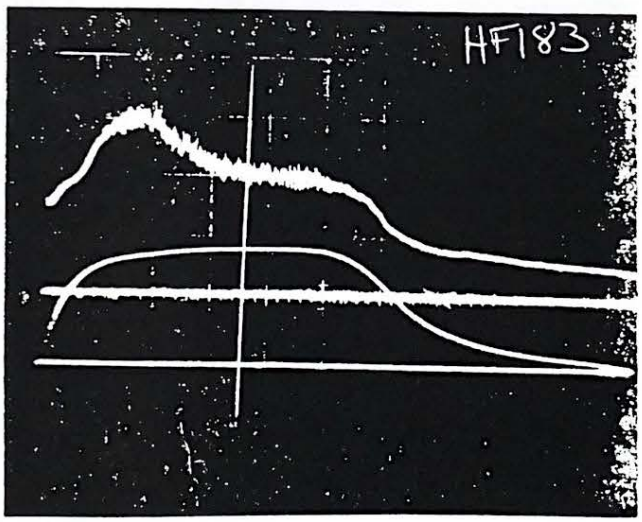

Figure 4.1

4.1.2 Voltage-Current Characteristics

Voltage current characteristics of the HSFAT were measured in both the Plexiglas and fiberglass vacuum facilities. Characteristics for 1.1, 2.2, and 3 g/s were measured in the plexiglas facility; voltages for 0.75, 1.5, and 3 g/s were measured in conjunction with thrust measurements in the fiberglass facility. The V-J curves for 1.1 and 2.2 g/s obtained in the Plexiglas facility displayed linear-cubic behavior of the same form seen in the Benchmark thruster:

$$V=2.05J +0.015J^3/\dot{m} + 30 \quad (4\text{-}1)$$

Characteristics for 0.75 and 1.5 g/s measured in the fiberglass facility displayed different behavior. Voltages at low currents agree with Plexiglas facility results; however, at currents greater than 9-10 kA, voltages for 1.5 and 0.75 g/s drop precipitously (Figure 4.3). This behavior has been observed in the HSFAT in the Plexiglas facility using other propellants such as Xenon and Krypton, but these results are preliminary and their cause remains unresolved (18). Terminal characteristics at 3 g/s in either facility agree well with one another, although their behavior differs from that seen in the low mass flow rates (Figure 4.2).

Full scale voltage also shows the characteristic behavior seen in previous experiments:

$$V = 1.18J + 0.018J^3/\dot{m} +33.1 \quad (4\text{-}2)$$

HALF SCALE FLARED ANODE
VOLTAGE CHARACTERISTICS, DIAGNOSTIC TANK

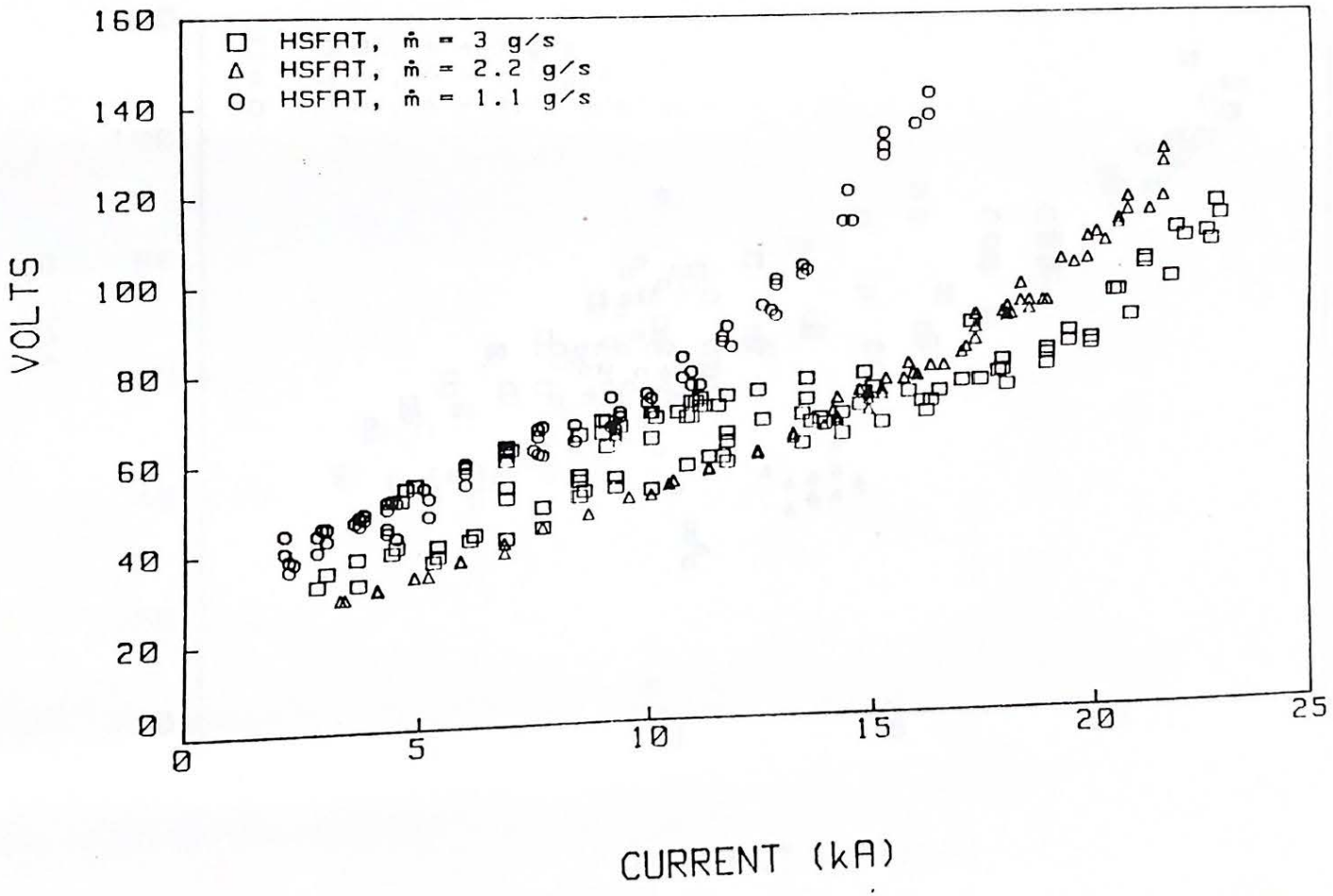

Figure 4.2

HALF SCALE FLARED ANODE
VOLTAGE CHARACTERISTICS, PERFORMANCE TANK

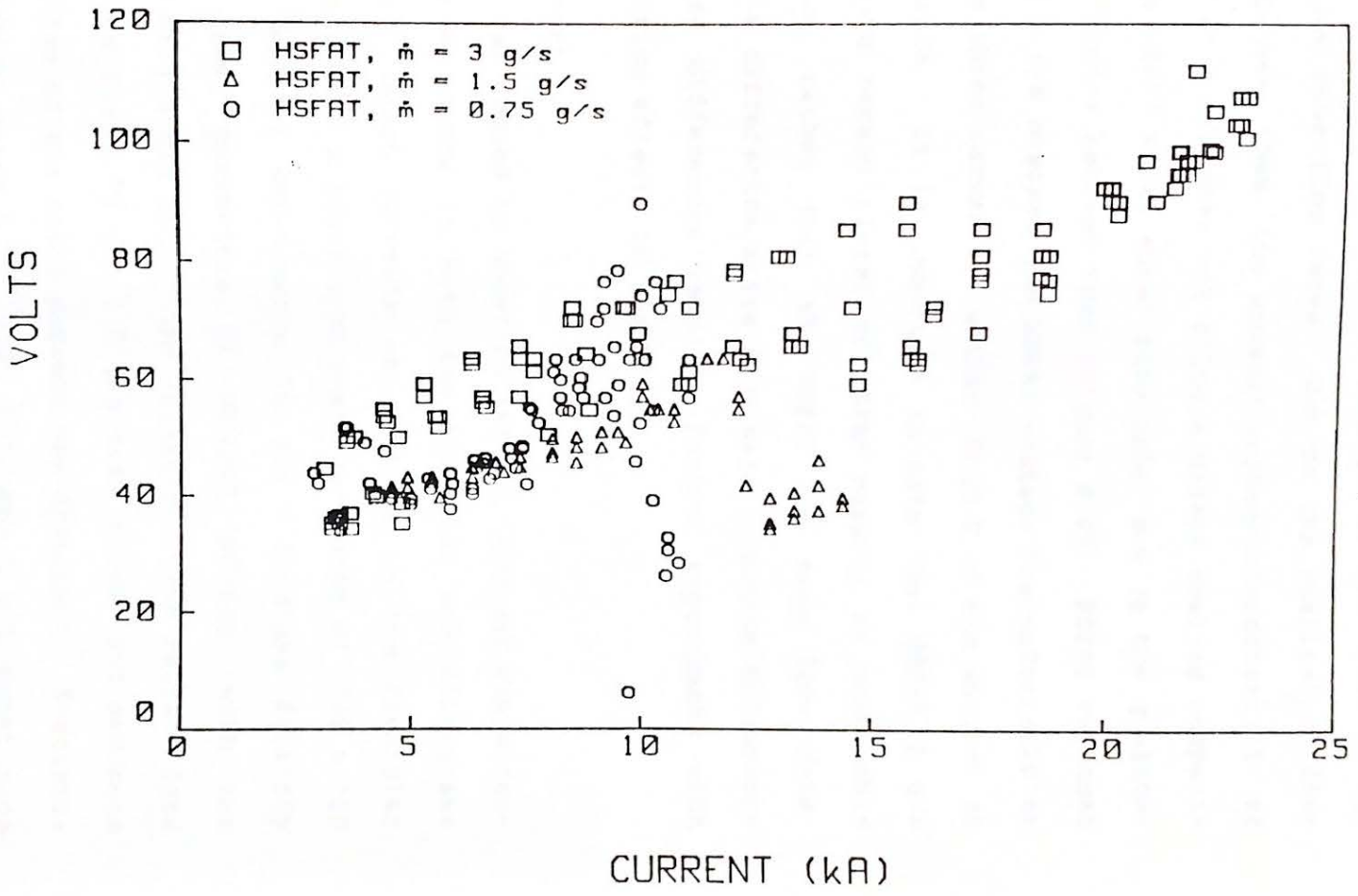

Figure 4.3

Again, the cubic term is quite similar to that seen in the HSFAT at low mass flow rates. Due to the qualitative differences between them, the unusual voltage characteristic of the HSFAT at 3 g/s does not allow a direct scaling comparison to the FSFAT at an equal flow rate, due to the qualitative differences between them (Figure 4.4). FSFAT voltages for 3 and 6 g/s bracket the HSFAT voltage characteristic at 3 g/s; the three curves are within 10-20 V of one another at high currents. It is important to note that HSFAT 3 g/s voltage data remain closer to FSFAT results at comparable flow rates, rather than the HSFAT low mass flow data. Whether the differences arise from mass injection differences or size differences requires further experiments with mass injection effects in the HSFAT.

4.1.3 Onset

The HSFAT was tested to onset during all terminal characteristics measurements in both the Plexiglas and fiberglass facilities. Onset currents as measured in the Plexiglas facility produced a consistent onset parameter of $J^2/\dot{m}$ = 180 kA^2-s/g. Similar experiments in the fiberglass facility produced onset parameters of 180-190 kA^2-s/g, with the exception of 1.5 g/s data. The fiberglass tank voltage data is scattered for 0.75 and 1.5 g/s mass flows, and accurate determination of the onset current was difficult. Statistical regression using 0.75, 1.1, 2.2, and 3 g/s onset data from the Plexiglas facility produced an onset parameter of

SCALING OF FLARED ANODE VOLTAGE CHARACTERISTICS

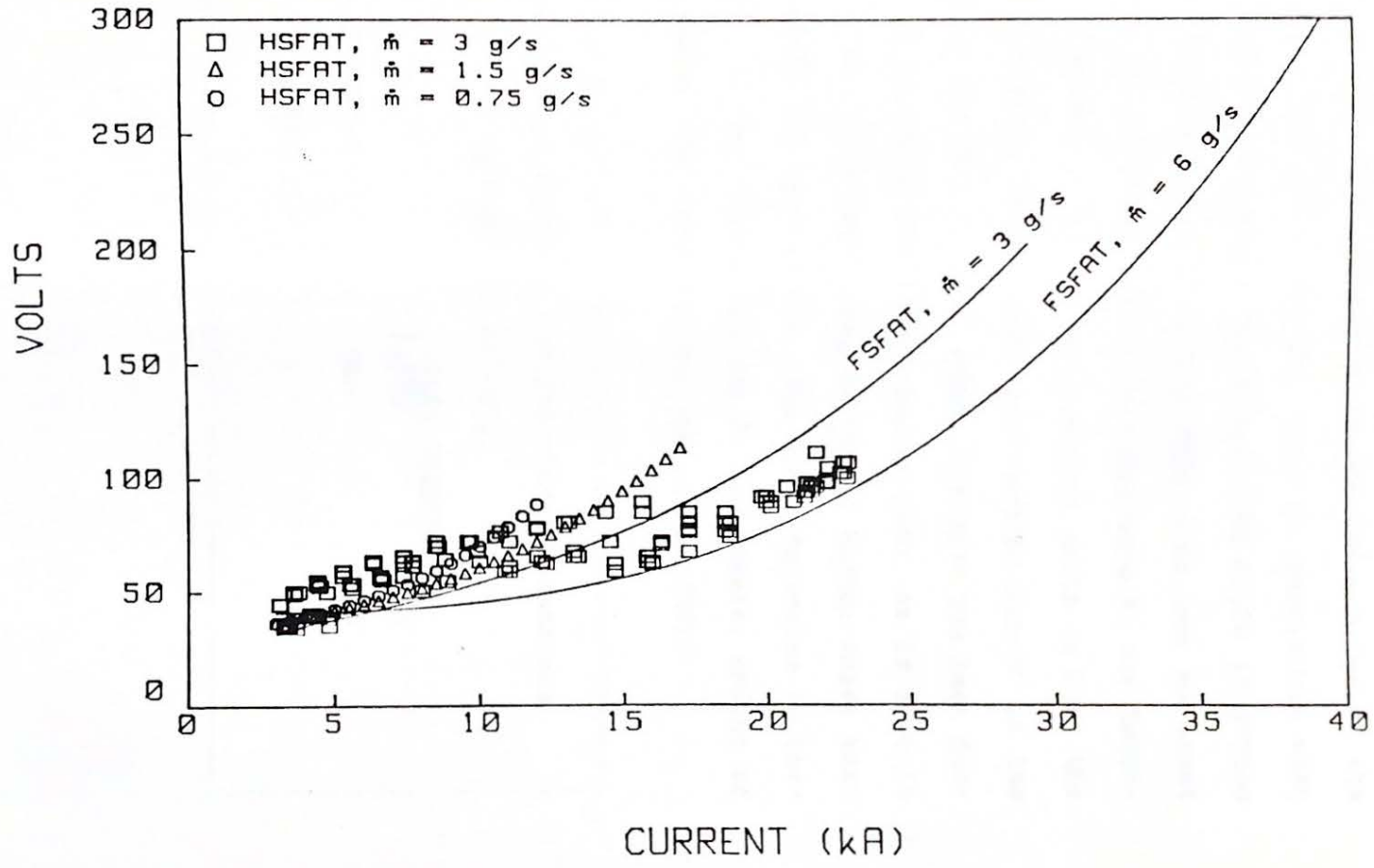

Figure 4.4

187 kA^2-s/g +/-3% standard deviation. The FSFAT with 0/100 flow has a higher onset parameter of 280 kA^2-s/g due to its all-outer mass injection design; this is consistent with experiments using Benchmark Thrusters with 0/100 injection (19). The FSFAT at 50/50, 6 g/s mass flow has an onset parameter of 73.5 kA^2-s/g, which is comparable to the Benchmark onset behavior. The outer injection ports in both the FSFAT 0/100 and the HSFAT 50/50 are located closer to the anode than in the FSFAT 50/50; anode injection has been demonstrated to increase the onset current (19), as is seen in this case. The HSFAT was found to have a higher onset than the FSFAT 50/50 for this reason; the onset parameter is lower than that of the 0/100 case due to the greater amount of mass injected at the anode in the case of the FSFAT.

Table 5: Flared Anode Thruster Onset Parameters

$(J^2/\dot{m})^*$ in kA^2-s/g

		Mass Injection 0/100	50/50
Thruster	FSFAT	280	73.5
	HSFAT	-	187

4.1.4 Thrust-Current Characteristics

Thrust performance of the Flared Anode design has been measured in both full and half scale. Full scale measurements were taken with 0/100 mass injection of 3 and 6 g/s Argon propellant. While thrust shows the predicted quadratic dependence upon current, performance is 20% lower than the value that had previously been derived from current mappings. Viscous losses, as discussed by Wolff (17), can account for some of this discrepancy.

HSFAT thrust was measured over a range of currents for mass flows of 0.75, 1.5, and 3.0 g/s (50/50 mass injection). Thrust data are plotted as a function of current for these mass flow rates in Figure 4.5. These data are shown in comparison to the theoretical curve for electromagnetic thrust using the geometric thrust coefficient, b, obtained from probing ($b=0.15$ N/kA^2). The quadratic curve which best fits the high current thrust values is also shown in the figure ($b=0.120$ N/kA^2). The inferiority of actual HSFAT performance compared to theoretical values is immediately apparent. In fact, the loss in performance is comparable to that seen in the FSFAT. As in the Benchmark thruster, thrust was found to be scale independent at high currents. Some dependence upon mass flow is seen; however, thrust data at equal mass flow rates show close agreement across scale (Figure 4.6).

HALF SCALE FLARED ANODE THRUST CHARACTERISTICS

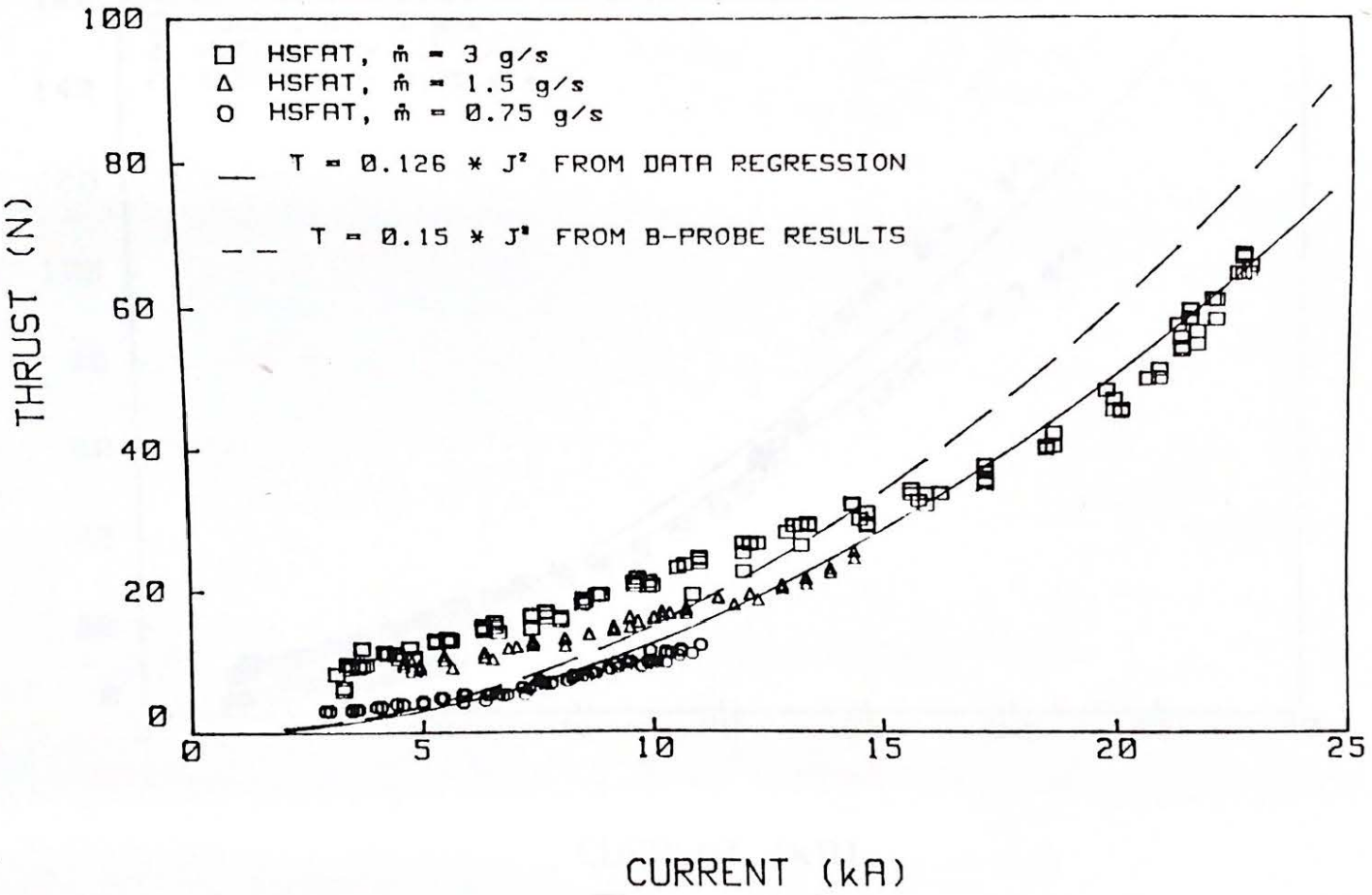

Figure 4.5

SCALING OF FLARED ANODE
THRUST CHARACTERISTICS

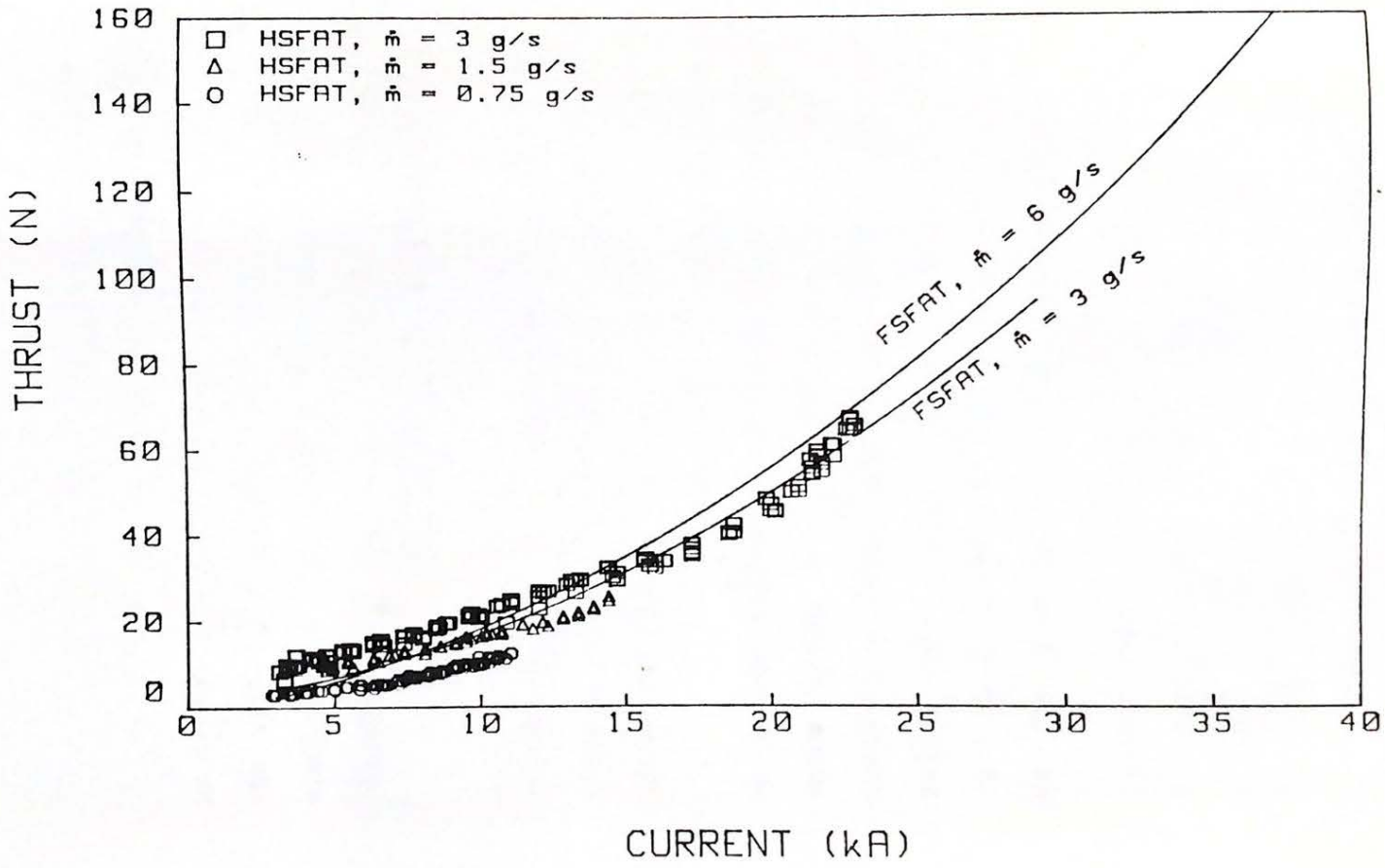

Figure 4.6

Table 6: HSFAT Experimental Thrust Coefficients

m(g/s)	b(N/kA²)	95% conf. int
0.75	0.105	0.103 - 0.107
1.5	0.127	0.120 - 0.133
3.0	0.121	0.120 - 0.123
All	0.120	0.119 - 0.122

The lower electromagnetic thrust coefficient can be interpreted as an effective electrode radius ratio of 1.6, corresponding to the smallest anode radius in the Flared Anode Thruster. The thrust coefficient based on current distributions, as shown above, indicates a larger anode radius of attachment; thus the thrust decrease cannot be explained on an electromagnetic thrust basis.

In his analysis of viscous drag in the Flared Anode Thruster, Wolff developed the following equation for viscous drag losses in a nozzle using a formulation for a conical nozzle arcjet:

$$D = 0.655R(\rho u)^{0.7} u \mu_r L^{0.7} \qquad (4\text{-}4)$$

where D=drag force, R=radius of the anode, ρ = density, u=flow velocity, μ_r =reference viscosity of the propellant=2.5x10E-4 kg/m-s for Argon. By replacing ρu with the known mass flux and u with $T/\dot{m}$, where T is the net thrust of the rocket, equation 4-4 can be expressed as

$$D=0.655R(\dot{m}/\pi R^2)^{0.7}((bJ^2-D)/\dot{m})\mu_r L^{0.7}$$

This can be reduced to

$$D = \frac{0.024\left[\frac{R}{m}\right]\left[\frac{mL}{R^2}\right]^{0.7}}{1 + 0.024\left[\frac{R}{m}\right]\left[\frac{mL}{R^2}\right]^{0.7}} bJ^2 = \frac{A}{1 + A} bJ^2 \qquad (4\text{-}5)$$

and thrust can be expressed as

$$T = \frac{1}{1 + 0.024\left[\frac{R}{m}\right]\left[\frac{mL}{R^2}\right]^{0.7}} bJ^2 = \frac{1}{1 + A} bJ^2 = b'J^2 \qquad (4\text{-}6)$$

In this formulation, drag is a function of scale and mass flow. Some sample calculations demonstrate the effects of scale and mass flow upon the coefficient b', shown in Table 3.

Table 7: Viscous Drag Scaling Calcuations

Scale	$\dot{m}$(g/s)	A/(1+A)	b'=b(1/1+A)(N/kA²)
Full	3	0.128	0.131
	6	0.100	0.134
Half	0.75	0.266	0.110
	1.5	0.128	0.131
	3	0.100	0.134

This analysis indicates that drag is dependent upon scale and mass flow rate. The calculations are invariant for a constant value of the parameter m/R, where R is the diameter of the thrust chamber. This quantity can also be written $U\rho\pi R^2/R$, or $\rho U \pi R$. The Reynolds number of the flow is $\rho UD/\mu$; with an assumption of constant gas viscosity, the parameter $\dot{m}/R$ is proportional to the flow Reynolds number

(20). It has been seen in low Reynolds number nozzle flow that viscous losses increase with decreasing Reynolds number (21); this scaling of losses according to Reynolds number agrees qualitatively with experimental results in the HSFAT, where the smaller device has been operated at values of $\dot{m}/R$ less than or equal to the lowest value of FSFAT operation. Thrust measurements at these lower Reynolds number conditions are inferior to those at the higher levels, even in the electromagnetic thrust regime (Figure 4.5). This behavior is also seen to a lesser extent in the Benchmark thruster, and indicates a need for higher mass flow rates in the Half Scale thrusters.

In contrast to viscous losses seen in the Flared Anodes, an offsetting gain in thrust performance over the predicted electromagnetic acceleration is seen at low currents. This phenomenon is particularly pronounced in the Flared thruster design, and may result from more effective conversion of thermal energy to directed kinetic energy by the nozzle. Thruster design obviously plays an important role in this behavior, since the Benchmark design shows little additional thrust at low currents.

4.2 B-Probing

The flared anode design has been probed under a variety of conditions, which are described in Figure 4.7. The FSFAT has been mapped for 50/50 and 0/100 mass flow; the HSFAT has

SUMMARY OF PROBING CONDITIONS
FLARED ANODE THRUSTER

THRUSTER SCALE	$\dot{m}$ g/s	FLOW SPLIT	J KA	J/J^*	$J^2/\dot{m}$ KA^2-s/g
FULL	6	50/50	20	0.95	66.7
	3	0/100	21.3	0.69	151
HALF	3	50/50	7.9	0.34	20.8
			17.8	0.76	106

Figure 4.7

been mapped for 50/50 flow at two current levels. Generally, the flared design can be divided into three regions of interest: the straight inlet, the flaring section, and the straight exit. The current mappings for both scales will be interpreted in terms of these regions.

Current contours of the FSFAT for both mass injection schemes are displayed in Figure 4.8. The top figure was done at 6 g/s, 50/50 mass flow at 20 kA (near onset); only the electrode surfaces were probed. Straight dashed lines link points of equal enclosed current value at each electrode. The inlet region current flows radially, with 20% of the current located within this section. Only 10% of the current attaches to the anode in the flaring section; current is distributed evenly over the cathode surface. A strong axial, or "blowing", component appears in the current within this region; this axial current continues into the exit section. 70% of the current attaches to the anode over this region; 50% attaches to the cathode. Current distribution on the electrodes is uniform until the exit, where concentration at the anode lip and cathode tip can be seen.

The lower figure (Figure 4.8b) is the FSFAT, 0/100, 3 g/s, at 21.3 kA. Current concentrates at the cathode root and flows axially to the anode exit region. Again, only 10% of the current reaches the anode in the flaring region. The beginning of the anode flare and the anode lip show the highest current concentrations, as do the cathode root and

ENCLOSED CURRENT CONTOURS
FULL–SCALE FLARED ANODE THRUSTER

0:100 MASS INJECTION 21.3 KA 3 g/s

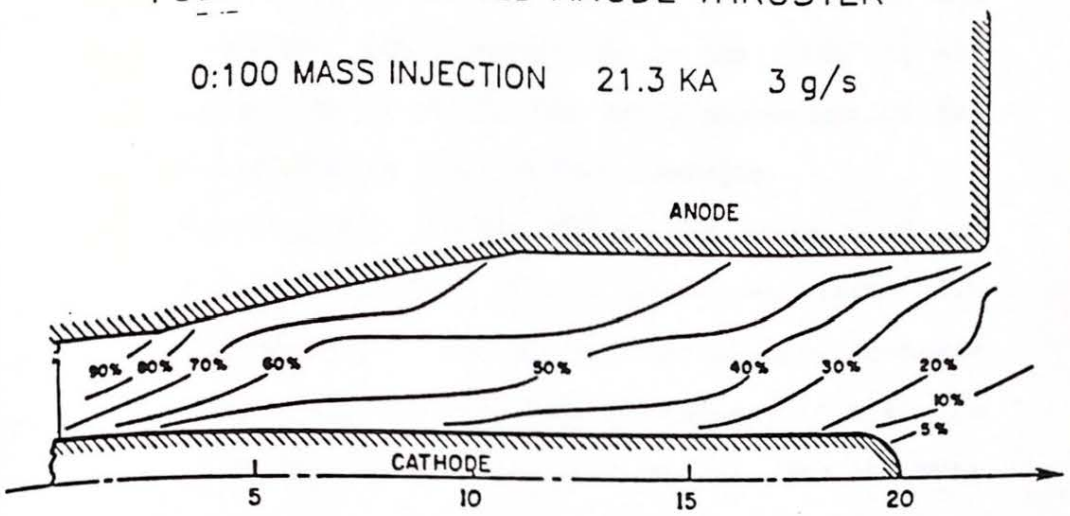

8(a) CURRENT DISTRIBUTION : J = 21.3 kA, m = 3g/sec

ENCLOSED CURRENT CONTOURS
FULL–SCALE FLARED ANODE THRUSTER

50:50 MASS INJECTION 20 KA 6 g/s

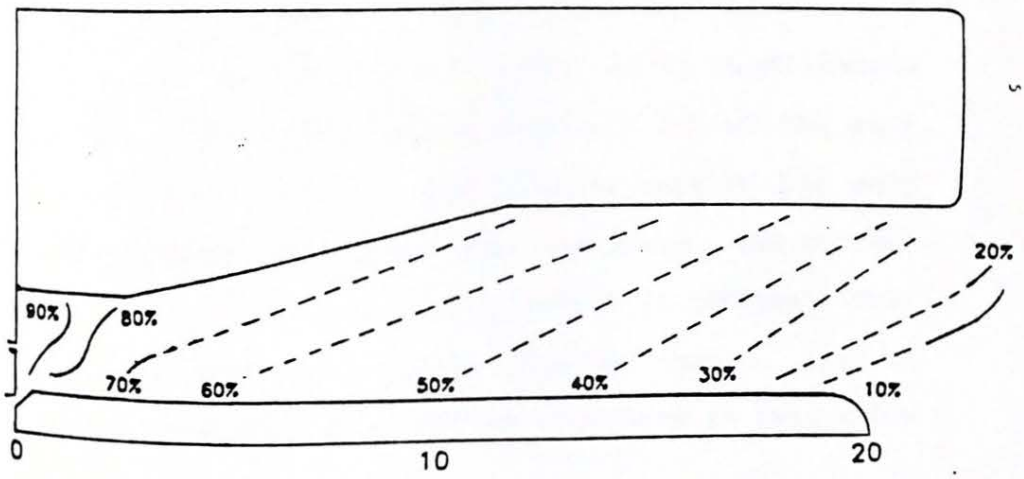

8(b)

Figure 4.8

tip (3). Less than 20% of the current is enclosed within the inlet. 60% of the current flows to the anode in the straight exit section; 50% concentrates at the anode lip and face. The current is blown in the axial direction in the flared and exit region, as in the first example.

Current distributions for the HSFAT were taken at 3 g/s 50/50 for two current levels. The first current level, 7.9 kA, is representative of the rectangular voltage waveform seen at low values of $J^2/\dot{m}$; the second current, 17.8 kA, is representative of the peaked voltage behavior. The low current mapping differs markedly from the full scale results, as well as from the high $J^2/\dot{m}$ half scale contours. At 7.9kA, current flow is primarily radial, and concentrates at the exit of the thruster (Figure 4.9a). 60% of the current attaches in the outer 3 cm of the anode exit region and within 4 cm of the cathode tip. Attachment elsewhere is diffuse, even in the inlet section.

The 17.8 kA high $J^2/\dot{m}$ condition for the HSFAT demonstrates behavior markedly different from the low current case, and quite similar to the FSFAT 50/50 distribution (Figure 4.9b). The inlet section contains 30% of the current, which flows radially. The flaring section has only 10% of the current distributed over the anode, and current distribution at the cathode in this region is diffuse. Current lines blow downstream to the straight region, just as in the FSFAT. The discharge current structure is less simi-

ENCLOSED CURRENT CONTOURS
HALF-SCALE FLARED ANODE THRUSTER

50:50 MASS INJECTION 17.8 KA 3 g/s

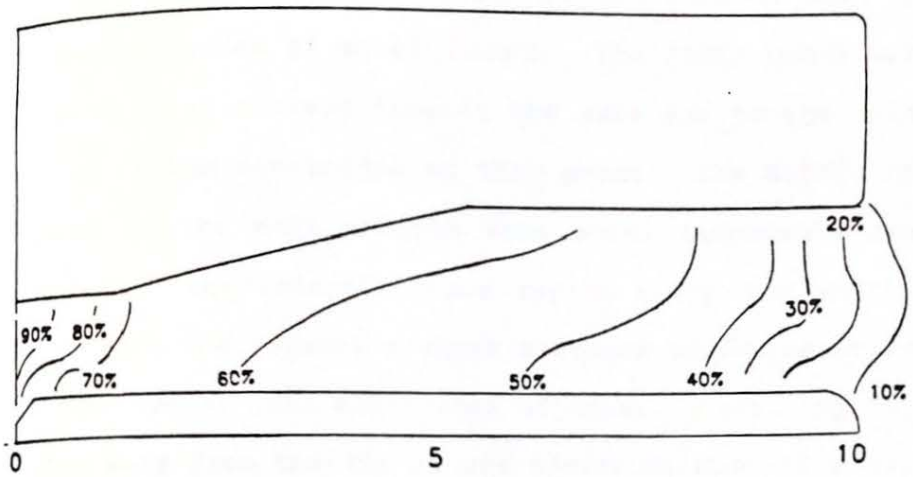

9(a)

ENCLOSED CURRENT CONTOURS
HALF-SCALE FLARED ANODE THRUSTER

50:50 MASS INJECTION 7.9 KA 3 g/s

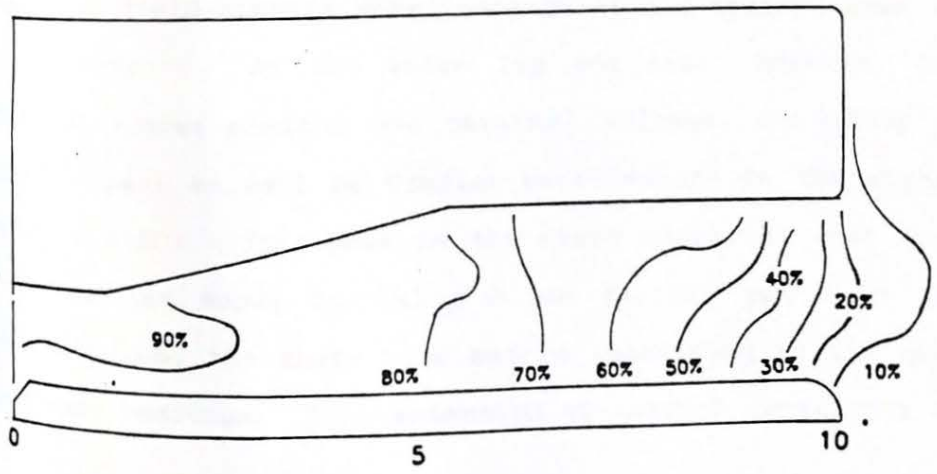

9(b)

Figure 4.9

lar in the exit section due to the slight difference in electrode construction between the two scales. The FSFAT has an anode which extends 2 cm beyond the cathode tip; the HSFAT has electrodes of equal length. The FSFAT configuration favors axial current flow at the exit due to the axial separation of the electrodes at this point. The HSFAT current lines at the exit exhibit some axial components near the center of the interelectrode region where the current flows out into the exhaust a short distance before returning to the electrodes. For electrodes of equal length, any current flow away from the tip of one electrode must flow back upstream to the other; whereas in the FSFAT, current flow downstream of the cathode can originate at the upstream edge of the anode, thus maintaining downstream flow at the exit of the thruster.

One additional characteristic of the HSFAT current distribution at high currents has been observed in the exit region near the anode. In most regions of the discharge, magnetic field signals were rectangular and steady, even at high currents. At the anode lip and face, however, the B-field traces mimiced the terminal voltage, including an initial peak as well as similar oscillations in the signal (Figure 4.10). This peak in the field indicated that current at the anode initially blows further out into the exhaust along the anode face before retreating to its quasisteady position. This extension of current represents an

B-FIELD BEHAVIOR IN ANODE REGION OF HSFAT

J = 17.8 KA 3 g/s 50:50

AWAY FROM ANODE:
z=8.0cm r=1.4cm

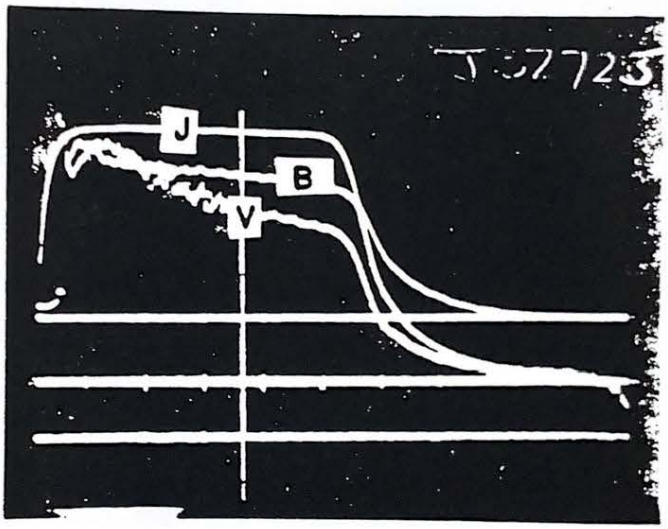

NEAR ANODE:
z=9.5cm r=2.3cm

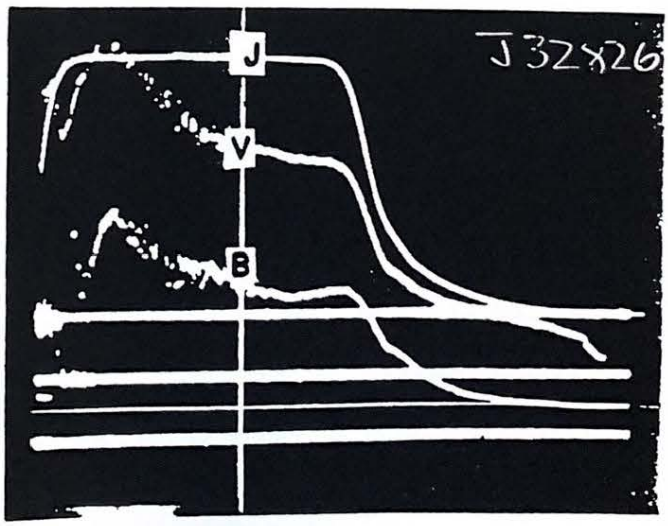

Figure 4.10

increase in the path followed by the electric field within the thruster, causing the voltage (E.dl) to be higher initially. This extension is shown in Figure 4.11, which shows the exit contours extending farther out into the discharge during the voltage peak. Initially, 30% of the current extends outward over the anode face before retreating to the quasisteady distribution shown earlier.

4.3 Summary

The effect of scaling upon the Flared Anode Thruster performance has been examined. As with the Benchmark, voltage and thrust terminal characteristics and current patterns of the HSFAT have been obtained and compared to FSFAT data. Current distributions show essentially similar patterns in both scales, although there is a noticeable difference in the HSFAT at low $J^2/\dot{m}$. Inferred electromagnetic thrust coefficients in both scales are approximately equal. Thrust measurements show the predicted thrust behavior and similar thrust coefficients in both scales. Thrust similarity is seen to include viscous losses in both devices, with increasing losses at low Reynolds numbers. Voltage measurements show the greatest variation across scale; characteristics at equal flow rates in both scales behave differently. The Flared Anode Thrusters show qualitative scaling similarity; however, the varying cross section electrode design appears to be more sensitive to changes in thruster size.

ENCLOSED CURRENT CONTOURS
HALF–SCALE FLARED ANODE THRUSTER
50:50 MASS INJECTION 17.8 KA 3 g/s

DATA TAKEN AT INITIAL PEAK OF B–FIELD TRACE

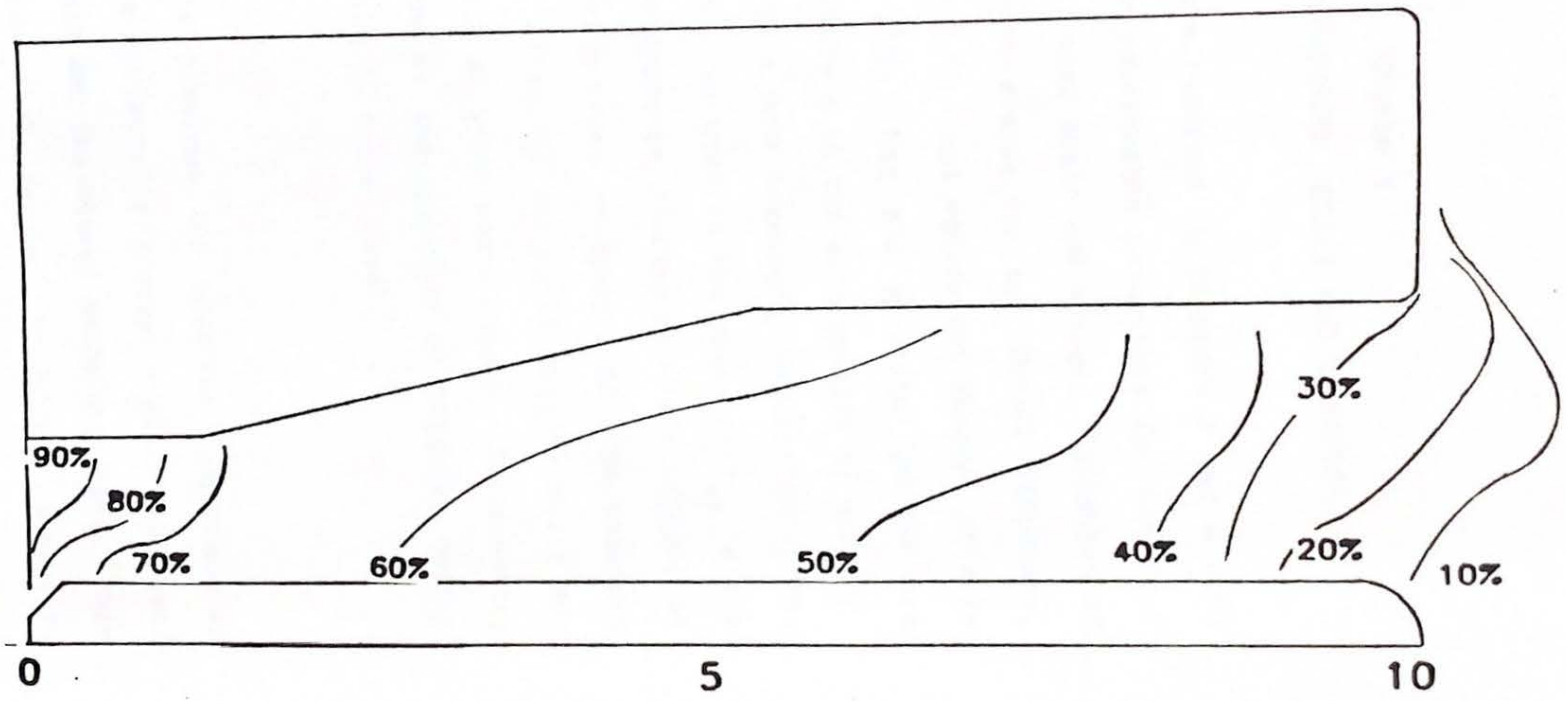

Figure 4.11

SCALE = 2:1

Chapter V

PERFORMANCE COMPARISON: SCALE AND GEOMETRY

The experimental data reported in Chapters 3 and 4 have been used to calculate performance parameters for the four combinations of MPD thruster scale and design. Variables of interest for performance evaluation are thrust efficiency ($T^2/2\dot{m}JV$), input power (JV), and equivalent exhaust velocity, U_{eq}, defined as $T/\dot{m}$. Ueq and specific impulse are related by $U_{eq}=gI_{sp}$, where g is the acceleration of gravity. U_{eq} is considered to be a more meaningful descriptor of the thrust process, and will be used in the place of I_{sp} in the performance in the performance discussion. The effects of scaling upon these performance parameters will be examined first to examine the potential merits of smaller scale MPD thrusters, particularly at lower power ranges. The geometry comparison will focus on the question of thruster design selection as a function fo thrust level.

5.1 Scaling

As was noted in the previous two chapters, experimental results show that performance is generally scale invariant for both the Benchmark and the Flared Anode thrusters. This is particularly true with respect to thrust behavior.

Thrust curves for a given thruster design overlay each other for both scales, regardless of scale. Some variation in thrust due to mass flow differences is evident at low currents, as noted in Chapter 4. At high currents, the electromagnetic thrust coefficient is independent of scale.

Terminal voltage characteristics display similar behavior with respect to scale. In both thruster configurations, the voltage is seen to be primarily a function of geometry, mass flow rate, and current. Voltage levels in the two scales are closest for equal mass flow and current. This is particularly true in the Benchmark thruster, in which the mass injection designs were equivalent in both scales. The Flared Anode design shows greater variation in voltage from scale to scale. HSFAT voltage data at low mass flow rates show the same behavior seen in the FSFAT and described using the linear-cubic function of Chapter 4; while voltage data taken at 3 g/s does not match full scale data taken at the same mass flow rate.

MPD performance parameters have been calculated from the experimentally measured current, voltage, thrust, and mass flow rates. Some initial conclusions of the effects of scaling can be drawn from the scaling of thrust and voltage described in the preceding chapters. In the case of thrust and U_{eq}, the behavior of a given design is seen to be scale independent. The scaling of U_{eq} with respect to current for both thruster designs is shown in Figures 5.1,2. Note that

SCALING OF BENCHMARK THRUSTER
THRUST PERFORMANCE

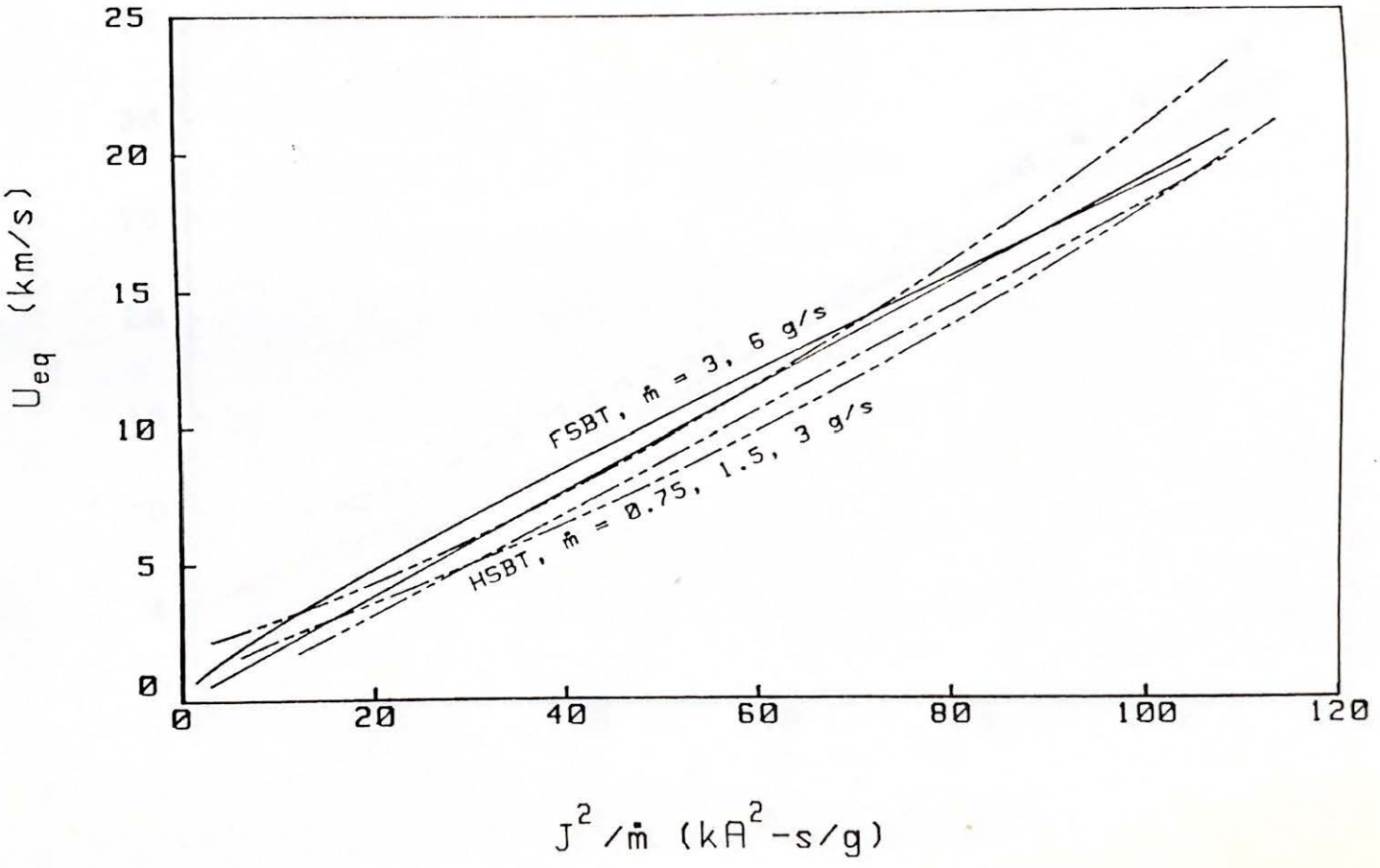

Figure 5.1

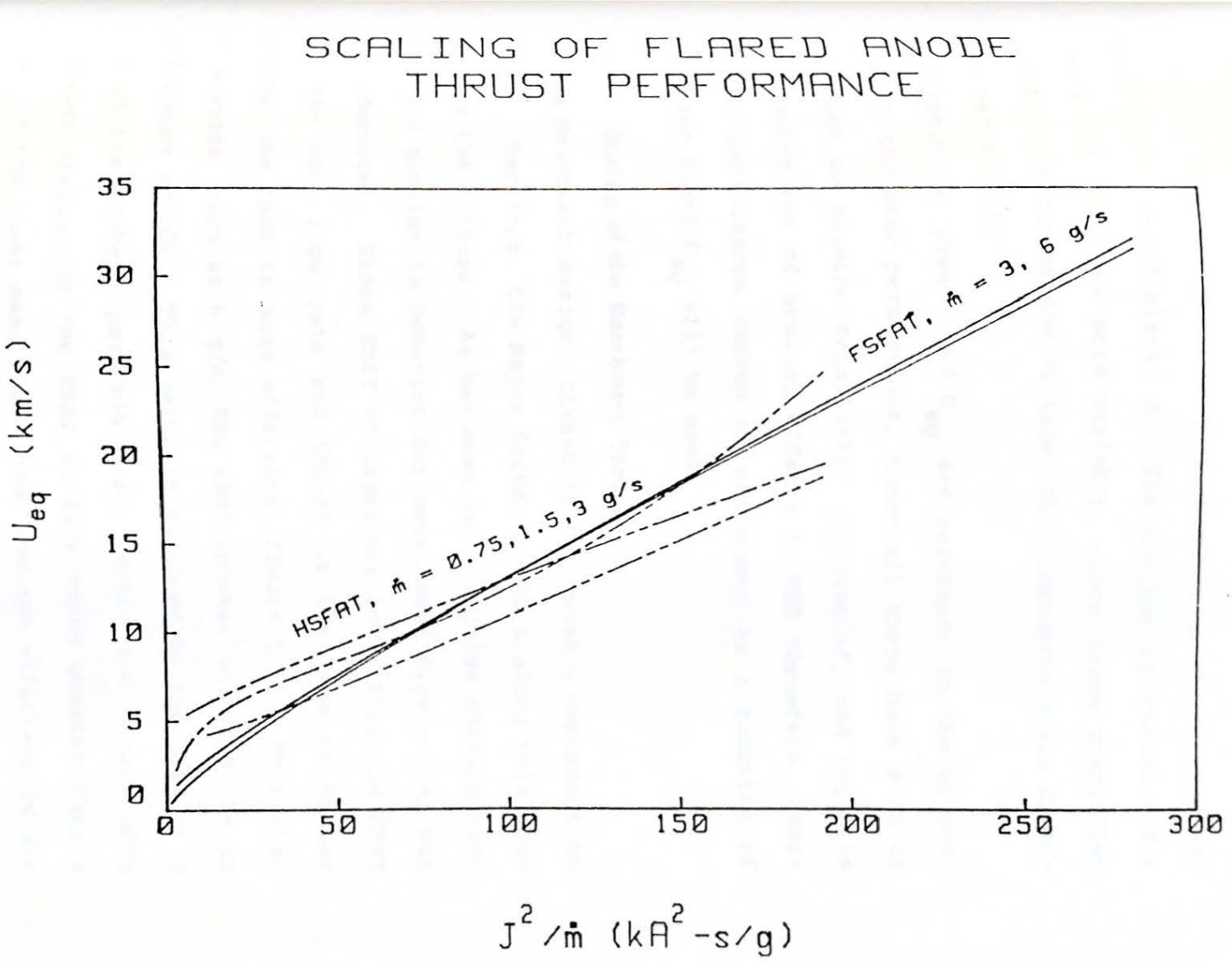
SCALING OF FLARED ANODE
THRUST PERFORMANCE
35
30
25
20
15
10
5
0
U_{eq} (km/s)
0
50
100
150
200
250
300
$J^2/\dot{m}$ (kA^2-s/g)
HSFAT, $\dot{m}$ = 0.75, 1.5, 3 g/s
FSFAT, $\dot{m}$ = 3, 6 g/s

Figure 5.2

the slope of lines shown in these figures is the electromagnetic thrust coefficient, b. The scaling of thrust efficiency and power is more variable, since these quantities include both thrust and voltage, which exhibits scale dependent variability.

Efficiency, power, and U_{eq} are pertinent to the evaluation of thruster performance, since all three have a major influence on mission capability. To simplify and organize the examination of scaling effects in MPD thrusters, families of performance curves of efficiency as a function of power for fixed U_{eq} will be used.

5.1.1 Scaling of the Benchmark Thruster

In the Benchmark design, thrust is only weakly dependent on scale. Therefore, the major factor in the scaling relationship is the voltage. As has been seen, voltage characteristics are similar in behavior for equal mass flow rates, but not identical. Since FSBT voltages are lower than the HSBT for the same flow rate and thrust is the same in either device, the FSBT is more efficient (Figure 5.3). At higher flow rates, such as 6 g/s, the FSBT reaches an asymptote in efficiency of 20%. This value is attained by the HSBT at 3 g/s at its highest possible power level, and should show behavior similar to the FSBT at flow rates greater than 3 g/s. At the lower mass flow rates, maximum efficiencies are 12% and 15%, respectively.

the slope of lines shown in these figures is the electromagnetic thrust coefficient, b. The scaling of thrust efficiency and power is more variable, since these quantities include both thrust and voltage, which exhibits scale dependent variability.

Efficiency, power, and U_{eq} are pertinent to the evaluation of thruster performance, since all three have a major influence on mission capability. To simplify and organize the examination of scaling effects in MPD thrusters, families of performance curves of efficiency as a function of power for fixed U_{eq} will be used.

5.1.1 Scaling of the Benchmark Thruster

In the Benchmark design, thrust is only weakly dependent on scale. Therefore, the major factor in the scaling relationship is the voltage. As has been seen, voltage characteristics are similar in behavior for equal mass flow rates, but not identical. Since FSBT voltages are lower than the HSBT for the same flow rate and thrust is the same in either device, the FSBT is more efficient (Figure 5.3). At higher flow rates, such as 6 g/s, the FSBT reaches an asymptote in efficiency of 20%. This value is attained by the HSBT at 3 g/s at its highest possible power level, and should show behavior similar to the FSBT at flow rates greater than 3 g/s. At the lower mass flow rates, maximum efficiencies are 12% and 15%, respectively.

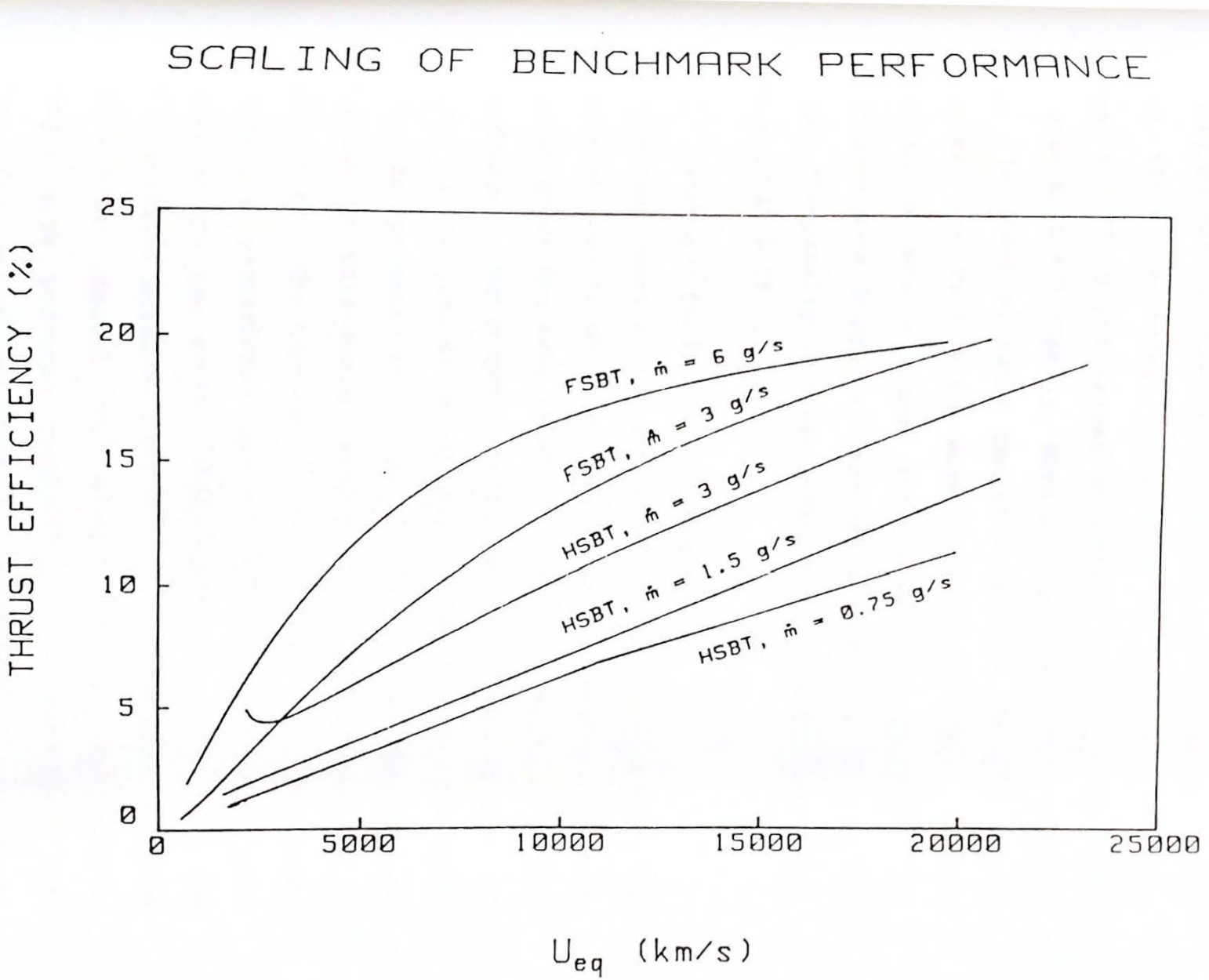
SCALING OF BENCHMARK PERFORMANCE
THRUST EFFICIENCY (%)
25
20
15
10
5
0
0
5000
10000
15000
20000
25000
FSBT, ṁ = 6 g/s
FSBT, ṁ = 3 g/s
HSBT, ṁ = 3 g/s
HSBT, ṁ = 1.5 g/s
HSBT, ṁ = 0.75 g/s
U_{eq} (km/s)

Figure 5.3

Judging the two Benchmark thrusters on the basis of the above three parameters, the FSBT is superior in all respects. For fixed values of exhaust velocity, the FSBT operates more efficiently, even at low power levels (Figure 5.4). In order to match the efficiency of the full scale thruster, the half scale must be used at higher powers, which would require higher flow rates than the FSBT. No advantages were found in operating at low mass flow rates; indeed, the penalty in lower efficiency is substantial, particularly at 0.75 g/s.

5.1.2 Scaling of the Flared Anode Thruster

Measured thrust in the FAT shows the same trends of scale invariance seen in the Benchmark design. Therefore, exhaust velocity shows the same invariant form as seen in the Benchmark design. One primary difference in the two scales, of course, is the greater onset levels attainable by the FSFAT due to its optimized mass injection design. Voltage characteristics in this design proved to be more sensitive to scale, so that the terminal voltage is once again the primary factor in performance scaling. For completeness, a comparison of the two scales' performance calculated from the actual voltages measured during thrust experiments is shown (Figure 5.5). Recall that these HSFAT voltages disagree strongly with previous measurements at comparable flow rates. For general performance modelling and comparisons, voltages based upon the function obtained from Plexiglas

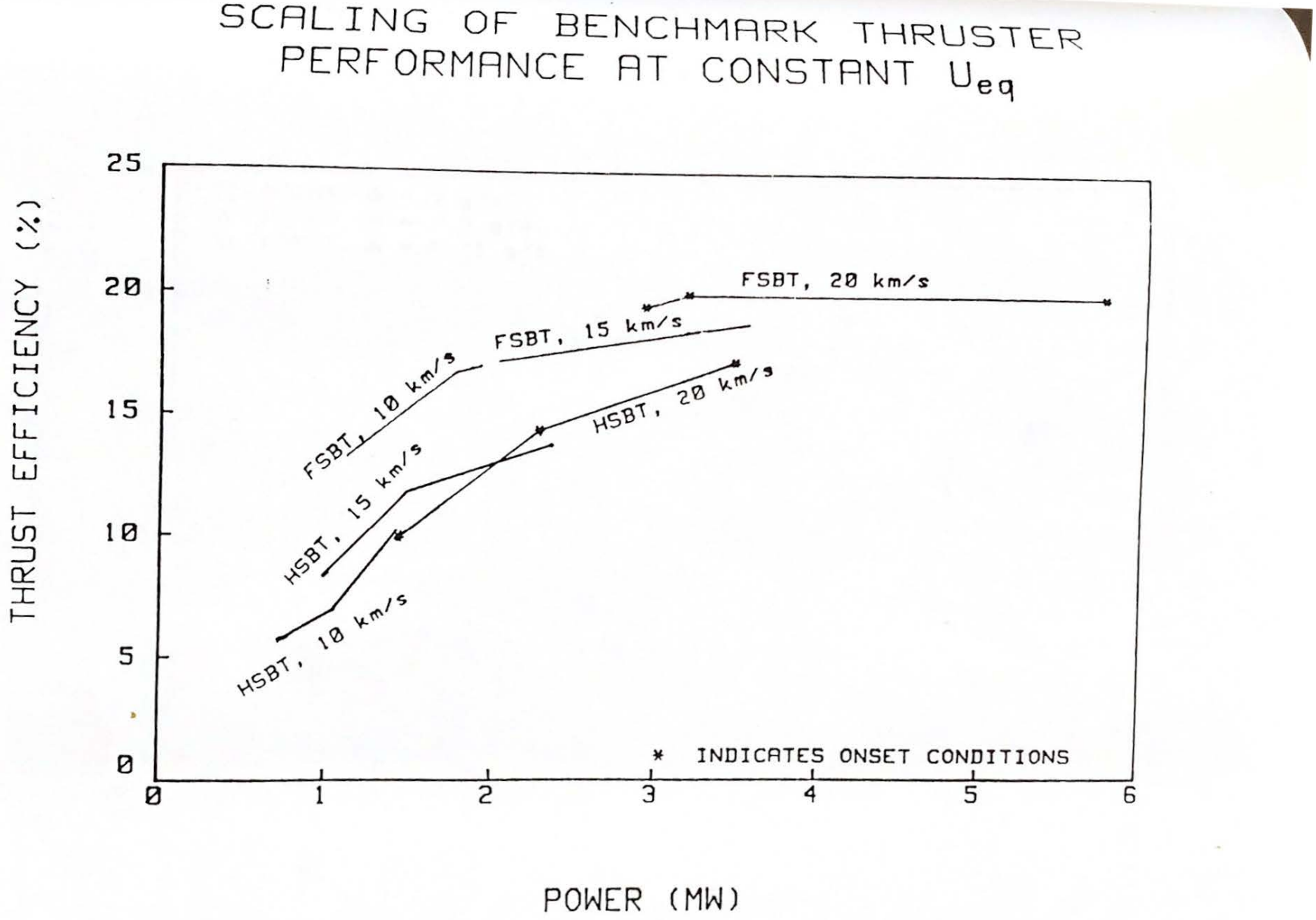
SCALING OF BENCHMARK THRUSTER PERFORMANCE AT CONSTANT U_{eq}
THRUST EFFICIENCY (%)
25
20
15
10
5
0
0
1
2
3
4
5
6
FSBT, 20 km/s
FSBT, 15 km/s
FSBT, 10 km/s
HSBT, 20 km/s
HSBT, 15 km/s
HSBT, 10 km/s
* INDICATES ONSET CONDITIONS
POWER (MW)

Figure 5.4

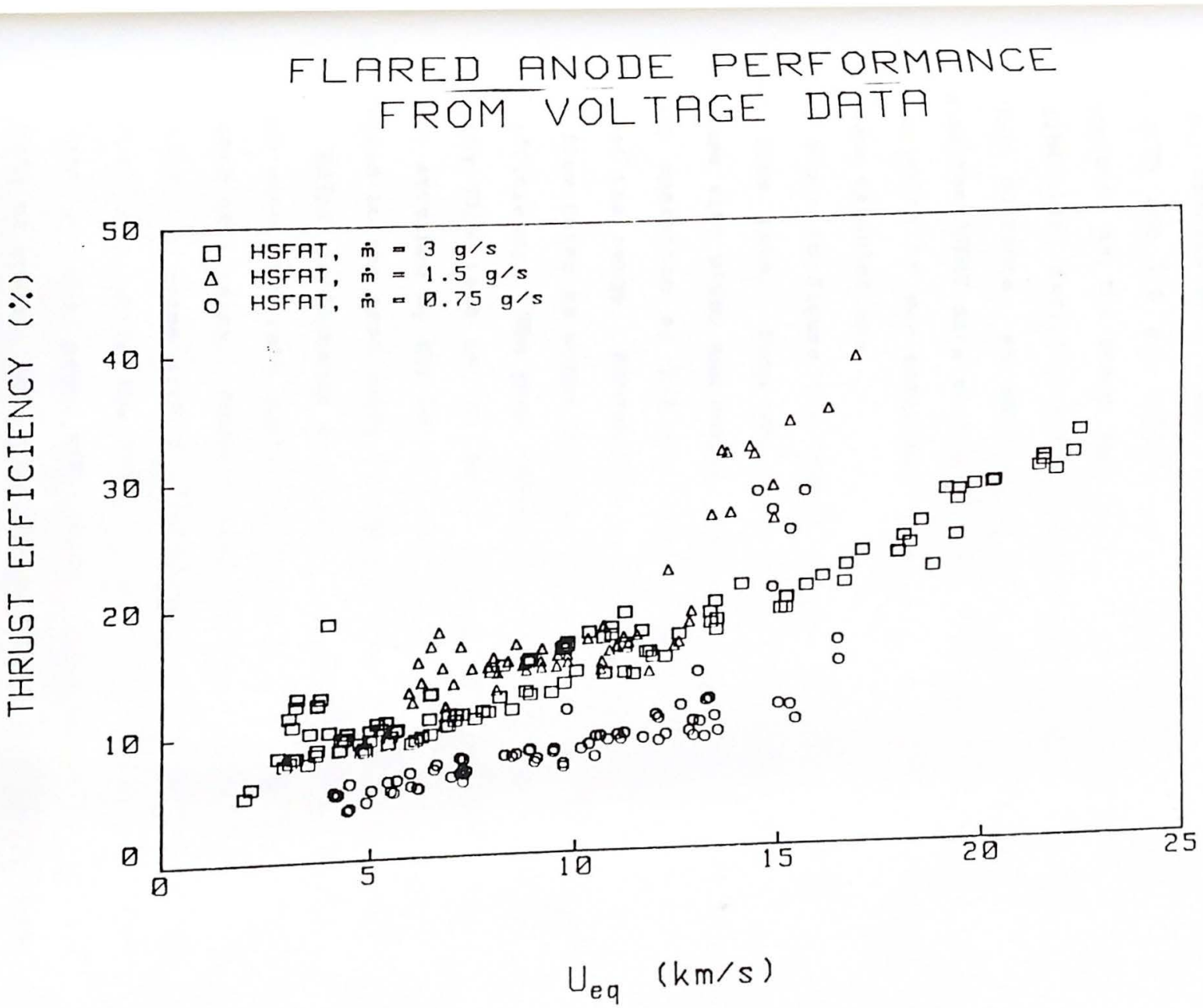
FLARED ANODE PERFORMANCE
FROM VOLTAGE DATA
HSFAT, ṁ = 3 g/s
HSFAT, ṁ = 1.5 g/s
HSFAT, ṁ = 0.75 g/s
THRUST EFFICIENCY (%)
0
10
20
30
40
50
0
5
10
15
20
25
U_{eq} (km/s)

Figure 5.5

facility results at 1.1 and 2.2 g/s will be used to calculate 0.75 and 1.5 g/s voltage characteristics in further discussions, as the steep declines in voltages measured in the fiberglass facility yield abnormally high efficiencies at high currents, as well as a great deal of scatter. Because the HSFAT data at 3 g/s is independent of the facility in which it was obtained, these data are used in performance calculations.

As shown in Figure 5.6, HSFAT thrust efficiency depends upon flow rate. Data at 0.75 and 3 g/s monotonically increase with power and exhaust velocity; whereas efficiency during operation at 1.5 g/s remains almost constant over most of its range. Performance of the HSFAT at the two low mass flow rates is worse than the full scale in terms of U_{eq} and efficiency. The peak exhaust velocity in either scale for any flow rate is the same; however, the maximum efficiency attained by the HSFAT at 0.75 or 1.5 g/s is only 15%, compared to the peak value of 24% achieved by the FSFAT at 3 g/s. HSFAT performance at 3 g/s follows FSFAT performance at the same flow rate quite closely until the FSFAT reaches its peak efficiency. Above this point HSFAT efficiency continues to increase with U_{eq} and power to an efficiency at onset of 32%, while the FSFAT at both 3 and 6 g/s remains constant at the peak efficiency independent of exhaust velocity or power. Note that although the increase of onset in the FSFAT allows for a greater range of exhaust velocity

SCALING OF FLARED ANODE PERFORMANCE

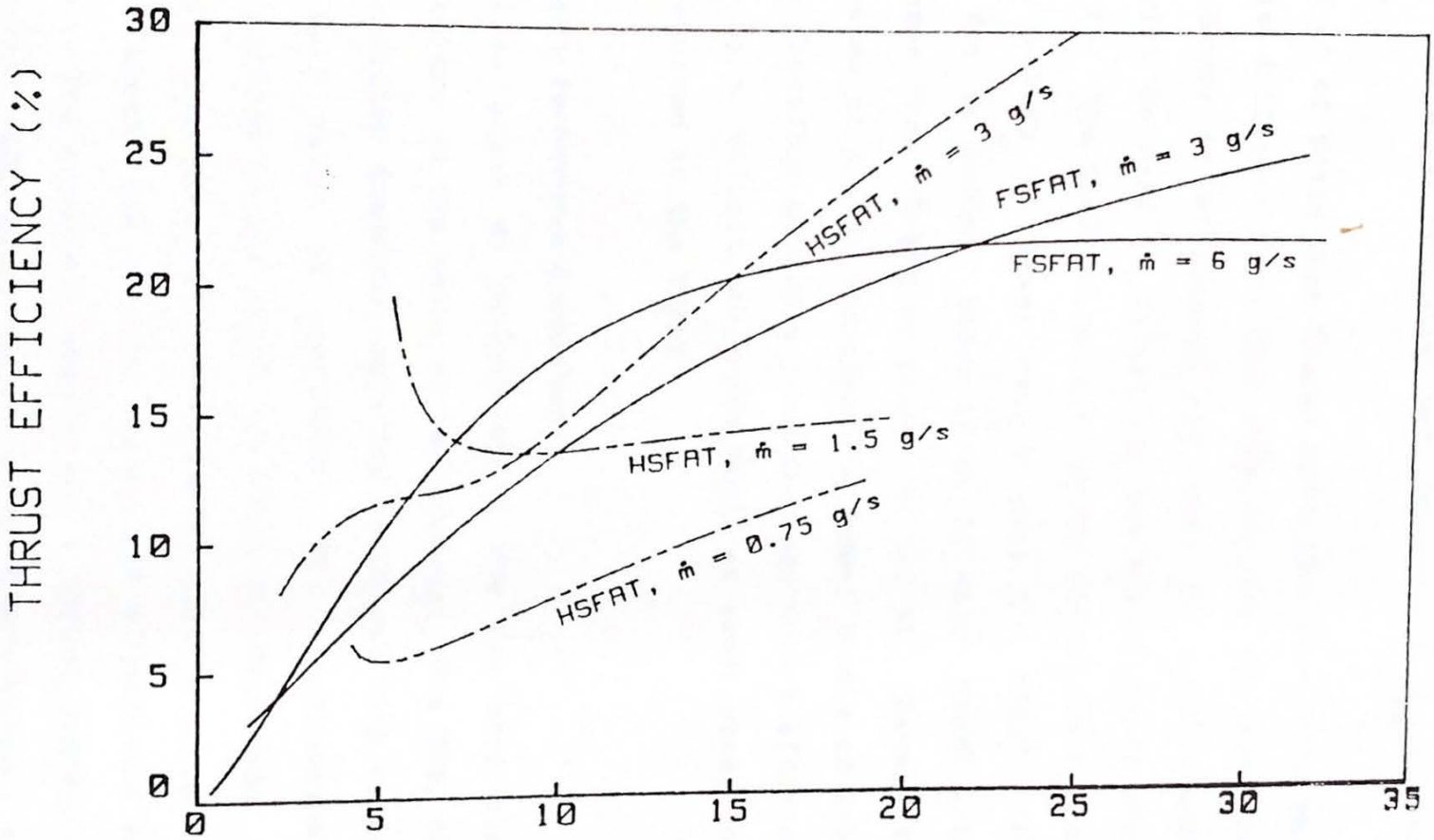

Figure 5.6

and power, the efficiency does not improve for U_{eq} greater than 20 km/s.

The effect of scale upon Flared Anode Thruster (FAT) performance is different from that observed for the Benchmark design. Curves of efficiency and power at fixed exhaust velocity will be used to illustrate the influence of scale (Figure 5.7). The HSFAT is able to reach comparable U_{eq} and efficiency values at lower powers than the FSFAT. For instance, for an exhaust velocity of 15 km/s, HSFAT efficiency ranges from 15-20% at powers of 1-2 MW, whereas the FSFAT operates at 17-20% efficiency at power levels of 2-3.5 MW. It is therefore possible to attain equivalent efficiencies and exhaust velocities in the HSFAT at lower power levels than required in the FSFAT.

5.2 Geometry Performance Comparison

The data also allow an evaluation of the two half scale thruster designs on the basis of performance. The HSBT follows the predicted quadratic behavior of thrust with current over its full range of operation. The electromagnetic thrust coefficient is 0.2 N/kA^2, or close to that value, for both scales. The HSFAT thrust characteristic is more varied, with a linear low current region and a quadratic high current one. The quadratic region has a thrust coefficient of b=0.12 N/kA^2, 60% lower than the Benchmark value. However, the HSFAT also has an onset parameter of 180 kA^2-s/g,

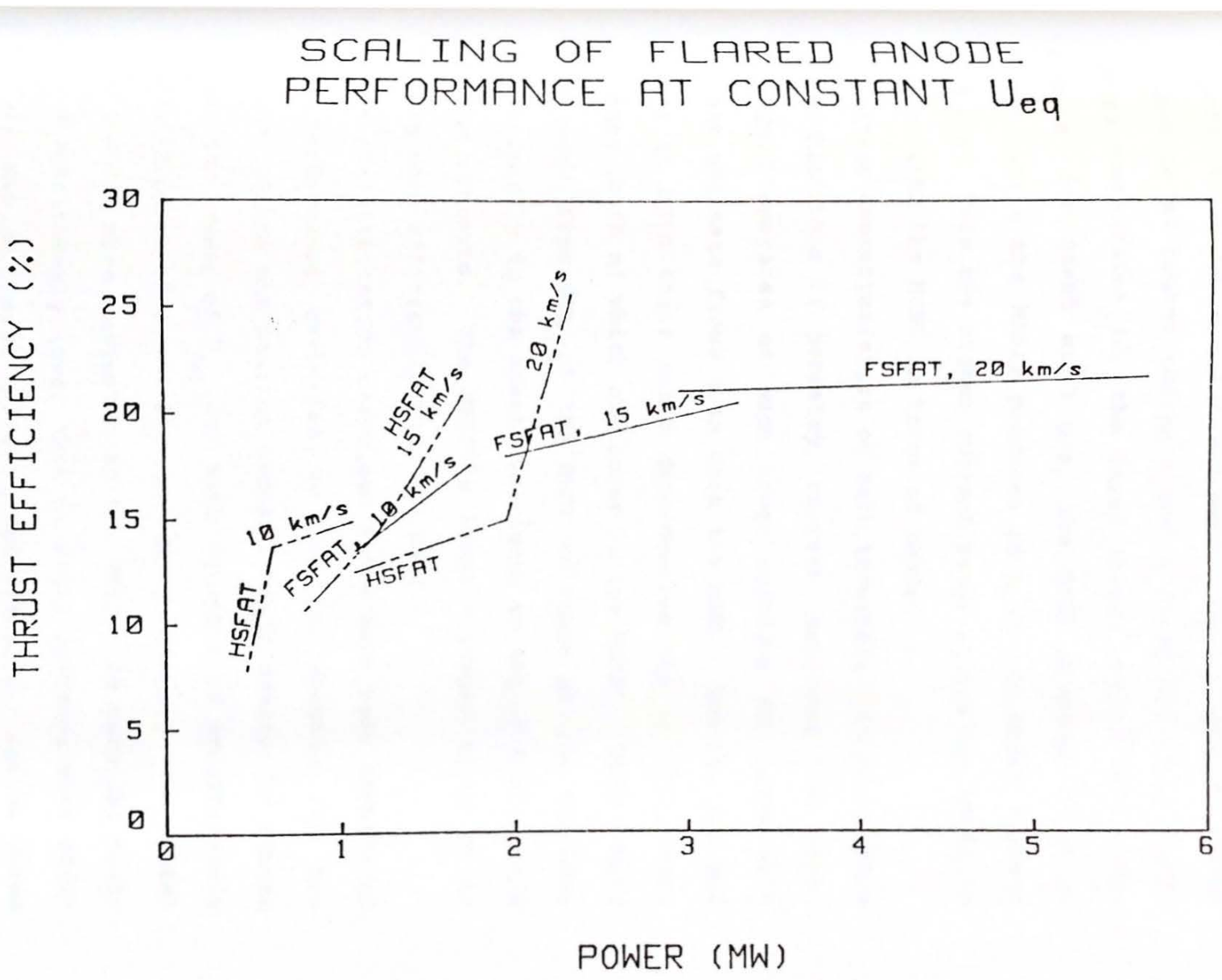
SCALING OF FLARED ANODE
PERFORMANCE AT CONSTANT U_{eq}
THRUST EFFICIENCY (%)
POWER (MW)
30
25
20
15
10
5
0
0
1
2
3
4
5
6
HSFAT
10 km/s
FSFAT, 10 km/s
HSFAT
15 km/s
20 km/s
FSFAT, 15 km/s
FSFAT, 20 km/s
HSFAT

Figure 5.7

compared to 90 kA^2-s/g for the HSBT. This allows the HSFAT to operate at higher currents for a given mass flow rate, and so compensates for the lower thrust coefficient. For example, for onset at 3 g/s, the HSBT produces 54 N of thrust, while the HSFAT produces 68 N at its onset current at 3 g/s. Thus the higher current range allows the HSFAT to compete with the HSBT in terms of thrust.

Voltage characteristics of both thrusters have been shown to be functions of geometry, current, and mass flow rate. The HSFAT operates at much lower voltages for comparable current and mass flows than does the HSBT. The two designs differ in both their cubic dependencies and in their fall voltages, both of which are lower in the HSFAT. HSFAT voltages range from 67% of the HSBT voltages at low currents (due primarily to the sheath voltages) to 45% of HSBT levels at high currents. The HSFAT's lower voltages allow it to perform more efficiently than the HSBT.

The characteristics described above have been translated into performance variables to use for judging the two designs. Since the maximum thrust of both designs is almost equal, the range of U_{eq} for each thruster is approximately equal (Figures 5.1, 5.2) For equal thrust, the HSFAT requires 30% more current than the HSBT; its terminal voltage is sufficiently lower that it still operates more efficiently and at lower power. Specifically, for a fixed exhaust velocity, the HSFAT is more efficient at lower pow-

ers than the HSBT (Figure 5.8). These results reflect the effects of design upon both thrust and voltage characteristics.

HSFAT - HSBT PERFORMANCE COMPARISON AT CONSTANT U_{eq}

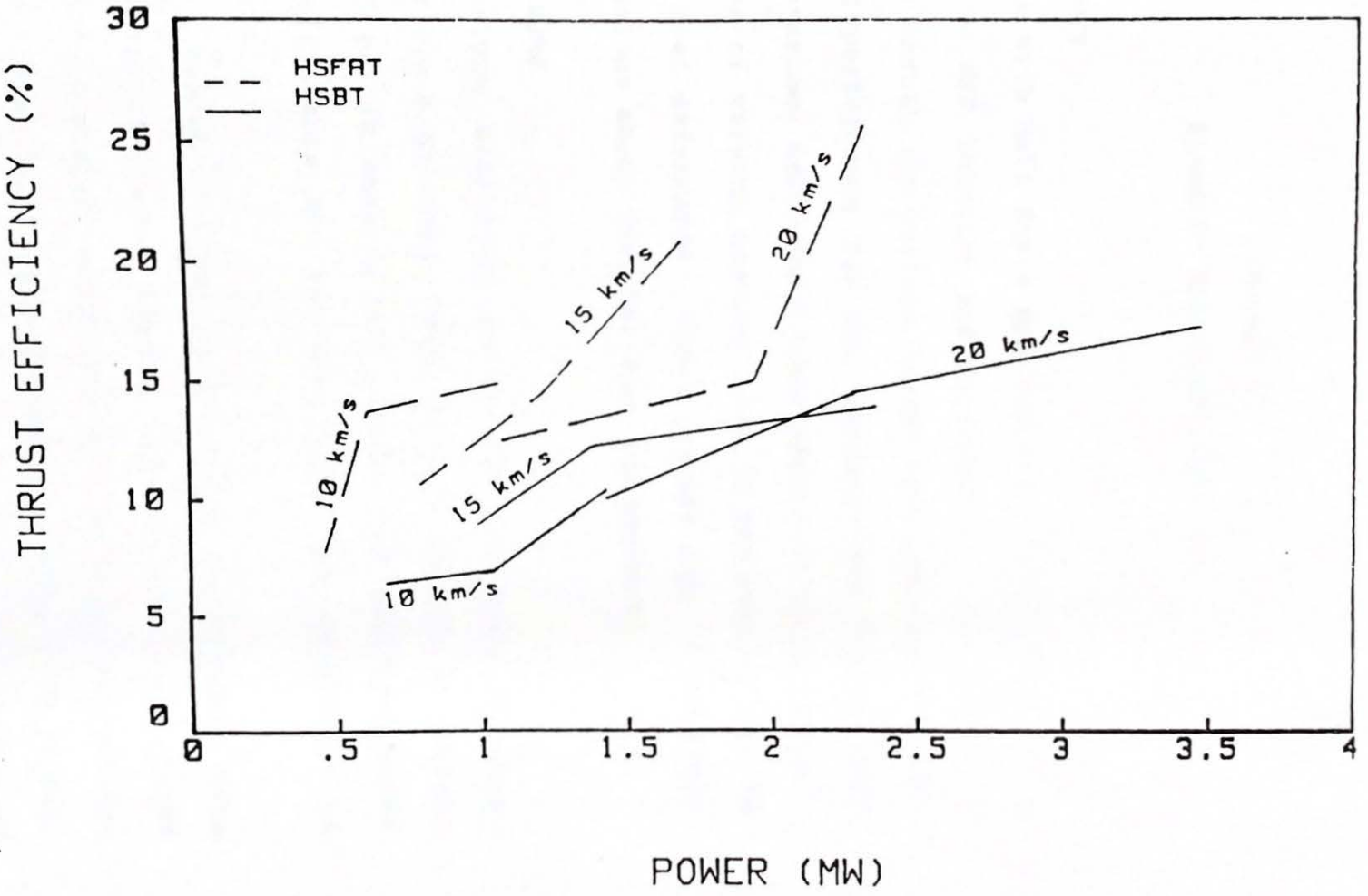

Figure 5.8

Chapter VI

SUMMARY AND CONCLUSIONS

6.1 Summary

Experiments with Half Scale MPD thrusters have provided new insight into MPD behavior and performance. The effect of scale upon thrust and voltage characteristics, current patterns, and performance for the Benchmark and Flared Anode has been examined using Half Scale models of these designs. The effects of varying geometry seen in the smaller devices have also been determined. These results lead to fundamental conclusions about thruster size and geometry.

6.1.1 Scaling

In both designs, similarity can be seen from scale to scale. Thrust follows a quadratic behavior with respect to current in both sizes; In keeping with theory, the electromagnetic thrust coefficients for the two scales are comparable in both designs.

A second result observed in the Flared Anode thrust data is the scaling of viscous losses. Losses seen in the FSFAT were present in similar magnitudes in the HSFAT; in particular, these losses show some dependence on flow rate as well as thruster size through scaling with the Reynolds number of

the flow. Such losses are observed in arcjet nozzle design and merit further investigation.

Terminal voltage is a function of mass flow rate and current, but not scale. Voltage characteristics in either scale are comparable at equal flow rates; in the case of the Benchmark Thruster, agreement is quite close. This correspondence can also be anticipated from calculations using a one- dimensional MHD model of the discharge.

The effect of scaling on thruster performance has been calculated from terminal characteristics in terms of equivalent exhaust velocity (U_{eq}), input power, and thrust efficiency. In the Benchmark Thruster, some similarity in performance can be seen at equal mass flow rates, where peak exhaust velocities and efficiencies are comparable; however, at comparable power levels the FSBT is superior in efficiency to the HSBT. The Flared Anode Thrusters show greater variation in performance across scale; the HSFAT shows superior efficiency at comparable exhaust velocities and power levels.

6.1.2 Geometry

In a comparison of half scale designs, the Flared Anode Thruster design emerges as being superior to the Benchmark. Although the FAT thrust coefficient is lower than the Benchmark's, the terminal voltage characteristic is also lower, resulting in a net gain in efficiency over the Benchmark. A higher onset current in the FAT also allows peak exhaust

velocities comparable to those seen in the Benchmark thrusters.

6.2 Conclusions

In terms of thruster design, several suggestions arise from the above results. For scaling, any downscaling should be done using propellant flow rates equal to those used in the larger device. The HSBT actually requires higher flow rates and powers to match the FSBT in exhaust velocity and efficiency. The Flared Anode design is a promising design for scaling; the HSFAT is comparable to the FSFAT in exhaust velocity and efficiency at lower powers, and despite its lower thrust coefficient, is generally superior to the HSBT.

Pertinent design considerations are maximizing thrust coefficients while minimizing terminal voltage and increasing onset. The Flared Anode design accomplishes the goal of low voltage; however, the electromagnetic thrust coefficient is much less than its predicted value. Onset can be increased using additional flow at the outer anode; this has already proven to be successful in both the FSFAT and the FSBT (17,19). Prime design considerations that are evident from this research are the tradeoffs between increasing thrust and decreasing voltage. The Flared Anode has shown that efficient performance can be achieved with a relatively low thrust coefficient, if the onset limit is high enough to allow the FAT to achieve comparable exhaust velocities. As

for the HSBT, mass injection near the anode has been shown to increase the onset level in both the full scale Flared Anode and Benchmark Thrusters (17,19). The HSFAT has already benefitted from outer injection; a similar injection scheme in the HSBT might allow it to achieve higher U_{eq} and efficiencies than it has presently achieved.

6.3 Future Work

Mass flow variation has a greater effect on thruster behavior and performance than does scale. Reducing the mass flow rate to less than 3 g/s has been found to impair the performance of both thruster designs. On the other hand, the lower limit of effective electromagnetic thrust has not yet been reached; this limit might be found at smaller scales and powers. A further reduction of scale, while retaining the mass flow rates used in the Half Scale research, would extend our knowledge of the interplay between mass flow rate and scale. The effects of mass injection location upon terminal characteristics, particularly onset, should be investigated to determine the maximum current range of half scale devices and to examine scaling further with respect to the flow fields of various scales.

An unsolved problem in the Flared Anode design is the viscous losses seen in both scales. Experimentally, the validity of the concept of viscous losses can be tried by testing shorter electrode thrusters, such as a short flared

anode, to see if losses are less. The boundary layers in a plasma flowing over an electrode in the presence of crossed electric and magnetic fields and current flow are not well understood. An understanding of the loss mechanisms present in the MPD nozzle might allow an improvement in Flared Anode performance in all scales and provide for improved performance for MPD devices at low mass flow rates and powers.

Appendix A

CALIBRATION PROCEDURES

A.1 Mass Flow Calibration

In quasisteady MPD thrusters, propellant is injected into the thrust chamber in a pulse 20-60 milliseconds long. The mass pulse starts 10-20 milliseconds prior to the initiation of the discharge to allow the mass distribution within the thruster to reach a steady state. Thus, the mass flow rate takes the form of a 20 - 60 ms long, approximately rectangular pulse, the the actual discharge occurring sometime during the plateau of the mass pulse.

Mass flow calibration of the plenum and choked nozzle injection system used the smaller diagnostic plexiglass facilty with the proper thruster and mass injection system installed. The tank was evacuated to pressures on the order of 10E-5 torr, and the tank was then sealed off from all pumps using a gate valve between the diffusion pumps and the vacuum chamber. Leakage of the tank over the time of any measurement was found to be negligible. Argon propellant was then injected into the tank using the standard pulse length. Tank pressure was then measured using a CVC Macleod guage in equilibrium with the chamber (after approximately 1

minute). The experiment was done for a variety of plenum pressures, using both single and multiple (5-10) shot measurements; close agreement was found between the two methods.

With accurate pressure measurements, the mass of the Argon injected during a single pulse can be calculated using the assumption of an ideal gas:

$$m = PV/RT$$

where P = chamber pressure, V = chamber volume, R = Argon gas constant, and T = gas temperature. Volume of the plexiglass facility has been calculated to be 1.16 m^3, T = 300K, and R = 208 J/kg-K for Argon. With all variables known or measured, the total mass per shot can be calculated.

Time of the mass pulse was calculated from the pressure pulse as measured by a Piezotronic piezoelectric pressure transducer located between the plenum and solenoid valve. The pressure pulse was stored in digital form using the Nicolet 2090-IIIA oscilloscope. The pulse waveform was then numerically integrated. The integral is then equated to an "ideal" rectangular pulse of the same amplitude as the steady portion of the measured pulse. The effective mass pulse time is

$$T = \frac{\int p \, \delta t}{p_o}$$

The total mass injected is then divided by the calculated mass pulse time. This method has been used previously by Merfeld (19), and has proved to be an effective means of calibration.

Both the HSBT and the HSFAT were calibrated using this method. The HSBT flow rates were found to be 33% higher than quoted by Kaplan or than calculated from theoretical choked flow calculations. HSFAT flow rates were found to be 47% higher than predicted from theory. Calibration curves for each thruster are shown in Figures A-1 and A-2.

A.2 Operation and Calibration of Magnetic Field Probes

The magnetic field probe, or B-probe, is based upon two of Maxwell's equations

$$\nabla \times \vec{E} = -\frac{\delta \vec{B}}{\delta t}$$

$$\nabla \times \vec{B} = \mu_o \vec{j} - \frac{\delta \vec{D}}{\delta t}$$

The B-probe is a coil of wire with its axis parallel to the direction of a magnetic field. Therefore, applying Faraday's Law to the coil and integrating over its cross-section perpendicular to the field, the relation becomes

$$V = -A_c(dB/dt) \qquad (3)$$

where V = emf through the coil and A_c = the coil area. The voltage between the two coil ends is proportional to the change of magnetic field strength through the center of the coil. Note that the above integration assumes that the field does not vary appreciably over the area enclosed by the coil.

HALF SCALE BENCHMARK THRUSTER MASS FLOW CALIBRATION

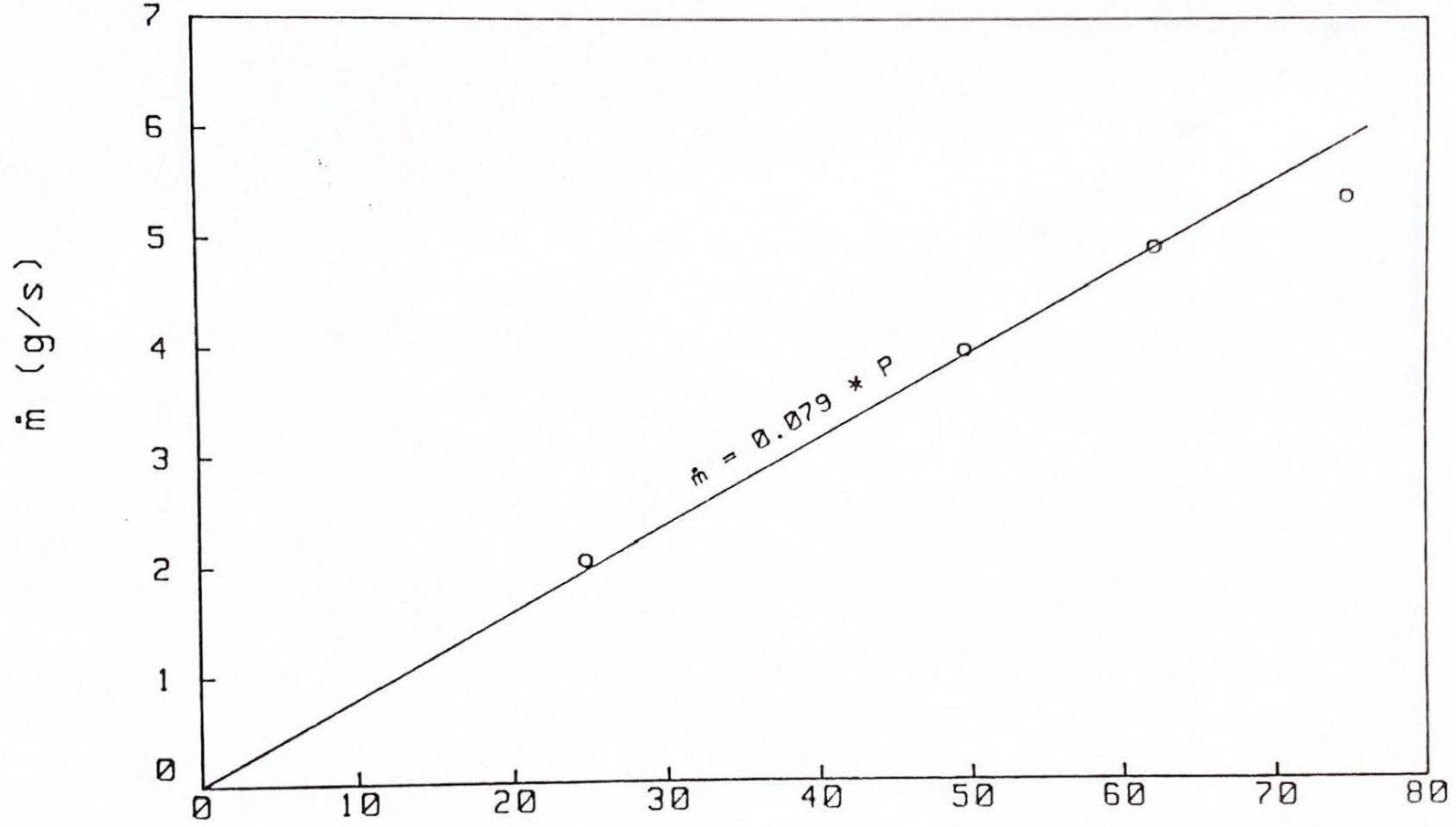

Figure A–1

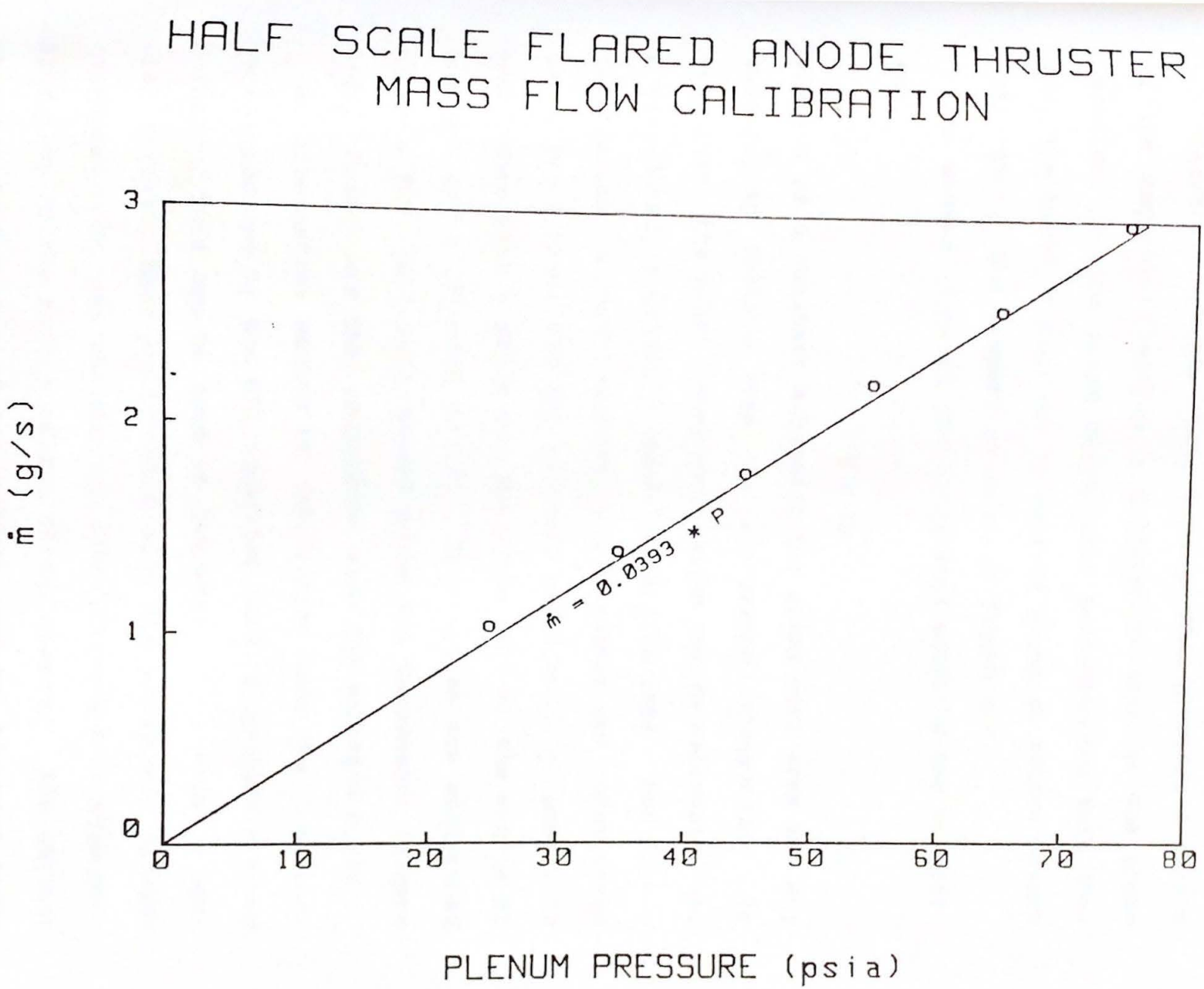
HALF SCALE FLARED ANODE THRUSTER
MASS FLOW CALIBRATION
ṁ (g/s)
3
2
1
0
ṁ = 0.0393 * P
0
10
20
30
40
50
60
70
80
PLENUM PRESSURE (psia)

Figure A–2

Integration of this probe voltage then provides a record of the magnetic field as a function of time at the probe location. In the probe experiments performed for this thesis, the probe signal was integrated using an active op-amp integrator. The circuit is shown in Figure A-3.

The general form of the integrated equation can be written

$$V = KB$$

where K is a constant subsuming the probe coil area and any multiplying factors from the electronic integration. In this form, the probe-integrator system can be calibrated and K calculated, provided a known B-field is used. For such a calibration, a known magnetic field source was constructed using two Skinner 120 VAC solenoid valve coils aligned with each other with a place for the probe coil at the middle of the two coils (Figures A-4,5). This system was calibrated using a F.H. Bell Hall Effect probe and Gaussmeter (Figure A-6). Probes are then calibrated with the solenoid coils.

An alternative method of calibration uses the high currents produced by the MPD capacitor bank to produce a known B-field. This can be done in two ways: 1.) Using a special thruster head constructed with the anode and cathode connected such that the current flows through a central metal column in the middle of the thrust chamber. The current is fixed at the axis of the chamber, and the magnetic field at any point in the thruster can be calculated to provide a

B-PROBE INTEGRATOR

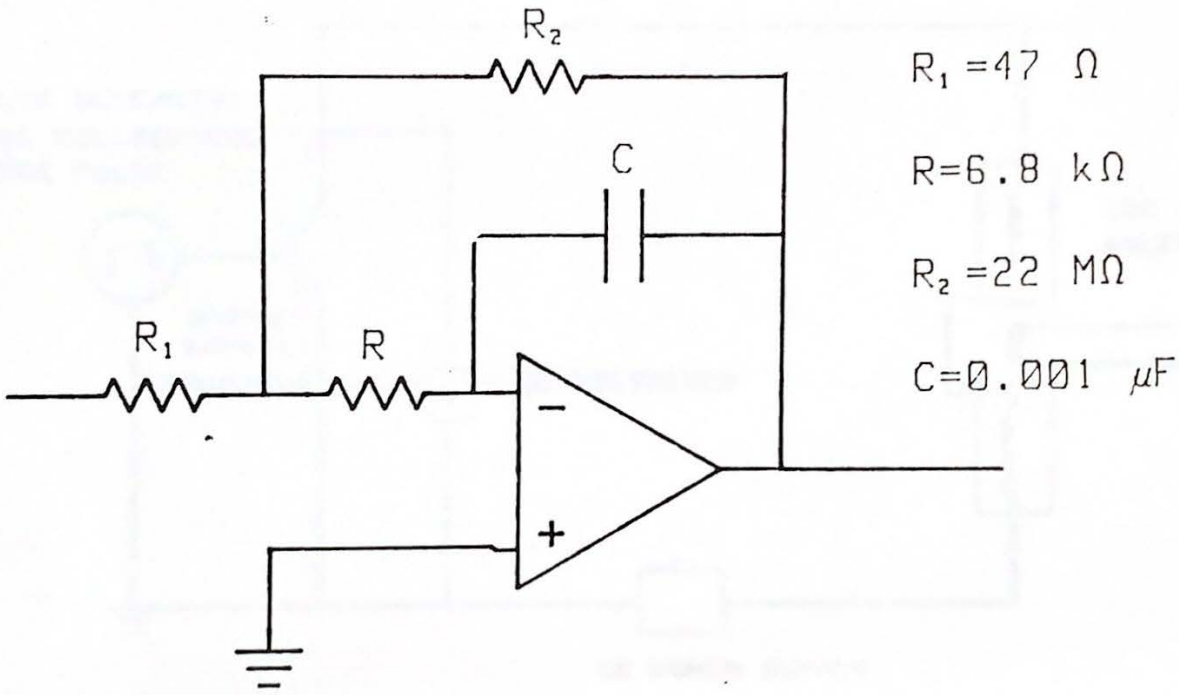

Figure A-3

B PROBE CALIBRATION STAND

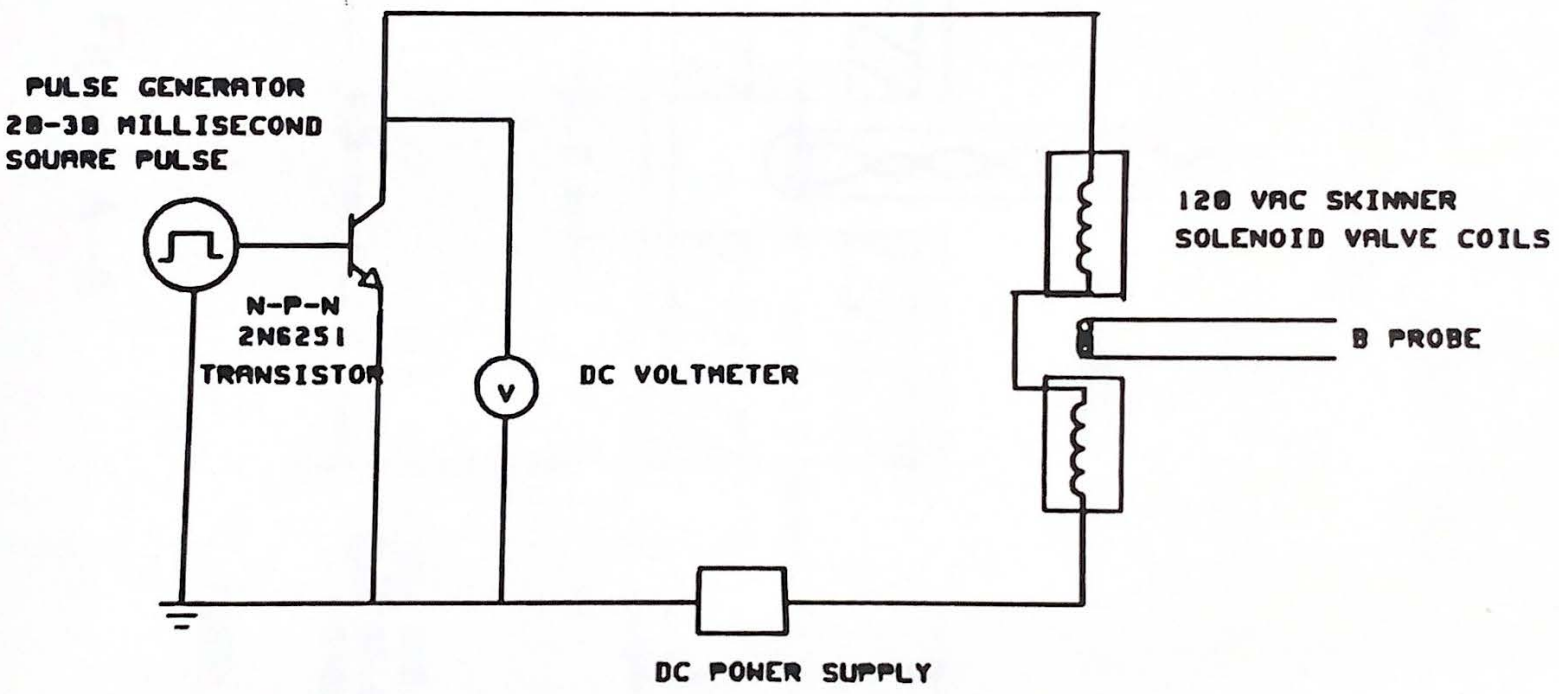

Figure A–4

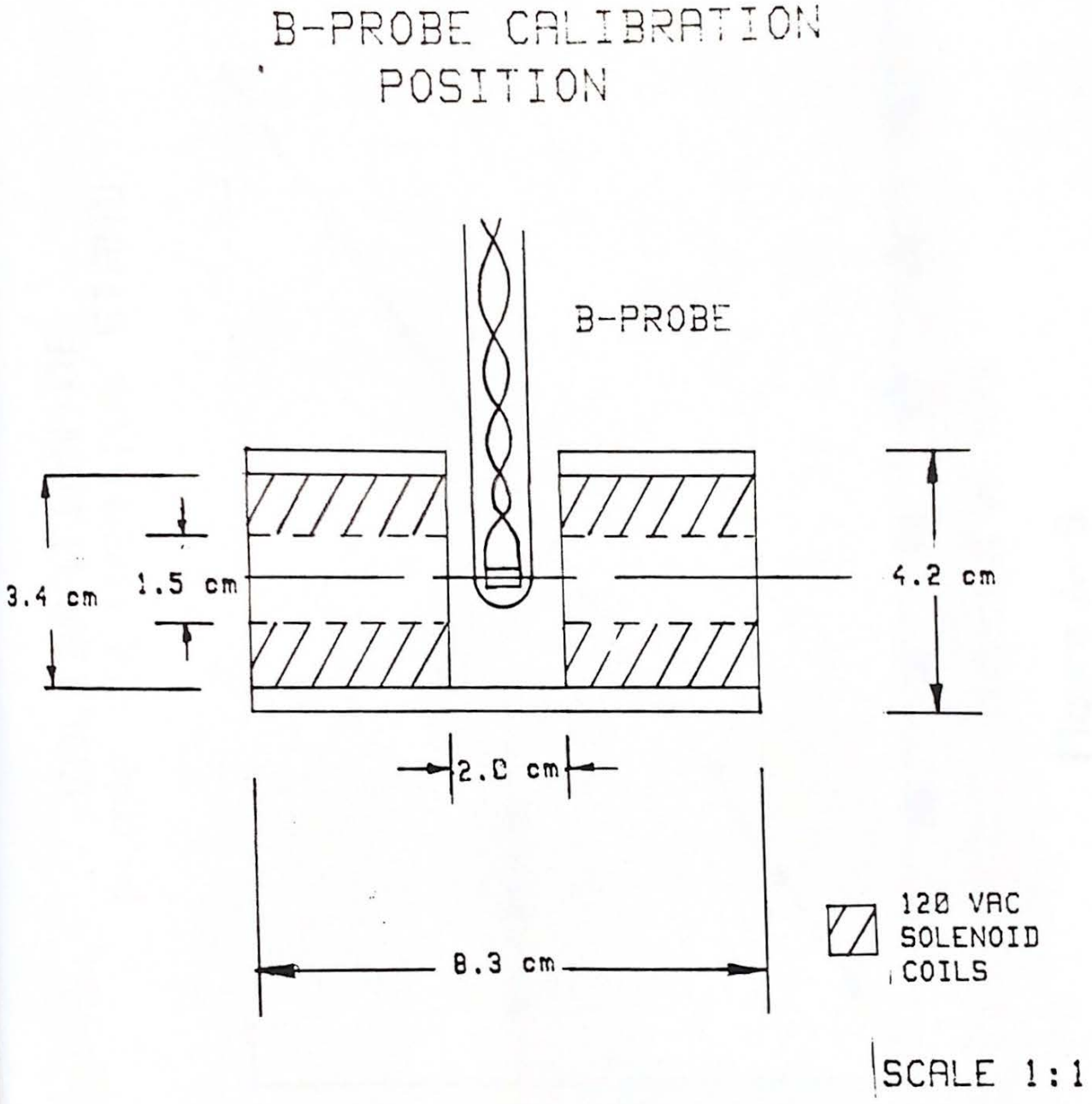
B-PROBE CALIBRATION
POSITION
B-PROBE
3.4 cm
1.5 cm
4.2 cm
2.0 cm
8.3 cm
120 VAC
SOLENOID
COILS
SCALE 1:1

Figure A–5

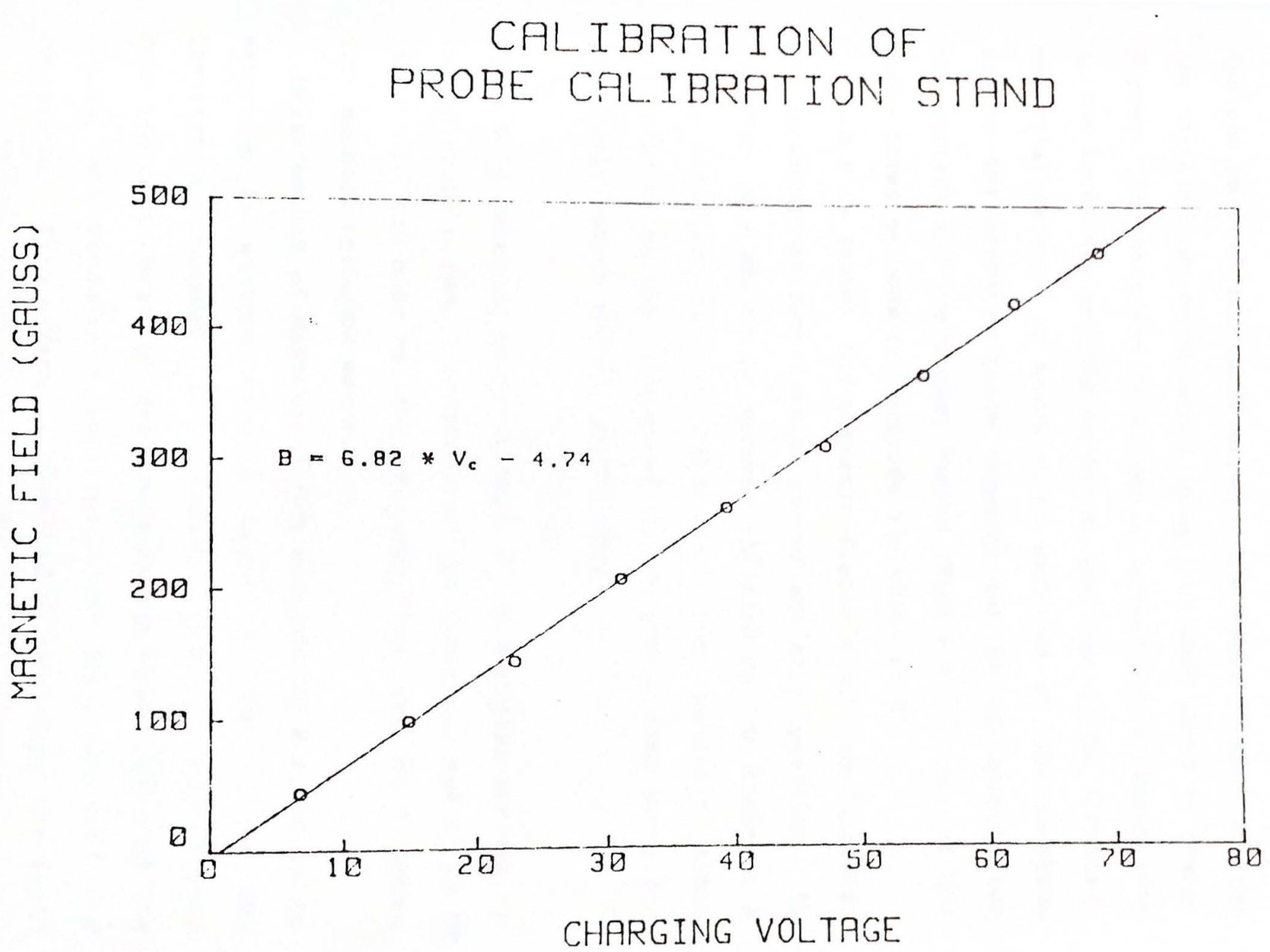
CALIBRATION OF
PROBE CALIBRATION STAND
MAGNETIC FIELD (GAUSS)
500
400
300
200
100
0
B = 6.82 * Vc - 4.74
0
10
20
30
40
50
60
70
80
CHARGING VOLTAGE

Figure A–6

known B-field for probe calibration. 2.) The actual thruster can be used for calibration. The total current through the thruster can be measured using a current shunt or transformer. If the probe is placed at a position adjacent both to the backplate and the anode, at the rear of the thruster, the total current is known to be enclosed at this location and so the magnetic field strength can be calculated from the current and the probes radius (Figure A-7). Any of the above three methods can provide the value of K.

Once K is known, the magnetic fields within the thruster can be mapped as functions of radius and axial position. In addition, the amount of current enclosed by the probe at a given location can be calculated from magnetic field strengths using the inverse of the relations used above for probe calibration within the thruster:

$$J_e = K'Vr$$

where V is measured probe voltage, J_e is enclosed current, r is the probe's radial location in the thruster, and K' is $2\pi/K\mu_o$. K' can also be obtained using the last two calibration methods outlined above.

Measurements of magnetic field strength were found to be sensitive to another form of signal present in the MPD thruster environment, electrostatic pickup. This arises form the capacitance present between the probe coil and the plasma, and produces a spurious input into the coil and integrator. This effect is detected by measuring the field

B-PROBE CALIBRATION METHODS

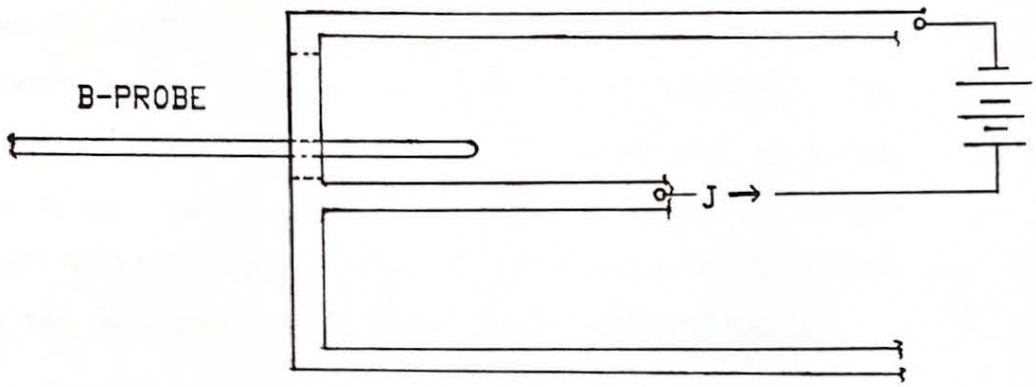

7a. Calibration Electrode

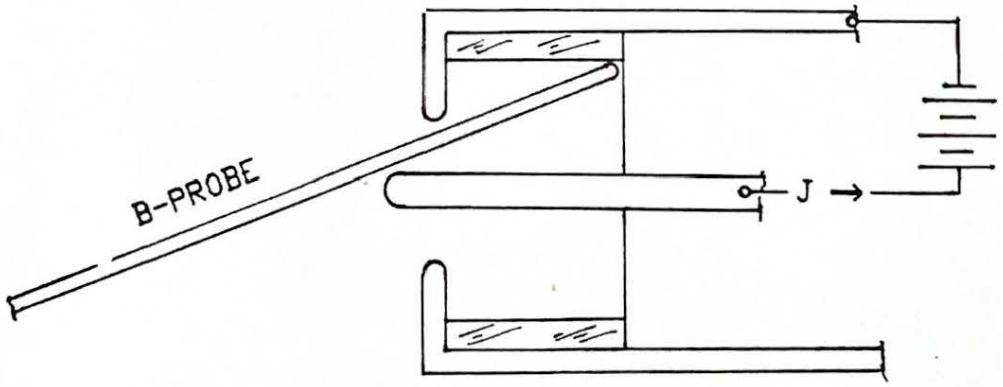

7b. Thruster Calibration

FIGURE A-7

strength at two diametrically opposed locations in the thruster. The flux at one location should be the negative of the other (since azimuthal symmetry is assumed); however, the electrostatic signal polarity remains constant, and so the two signals are not exact reflections of one another.

The method used to eliminate this problem is to install 50 ohm terminators between the probe and integrator. The terminator forms a circuit with the coil that acts as a low frequency filter which effectively eliminates the DC offset introduced by the electrostatic effect. This solution was found in the excellent reference by R. H. Lovberg (22).

REFERENCES

1. D. Q. King and L. K. Rudolph. "100 kWe MPD Thruster System Design," AIAA 82-1897, 1982.
2. R. G. Jahn. Physics of Electric Propulsion McGraw Hill, NY, 1968.
3. K. E. Clark. "Quasisteady Plasma Acceleration," Ph.D. Thesis, Princeton University, Princeton, NJ, May 1969.
4. L. K. Rudolph. "The MPD Thruster Onset Current Performance Limitation," Ph.D. Thesis, Princeton University, Princeton NJ, Sept. 1980.
5. M. Wolff et. al. "A High Performance MPD Thruster," 17th International Electric Propulsion Conference, IEPC 84-32, Tokyo, Japan, 1984.
6. F. M. Mead and R. G. Jahn. "Scaling of MPD Thrusters," AIAA 79-2075, 1979.
7. D. I. Kaplan. "Performance Characteristics of Geometrically Scaled MPD Thrusters," M.S.E. Thesis, Princeton University, Princeton NJ, Feb. 1982.
8. D. Q. King. "Effect of Choked Flow on Terminal Characteristics of MPD Thrusters," AIAA 81-0686, 1981.
9. J. W. Barnett. "Operation of the MPD Thruster with Stepped Current Input," Ph.D. Thesis, Princeton University, Princeton NJ, April 1985.

10. R. L. Burton, et. al. "Thrust and Efficiency of a Self Field MPD Thruster," AIAA-81-0686, 1981.

11. M. J. Boyle and R. G. Jahn. "Effects of Insulator Ablation on the Operation of a Quasi-steady MPD Arc," AIAA-73-1090, 1973.

12. M. J. Boyle, K. E. Clark, and R. G. Jahn. "Flowfield Characteristics and Performance Limitations of Quasi-Steady Magnetoplasmadynamic Accelerators," AIAA Journal, Vol. 14, No. 7, July 1975, pp. 955-962.

13. F. G. Baksht, et. al. "Critical Regime of a Plasma Accelerator," Sov. Phys. Tech. Phys., Vol. 18, No. 12, June 1974.

14. P. J. Devillers. "The Acceleration Processes in Magneto Plasma Dynamic Arcs," Ph.D. Thesis, University of California at San Diego, San Diego, CA 1971.

15. A. C. Malliaris, et. al. "Quasisteady MPD Propulsion at High Power," Final Technical Report AVSD-0146-71-RR Avco Corporation, Wilmington MA, February, 1971.

16. D. Q. King. "Magnetoplasmadynamic Channel Flow for Design of Coaxial MPD Thrusters," Ph.D. Thesis, Princeton University, Princeton, NJ, Dec. 1981.

17. M. Wolff. "A High Performance MPD Thruster," M.S.E. Thesis, Princeton University, Princeton NJ, Oct. 1983.

18. E. Y. Choueiri. "The Manifestation of Alfven's Hypothesis of Critical Ionization Velocity in the Performance of MPD Thrusters," AIAA-85-2037, 1985.

19. D. M. Merfeld. "MPD Thruster Performance: Propellant Injection and Species Effects," M.S.E Thesis, Princeton University, Princeton NJ, 1985.

20. J. R. Brophy, T. J. Pivirotto, D. Q. King. "Investigation of Arcjet Nozzle Performance," AIAA-85-2016, 1985.

21. C. K. Murch, et. al. "Performance Losses in Low Reynolds Number Nozzles," Journal of Spacecraft and Rockets, Vol. 5, No. 9, Sept. 1968, PP. 1090-1094.

22. R. H. Lovberg. "Magnetic Probes," Plasma Diagnostic Techniques. Huddlestone and Lennard, ed., Academic Press, NY, 1965.